Studies on the cell-to-cell movement mechanism of red clover necrotic mosaic virus via analysis of intracellular dynamics of double-stranded RNA and movement protein

Shota Takata

2024

CONTENTS

GENERAL INTRODUCTION

Plant viruses cause severe symptoms such as yellowing, necrosis and dwarf symptoms, resulting in a significant reduction in commercial value and yield (Scholthof *et al*., 2011). Global climate change is progressively increasing and is projected to intensify in the future (Singh *et al*., 2023). Climate change may affect the virulence and pathogenicity of plant viruses as well as the habitats of vector insects, increasing the frequency and magnitude of disease outbreaks (Singh *et al*., 2023; Trebicki, 2020). The development of agrochemicals and breeding for resistance are urgent issues, and elucidating the mechanism of virus infection is essential.

Although plant viruses are highly diverse, encompassing viruses of various natures, positive-sense single-stranded RNA (+ssRNA) viruses are the most frequently identified and well-studied (Dolja and Koonin, 2011; Fauquet, 2008). +ssRNA virus is characterized by its genomic RNA being directly translated as mRNA to produce its RNA-dependent RNA polymerase without the need for a complementary RNA intermediate (Matthew, 2012). The +ssRNA viruses include agriculturally important species such as *Barley stripe mosaic virus*, *Beet necrotic yellow vein virus*, *Cowpea mosaic virus, Grapevine leafroll-associated virus 3*, *Plum pox virus, Potato virus X*, *Soil-borne wheat mosaic virus, Tobacco mosaic virus*, and *Turnip yellow mosaic virus* (Fauquet, 2008, Mayo and Brunt, 2001; Scholthof *et al*., 2011).

+ssRNA virus invades plant cells via wounds or vectors such as fungi and insects (Adams, 1991; Dietzgen *et al*., 2016; Shaw, 1999). Once inside the cell, the viral particles become unstable, and the viral genomic nucleic acids are released into the cytoplasm. This disassembly mechanism is known as “uncoating" (Zaitlin and Hull, 1987). In the case of tobacco mosaic virus (TMV), the outer coat protein is partially dissociated at the

5' end of the genomic RNA, allowing translation factors and ribosomes to access the exposed 5' end. This process is thought to cause uncoating in parallel with translation (Wilson, 1984; Shaw *et al*, 1986). The uncoating of spherical viruses, such as cowpea chlorotic mottle virus (CCMV), is thought to involve pH-dependent particle swelling or structural changes (Wilts *et al*., 2015).

For efficient "translation" of eukaryotic mRNAs, two features are important: the 5′m7G(5′)ppp(5′)N cap and the 3′ poly(A) tail. The interaction of initiation factor 4E (eIF4E) with the cap structure and the interaction of poly(A)-binding protein (PABP) with the poly(A) tail promote translation initiation (Kahvejian *et al*. 2005; von der Haar *et al*., 2004). Nevertheless, these features are present in only a subset of RNA viruses. Viral genomic RNAs lacking a cap structure often possess a small protein called VPg covalently attached to the 5' end, which is crucial for translation (Kneller *et al*., 2006). Furthermore, viral genomic RNAs without both cap structure and VPg possess unique sequences and RNA structures in the 3' untranslated region to recruit translation factors and ribosomes (Guo *et al*., 2001; Mizumoto *et al*., 2003).

The initiation of +ssRNA viral "replication" occurs after the translation of RNA replication enzyme component proteins with RNA-dependent RNA polymerase domain, helicase domain and methyltransferase domain in general (van der Heijden and Bol, 2002). +ssRNA viruses utilize replication enzyme component proteins to modify the intracellular membrane system, forming viral replication complexes (VRCs), which are sites for RNA replication (den Boon and Ahlquist, 2010; Heinlein *et al*., 1998; Jin *et al*., 2018; Laliberté and Sanfaçon, 2010; Mine and Okuno, 2012). Different viruses use varied membrane systems as their replication sites. For instance, TMV, BMV, potato virus X (PVX), and turnip mosaic virus use the endoplasmic reticulum (ER). Melon necrotic spot virus and

carnation Italian ringspot virus uses mitochondria. Meanwhile, tomato bushy stunt virus and cucumber necrosis virus use peroxisome (Laliberté and Sanfaçon, 2010). VRCs assemble and form vesicle-like spherules in host membranes. These membranous compartments seemingly shield RNA replication intermediates from host defense responses activated by double-stranded (ds) RNA (den Boon and Ahlquist, 2010).

Because plant viruses encode a relatively small number of proteins (e.g., four for TMV), they are thought to rely on host factors for replication. From genetic analyses using positional cloning of *Arabidopsis* mutants resistant to TMV, *TOM1*, *TOM2A*, and *TOM3* were identified. The proteins encoded by these genes are membrane proteins with transmembrane domains and are crucial for the formation of VRCs (Tsujimoto *et al*., 2003; Yamanaka *et al*., 2002). Screening using the yeast and mini-replicon system has also identified several host factors involved in BMV replication, including reticulon and Δ9 fatty acid desaturase (Diaz *et al*., 2010; Lee *et al*., 2001).

After the replication in infected cells, the newly synthesized virion or viral genome RNA is transported to the plasmodesmata (PD). It moves through the PD to neighboring cells in a process called “cell-to-cell movement”. Subsequently, the virus enters vascular tissue, undergoes long-distance movement via the phloem, and establishes a systemic infection within the plant (Hipper *et al*., 2013). PD traverse the cell wall, with both the plasma membrane and the ER membrane extending through them. These structures are pivotal for connecting plant cells and play a significant role in molecular transport (Faulkner, 2018). However, PD have a size exclusion limit (SEL), which does not allow the passage of large molecules, including viral particles and nucleic acids of the viral genome (Tucker *et al*., 1982; Wolf *et al*., 1989; Oparka *et al*., 1999). Therefore, plant viruses encode a specialized protein, known as movement protein (MP), which facilitates

cell-to-cell movement via the PD (Lucas, 2006). Although there is little sequence conservation among viral MPs, the MPs possess properties that allow them to bind nucleic acid, localize to PD and increase SEL (Benitez-Alfonso *et al*., 2010; Lucas, 2006; Melcher, 1990, 2000; Waigmann *et al*., 2004). The precise mechanism underlying the increase in SEL remains not fully understood. In the case of TMV, it is proposed that MP recruits ankyrin repeat-containing proteins (ANKs) to the PD. This recruitment results in suppressing callose accumulation, consequently increasing SEL (Ueki *et al*., 2010).

Recently, a proposal suggested a close relationship between viral cell-to-cell movement and viral replication (Heinlein, 2015). The MPs of several +ssRNA viruses, such as TMV, PVX, and BMV have been reported to colocalize with membrane-associated inclusions that contain their respective VRCs (Asurmendi *et al*., 2004; Bamunusinghe *et al*., 2009; Dohi *et al*., 2001; Heinlein *et al*., 1998; Kawakami *et al*., 2004; Tilsner *et al*., 2012, 2013). In the case of TMV, it has been proposed that cell-to-cell movement occurs in the form of VRCs containing MP:vRNA and replication enzymes (Kawakami *et al*., 2004; Peña *et al*., 2014; Hirashima and Watanabe, 2001, 2003). Triple gene blocks, the MPs of PVX, localize to VRCs formed in the PD orifice and are proposed to send partially encapsidated RNA into the PD (Tilsner *et al*., 2013; Verchot-Lubicz *et al*., 2010). Thus, MP localization to VRCs is thought to be important for efficient cell-to-cell movement linked to replication, but the molecular background of how MPs localize is not well understood.

In this thesis, I focus on *Red clover necrotic mosaic virus*, which belongs to the genus *Dianthovirus* in the family *Tombusviridae*. Red clover necrotic mosaic virus (RCNMV) is a positive-stranded RNA virus with a bipartite genome. In contrast, well-studied plant viruses such as TMV and tomato bushy stunt virus (TBSV) possess unsegmented

genomes (Dawson *et al*., 1986; Gould *et al*., 1981; Hearne *et al*., 1990). Since RCNMV encodes only four proteins (Xiong and Lommel, 1989; Xiong *et al.,* 1993a, 1993b; Zavriev *et al*., 1996), it serves as an efficient model virus for studying the interaction between its two genome segments during viral replication, translation, and cell-to-cell movement.

Recent studies have explored the relationship between cell-to-cell movement and the localization of RCNMV MP (Kaido *et al*., 2009, 2011, 2014). The subcellular localization of RCNMV MP and sGFP fusion proteins has been characterized. MP:sGFP expressed from the recombinant virus localizes to the PD early in infection and eventually forms aggregated structures on the cortical ER (Kaido *et al*., 2009). These aggregated structures are VRCs of RCNMV, including the ER membrane, p27 protein, and dsRNA (Kaido *et al*., 2009, 2014). The 70 amino acids at the C-terminus of MP are required for localization to the VRCs. The cell-to-cell movement efficiency of a mutant RCNMV lacking its C-terminal 70 amino acids is remarkably reduced (Kaido *et al*., 2011). In addition, a search for host factors revealed that NbGAPDH-A is required for cell-to-cell movement. In *N. benthamiana* with a *NbGAPDH-A* gene knockdown, the efficiency of cell-to-cell movement and the localization of MP to the surface VRC is significantly reduced (Kaido *et al*., 2014). These results suggest that MP is recruited to VRCs on the cortical ER membrane via its C-terminal 70 amino acids and NbGAPDH-A, thereby facilitating viral intercellular movement. These localization analyses emphasize the importance of localization to both PD and VRCs. However, the exact mechanisms underlying the localization to these sites remain elusive.

In this thesis, I aimed to elucidate the mechanism of intercellular movement of RCNMV by analyzing the dynamics of dsRNA, which represents the replication site, and

conducting localization analyses using mutants of secondary structures of MP. In Chapter I, I performed an in-depth dynamic analysis of MP and dsRNA using B2-GFP plants (Monsion *et al*., 2018), reporter plants designed to detect dsRNA, representing the replication site. During the initial stages of infection, granular structures of dsRNA formed on the cell surface, while MP granule structures appeared separately. However, in the later stages, both dsRNA and MP granule structures aggregated and colocalized. To assess the necessity of MP for dsRNA aggregation, I examined the dsRNA dynamics in a mutant virus that does not express MP. Notably, dsRNA granule structures aggregated regardless of the presence or absence of MP, indicating that MP is not required for dsRNA aggregation. These results suggest that the granule structures of dsRNA and MP form independently in different cellular locations, and MP is subsequently recruited to colocalize with aggregated dsRNA structures.

In Chapter II, I investigated the transport pathways responsible for targeting MP to the PD. I focused on the cytoskeleton and vesicular transport system, given their reported association with MPs of other viruses. However, upon treating cells with various inhibitors, none were found to impede the localization of RCNMV MP to the PD. This finding suggests that RCNMV MP may use an unknown transport system to localize to the PD. Finally, I searched for functional regions within MP that are involved in its subcellular localization. Since neither transmembrane domains nor signal sequences were predicted within MP, I focused on the α-helix, a foundational structural element of the protein. After introducing mutations in the predicted α-helix regions, analysis revealed that specific amino acids within these α-helices of MP play a crucial role for the localization to PD and replication sites and facilitating cell-to-cell movement.

REFERENCES

Adams, M. J. (1991). Transmission of plant viruses by fungi. Ann. appl. Biol., 118, 479-492.

Asurmendi, S., Berg, R. H., Koo, J. C., Beachy, R. N. (2004). Coat protein regulates formation of replication complexes during tobacco mosaic virus infection. Proc. Natl. Acad. Sci. U. S. A., 101(5), 1415-1420.

Bamunusinghe, D., Hemenway, C. L., Nelson, R. S., Sanderfoot, A. A., Ye, C. M., Silva, M. A., Payton, M., Verchot-Lubicz, J. (2009). Analysis of potato virus X replicase and TGBp3 subcellular locations. Virology, 393(2), 272-285.

Benitez-Alfonso, Y., Faulkner, C., Ritzenthaler, C., Maule, A. J. (2010). Plasmodesmata: gateways to local and systemic virus infection. Mol. Plant Microbe Interact., 23(11), 1403-1412.

Dawson, W. O., Beck, D. L., Knorr, D. A., Grantham, G. L. (1986). cDNA cloning of the complete genome of tobacco mosaic virus and production of infectious transcripts. Proc. Natl. Acad. Sci. U. S. A., 83(6), 1832-1836.

den Boon, J. A., Ahlquist, P. (2010). Organelle-like membrane compartmentalization of positive-strand RNA virus replication factories. Annu. Rev. Microbiol., 64, 241-256.

Diaz, A., Wang, X., Ahlquist, P. (2010). Membrane-shaping host reticulon proteins play crucial roles in viral RNA replication compartment formation and function. Proc. Natl. Acad. Sci. U. S. A., 107(37), 16291-16296.

Dietzgen, R. G., Mann, K. S., Johnson, K. N. (2016). Plant virus-insect vector interactions: current and potential future research directions. Viruses, 8(11), 303.

Dohi, K., Mori, M., Furusawa, I., Mise, K., Okuno, T. (2001). Brome mosaic virus replicase proteins localize with the movement protein at infection-specific cytoplasmic inclusions in infected barley leaf cells. Arch. Virol., 146(8), 1607-1615.

Dolja, V. V., Koonin, E. V. (2011). Common origins and host-dependent diversity of plant and animal viromes. Curr. Opin. Virol., 1(5), 322-331.

Faulkner, C. (2018). Plasmodesmata and the symplast. Curr. Biol., 28(24), R1374-R1378.

Fauquet, C. M. (2008). Taxonomy, classification and nomenclature of viruses. Encyclopedia of Virology, 9-23.

Gould, A. R., Francki, R. I., Hatta, T., Hollings, M. (1981). The bipartite genome of red clover necrotic mosaic virus. Virology, 108(2), 499-506.

Guo, L., Allen, E. M., Miller, W. A. (2001). Base-pairing between untranslated regions facilitates translation of uncapped, nonpolyadenylated viral RNA. Mol. Cell, 7(5), 1103-1109.

Hearne, P. Q., Knorr, D. A., Hillman, B. I., Morris, T. J. (1990). The complete genome structure and synthesis of infectious RNA from clones of tomato bushy stunt virus. Virology, 177(1), 141-151.

Heinlein, M. (2015). Plant virus replication and movement. Virology, 479-480, 657-671.

Heinlein, M., Padgett, H. S., Gens, J. S., Pickard, B. G., Casper, S. J., Epel, B. L., Beachy, R. N. (1998). Changing patterns of localization of the tobacco mosaic virus movement protein and replicase to the endoplasmic reticulum and microtubules during infection. Plant Cell, 10(7), 1107-1120.

Hipper, C., Brault, V., Ziegler-Graff, V., Revers, F. (2013). Viral and cellular factors involved in Phloem transport of plant viruses. Front. Plant Sci., 24, 4:154.

Hirashima, K., Watanabe. Y. (2001). Tobamovirus replicase coding region is involved in cell-to-cell movement. J. Virol., 75(18), 8831-8836.

Hirashima, K., Watanabe, Y. (2003). RNA helicase domain of tobamovirus replicase executes cell-to-cell movement possibly through collaboration with its nonconserved region. J. Virol., 77(22):12357-12362.

Jin, X., Cao, X., Wang, X., Jiang, J., Wan, J., Laliberté, J. F., Zhang, Y. (2018). Three-dimensional architecture and biogenesis of membrane structures associated with plant virus replication. Front. Plant Sci., 9, 57.

Kahvejian, A., Svitkin, Y. V., Sukarieh, R., M'Boutchou, M. N., Sonenberg, N. (2005). Mammalian poly(A)-binding protein is a eukaryotic translation initiation factor, which acts via multiple mechanisms. Genes Dev., 19(1), 104-113.

Kaido, M., Abe, K., Mine, A., Hyodo, K., Taniguchi, T., Taniguchi, H., Mise, K., Okuno, T. (2014). GAPDH-A recruits a plant virus movement protein to cortical virus replication complexes to facilitate viral cell-to-cell movement. PLoS Pathog., 10(11), e1004505.

Kaido, M., Funatsu, N., Tsuno, Y., Mise, K., Okuno, T. (2011). Viral cell-to-cell movement requires formation of cortical punctate structures containing red clover necrotic mosaic virus movement protein. Virology, 413(2), 205–215.

Kaido, M., Tsuno, Y., Mise, K., Okuno, T. (2009). Endoplasmic reticulum targeting of the Red clover necrotic mosaic virus movement protein is associated with the replication of viral RNA1 but not that of RNA2. Virology, 395(2), 232–242.

Kawakami, S., Watanabe, Y., Beachy, R. N. (2004). Tobacco mosaic virus infection spreads cell to cell as intact replication complexes. Proc. Natl. Acad. Sci. U. S. A., 101(16), 6291-6296.

Kneller, E. L., Rakotondrafara, A. M., Miller, W. A. (2006). Cap-independent translation of plant viral RNAs. Virus Res., 119(1), 63-75.

Laliberté, J. F., Sanfaçon, H. (2010). Cellular remodeling during plant virus infection. Annu. Rev. Phytopathol., 48, 69-91.

Lee, W. M., Ishikawa, M., Ahlquist, P. (2001). Mutation of host delta9 fatty acid desaturase inhibits brome mosaic virus RNA replication between template recognition and RNA synthesis. J. Virol., 75(5), 2097-2106.

Lucas, W. J. (2006). Plant viral movement proteins: agents for cell-to-cell trafficking of viral genomes. Virology, 344(1), 169-184.

Matthews, R. E. F. (2012). Fundamentals of plant virology. Academic press, 1-403.

Mayo, M. A., Brunt, A. A. (2001). The current state of plant virus taxonomy. Mol. Plant Pathol., 2(2), 97-100.

Melcher, U. (1990). Similarities between putative transport proteins of plant viruses. J. Gen. Virol., 71(Pt 5), 1009-1018.

Melcher, U. (2000). The '30K' superfamily of viral movement proteins. J Gen Virol. 81(Pt 1), 257-266.

Mine, A., Okuno, T. (2012). Composition of plant virus RNA replicase complexes. Curr. Opin. Virol., 2(6), 669-675.

Mizumoto, H., Tatsuta, M., Kaido, M., Mise, K., Okuno, T. (2003). Cap-independent translational enhancement by the 3' untranslated region of red clover necrotic mosaic virus RNA1. J. Virol., 277(22), 12113-12121.

Monsion, B., Incarbone, M., Hleibieh, K., Poignavent, V., Ghannam, A., Dunoyer, P., Daeffler, L., Tilsner, J., Ritzenthaler, C. (2018). Efficient detection of long dsRNA in vitro and in vivo using the dsRNA binding domain from FHV B2 protein. Front. Plant Sci., 9, 1–16.

Oparka, K. J., Roberts, A. G., Boevink, P., Santa, Cruz, S., Roberts, I., Pradel, K. S., Imlau, A., Kotlizky, G., Sauer, N., Epel, B. (1999). Simple, but not branched, plasmodesmata allow the nonspecific trafficking of proteins in developing tobacco leaves. Cell, 97(6), 743-754.

Peña, E. J., Ferriol, I., Sambade, A., Buschmann, H., Niehl, A., Elena, S. F., Rubio, L., Heinlein, M. (2014). Experimental virus evolution reveals a role of plant microtubule dynamics and TORTIFOLIA1/SPIRAL2 in RNA trafficking. PLoS One, 9(8), e105364.

Scholthof, K. B., Adkins, S., Czosnek, H., Palukaitis, P., Jacquot, E., Hohn, T., Hohn, B., Saunders, K., Candresse, T., Ahlquist, P., Hemenway, C., Foster, G. D. (2011). Top 10 plant viruses in molecular plant pathology. Mol. Plant Pathol., 12(9), 938-954..

Shaw, J. G. (1999). Tobacco mosaic virus and the study of early events in virus infections. Philos. Trans. R. Soc. Lond. B. Biol. Sci., 354(1383), 603-611.

Shaw, J. G., Plaskitt, K. A., Wilson, T. M. (1986). Evidence that tobacco mosaic virus particles disassemble contranslationally in vivo. Virology, 148(2), 326-336.

Singh, B. K., Delgado-Baquerizo, M., Egidi, E., Guirado, E., Leach, J. E., Liu, H., Trivedi, P. (2023). Climate change impacts on plant pathogens, food security and paths forward. Nat. Rev. Microbiol., 21(10), 640-656.

Tilsner, J., Linnik, O., Louveaux, M., Roberts, I. M., Chapman, S. N., Oparka, K. J. (2013). Replication and trafficking of a plant virus are coupled at the entrances of plasmodesmata. J. Cell Biol., 201(7), 981-995.

Tilsner, J., Linnik, O., Wright, K. M., Bell, K., Roberts, A. G., Lacomme, C., Santa, Cruz, S., Oparka, K. J. (2012). The TGB1 movement protein of Potato virus X reorganizes actin and endomembranes into the X-body, a viral replication factory. Plant Physiol., 158(3), 1359-1370.

Trebicki, P. (2020). Climate change and plant virus epidemiology. Virus Res., 286, 198059.

Tsujimoto, Y., Numaga, T., Ohshima, K., Yano, M. A., Ohsawa, R., Goto, D. B., Naito, S., Ishikawa, M. (2003). Arabidopsis TOBAMOVIRUS MULTIPLICATION (TOM) 2

locus encodes a transmembrane protein that interacts with TOM1. EMBO J., 22(2), 335-343.

Tucker, E. B. (1982). Translocation in the stamina hairs of Setcreasea purpuerea. 1. A study of cell ultrastructure and cell-to-cell passage of molecular probes. Protoplasma, 113, 193-201.

Ueki, S., Spektor, R., Natale, D. M., Citovsky, V. (2010). ANK, a host cytoplasmic receptor for the Tobacco mosaic virus cell-to-cell movement protein, facilitates intercellular transport through plasmodesmata. PLoS Pathog., 6(11), e1001201.

van der Heijden, M. W., Bol, J. F. (2002). Composition of alphavirus-like replication complexes: involvement of virus and host encoded proteins. Arch. Virol., 147(5), 875-898.

Verchot-Lubicz, J., Torrance, L., Solovyev, A. G., Morozov, S. Y., Jackson, A. O., Gilmer, D. (2010). Varied movement strategies employed by triple gene block-encoding viruses. Mol. Plant Microbe Interact., 23(10), 1231-12347.

von der Haar, T., Gross, J. D., Wagner, G., McCarthy, J. E. (2004). The mRNA cap-binding protein eIF4E in post-transcriptional gene expression. Nat. Struct. Mol. Biol., 11(6), 503-511.

Waigmann, E., Ueki, S., Trutnyeva, K., Citovsky, V. (2004). The ins and outs of nondestructive cell-to-cell and systemic movement of plant viruses. Crit. Rev. Plant Sci., 23, 195–250.

Wilson, T. M. (1984). Cotranslational disassembly of tobacco mosaic virus in vitro. Virology, 137(2), 255-265.

Wilts, B. D., Schaap, I. A. T., Schmidt, C. F. (2015). Swelling and softening of the cowpea chlorotic mottle virus in response to pH shifts. Biophys. J., 108(10), 2541-2549.

Wolf, S., Deom, C. M., Beachy, R. N., Lucas, W. J. (1989). Movement protein of tobacco mosaic virus modifies plasmodesmatal size exclusion limit. Science, 246(4928), 377-379.

Xiong, Z., Kim, K. H., Giesman-Cookmeyer, D., Lommel, S. A. (1993a). The roles of the red clover necrotic mosaic virus capsid and cell-to-cell movement proteins in systemic infection. Virology. 192(1), 27–32.

Xiong, Z., Kim, K. H., Kendall, T. L., Lommel, S. A. (1993b). Synthesis of the putative red clover necrotic mosaic virus RNA polymerase by ribosomal frameshifting in vitro. Virology, 193(1), 213–221.

Xiong, Z., Lommel, S. A. (1989). The complete nucleotide sequence and genome organization of red clover necrotic mosaic virus RNA-1. Virology, 171(2), 543–554.

Yamanaka, T., Imai, T., Satoh, R., Kawashima, A., Takahashi, M., Tomita, K., Kubota, K., Meshi, T., Naito, S., Ishikawa, M. (2002). Complete inhibition of tobamovirus multiplication by simultaneous mutations in two homologous host genes. J. Virol., 76(5), 2491-2497.

Zaitlin, M., Hull, R. (1987). Plant virus-host interactions. Ann. Rev. Plant Physiol., 38, 291-315.

Zavriev, S. K., Hickey, C. M., Lommel, S. A. (1996). Mapping of the red clover necrotic mosaic virus subgenomic RNA. Virology, 216(2), 407–410.

CHAPTER I

Subcellular dynamics of red clover necrotic mosaic virus double-stranded RNAs in infected plant cells

INTRODUCTION

Most positive-strand RNA viruses modify the membrane structure of cellular organelles, such as the endoplasmic reticulum (ER), peroxisomes, and Golgi apparatus, to form viral replication complexes (VRCs) and synthesize viral RNA (den Boon *et al*., 2010; Heinlein *et al*., 1998; Laliberté and Sanfaçon, 2010; Laliberté and Zheng, 2014; Mine and Okuno, 2012). As viruses encode only a few proteins, they must utilize several host proteins to form a suitable microenvironment for replication (Hyodo and Okuno, 2014, 2016, 2020; Nagy and Feng, 2021). VRCs contain viral replicase, genomic RNA, double-stranded RNA (dsRNA), an intermediate product of viral replication, and host proteins. Replicase alters the membrane structure of the host cell organelle, resulting in the reorganization of the endomembrane upon VRC formation (den Boon and Ahlquist, 2010). Electron microscopy analysis of yeast cells expressing the 1a protein, a replicase component of brome mosaic virus, showed the formation of spherules about 50 nm in diameter that contain the viral replicase proteins (Schwartz *et al*., 2002). The formation of spherules involves endosomal sorting complexes required for transport (ESCRT) and the reticulon, which functions during ER remodeling-associated processes, such as membrane detachment and bending (Diaz *et al*., 2010, 2015). These structures are thought to be the sites of viral replication; they protect the viral dsRNA from host RNase (Schwartz *et al*., 2002, 2004).

VRCs formed by several types of viruses are not static and change their sizes and

subcellular localization as the infection progresses. During cowpea mosaic virus (CPMV) infection, CPMV VRCs are distributed as spot-like structures throughout the cytoplasm at an early stage of infection, while larger bodies are formed in the center of cells, often near the nucleus at a late stage of infection (Carette *et al*., 2002). Tobacco mosaic virus (TMV) viral RNA is recruited to the ER membrane via the 5′ cap structure, and then, the initial VRCs are formed as small granules (Christensen *et al*., 2009). TMV VRCs move along the microfilaments and accumulate at the junction between the cortical ER–actin network with microtubules; these junctions are called cortical microtubule-associated ER sites (cMERs). The initial VRCs collected in the cMERs are targeted to the plasmodesmata (PD) for viral cell-to-cell movement or form larger aggregates (Sambade *et al*., 2008). Potato virus X (PVX) induces the formation of ER-derived granular VRCs at an early stage of infection (Bamunusinghe *et al*., 2009) and forms large aggregates called X-bodies or inclusion bodies at a late stage of infection (Linnik *et al*., 2013; Tilsner *et al*., 2012). Aggregates formed during the late stage are believed to be the sites for enhancing the efficiency of viral replication and virion formation via the sequestration of various host proteins and the cytoskeleton. Thus, the transition of VRCs from smaller granular structures to the larger aggregates represents a widely conserved feature of plant virus infection. However, the process of VRC formation and the transition from the smaller VRCs to the larger aggregates remain poorly understood.

Plant viruses move via the PD to adjacent cells (Lucas, 2006; Reagan and Burch-Smith, 2020; Tilsner *et al*., 2014; Waigmann *et al*., 2004). Movement proteins (MPs) function to increase the size exclusion limit of the PD and transfer RNA–MP complexes by binding to viral RNAs (Benitez-Alfonso *et al*., 2010; Kumar and Dasgupta, 2021; Sambade *et al*., 2008; Waigmann *et al*., 2004). Several types of viral MPs colocalize with

VRCs. Turnip mosaic virus (TuMV) encodes P3N-PIPO protein as a dedicated MP (Cui *et al*., 2017; Yang *et al*., 2021). P3N-PIPO localizes at PD to support the recruitment of cylindrical inclusion (CI) protein to PD and subsequent intercellular trafficking of virion or CP/vRNP. In addition, P3N-PIPO colocalizes with 6K2-containing vesicles, which are thought to be components of VRCs. Multipartite interaction between TuMV-encoded proteins, such as 6K2, P3, P3N-PIPO, and CI may be involved in transporting 6K2-containing vesicles to the entrance of PD, possibly facilitating the cell-to-cell movement of TuMV (Chai *et al*., 2020; Wang, 2021). Barley stripe mosaic virus (BSMV) encodes three types of MPs (triple gene block (TGB) 1, 2, and 3). TGB2 and TGB3 are recruited by the viral γb protein into chloroplasts, where VRCs are formed, and enhance viral cell-to-cell movement (Jiang *et al*., 2020). These results suggest that viral replication and cell-to-cell movement are tightly linked and that the colocalization of MPs with VRCs may be necessary for the efficient viral cell-to-cell movement.

Thus far, VRC localization in living cells has been investigated by using fluorescent protein (FP)-tagged viral proteins. As FP-tagged viruses usually have a lower replication capacity than wild type (wt) viruses, it is quite difficult to monitor the dynamics of the VRCs. Recently, Monsion *et al*. (2018) have developed a transgenic *Nicotiana benthamiana* (B2-GFP plant) expressing the GFP-tagged dsRNA-binding domain of the B2 protein encoded by Flock House virus (B2-GFP). B2-GFP binds to, and detects the localization of, dsRNAs that are more than 80 nucleotides long in living infected cells. Punctate-like dsRNA structures (dsRNA granules) and larger aggregated structures were formed only upon viral infection. The aggregated dsRNA structures colocalized with the viral coat protein (CP), MPs, viral genomic RNA, and viral replicase, suggesting that these structures are components of VRCs. Therefore, B2-GFP plants have the potential to

be used for monitoring the dynamics of VRCs in living cells.

Red clover necrotic mosaic virus (RCNMV) is a positive-stranded RNA virus with a bipartite genome; it belongs to the genus *Dianthovirus* in the family *Tombusviridae*. Genomic RNA1 encodes the p27 auxiliary replication protein, p88 RNA-dependent RNA polymerase, and CP (Xiong and Lommel, 1989; Xiong *et al*., 1993b; Zavriev *et al*., 1996). RNA2 encodes an MP that is required for viral cell-to-cell movement and belongs to the 30K superfamily (Fujiwara *et al*., 1993; Xiong *et al*., 1993a). p27 and p88 localize at the ER (Turner *et al*., 2004) and form 480-kDa complexes, which are components of VRCs, by binding with several host proteins (Hyodo and Okuno, 2014, 2020). GFP-tagged p27 coexpressed with p88 and RNA2 via agroinfiltration localizes at small punctates along ER filaments. Later, larger aggregates containing the modified ER are formed at the perinuclear region (Kusumanegara *et al*., 2012), suggesting that the localization and morphology of VRCs change along with RCNMV infection.

Expression of GFP-tagged MPs from the CP-encoding region of RCNMV RNA1 makes it possible to monitor the localization of the MPs in living cells (Tremblay *et al*., 2005; Kaido *et al*., 2009). This recombinant system revealed that the MP-GFP localizes at the PD at an early infection stage, and later, forms cortical punctate structures. Eventually, larger aggregates are formed adjacent to the nucleus. Immunostaining analysis showed that the MP-GFP colocalized with p27 and dsRNA, which are components of VRCs (Kaido *et al*., 2009, 2014). Furthermore, 70 C-terminal amino acids of RCNMV MPs are required for both the localization to cortical punctate structures (that are VRCs) and viral cell-to-cell movement (Kaido *et al*., 2011). In addition, the search for host factors that facilitate the movement of RCNMV revealed that the glyceraldehyde 3-phosphate dehydrogenase A of *N. benthamiana* (NbGAPDH-A) is involved in viral

cell-to-cell movement by influencing the localization of MPs to VRCs (Kaido *et al*., 2014). These results suggest that RCNMV MPs localize at VRCs via 70 C-terminal amino acids with NbGAPDH-A and that the colocalization of MPs with VRCs is essential for efficient viral cell-to-cell movement. However, fundamental questions regarding how VRCs grow and increase in size, and how and when MPs colocalize with VRCs, remain unanswered.

In this study, I investigated the dynamics of dsRNA structures formed during RCNMV infection in B2-GFP plants to gain insights into the formation and transition processes of VRCs. Upon RCNMV infection, cortical punctate dsRNA granules were formed during an early infection stage; these granules then coalesced with each other to form larger aggregates. The colocalization of dsRNA granules with viral replicase was confirmed, indicating that these dsRNA structures are components of VRCs. Remarkably, large aggregates containing the ER colocalized strongly with MPs, while tiny dsRNA granules were weakly associated with both the membrane and MPs. Herein, I present novel findings stating that VRCs containing dsRNA and granular structures containing MPs are formed separately and that the size of VRCs is relevant to their colocalization with MPs.

MATERIALS AND METHODS

Plasmid construction

Plasmids given the prefix “pBIC” were used for agroinfiltration, and “pUC” were used for *in vitro* transcription. The plasmids pBICp88, pBICRC2 and pUCR1 were described previously (Figure I-1, Takeda *et al*., 2005).

All plasmids were amplified using Escherichia coli DH5α strain. All PCR reactions were performed using KOD One PCR master mix (Toyobo, Osaka, Japan), and all the PCR-amplified regions were verified by sequencing. The primers used in this study are listed in Table I-1.

The binary vector pBICP35 (Mori *et al*., 1991) was digested with ClaI, blunt-ended with T4 DNA polymerase (Takara Bio, Shiga, Japan) treatment to eliminate ClaI site, and self-ligated, producing pBICP35 (-ClaI).

A DNA fragment containing ER targeting peptide coding region was amplified from pBICER-mCherry (Kaido *et al*., 2009) using primers 1 and 2. A DNA fragment containing mScarlet-i coding region was amplified from pmScarlet-i_C1 (Addgene, Watertown, MA, USA) using primers 3 and 4. These fragments were mixed and used as the template for recombinant PCR using primers 1 and 4. The amplified PCR product was digested with BamHI/KpnI and inserted into the corresponding site of pBICP35 (-ClaI), producing pBICER-mSi.

A DNA fragment containing mSi coding region was amplified from pBICER-mSi using primers 5 and 6. A DNA fragment containing p27 coding region was amplified from pUCR1 using primers 7 and 8. These fragments were mixed and used as the template for recombinant PCR using primers 5 and 8. The amplified PCR product was digested with BamHI/KpnI and inserted into the corresponding site of pBICP35 (-ClaI), producing

pBICp27-mSi (Figure I-1).

A DNA fragment containing mSi peptide coding region was amplified from pBICER-mSi using primers 9 and 10. The amplified PCR product was digested with MluI/ClaI and inserted into the corresponding site of pUCR1-MsG (Kaido *et al*., 2009), producing pUCR1-MmSi (Figure I-1).

pUCR1-MmSi was digested with MluI/ClaI and inserted into the corresponding site of pR1-sGFP (Kaido *et al*., 2009), producing pR1-mSi. pR1-mSi was digested with SmaI/XhoI and inserted into the corresponding site of pUCR1, producing pUCR1-mSi (Figure I-1).

Plant growth conditions

N. benthamiana expressing B2-GFP (B2-GFP plants) were grown on commercial soil (Sumirin-Ryokka, Tokyo, Japan) at 25 ± 2 ◦ C and under long-day conditions with 16 h illumination per day. 4- or 5-week-old plants were used for viral RNA inoculation and 5- or 6-week-old plants were used for agroinfiltration or inhibitor treatment.

Inoculation of plants with viral RNA

RCNMV RNA was transcribed *in vitro* from plasmids given the prefix ‘pUC’ by using T7 RNA polymerase (Takara Bio) and the concentration of RCNMV was adjusted to 1.0 μg/μl. 4- or 5-week-old wt *N. benthamiana* or B2-GFP plants were rub-inoculated with a mixture of *in vitro* transcripts of RCNMV RNA by using carborundum (Nacalai Tesque, Kyoto, Japan) and incubated at 17 ◦C under long-day conditions with 16 h illumination per day.

Microscopy

Subcellular localization of proteins tagged with FPs was observed using an Olympus FluoView FV1200 confocal laser scanning microscope (CLSM). A 40 × Plan Apo objective lens (numerical aperture 0.95) or 60 × Plan Apo (numerical aperture 1.35) oil immersion objective lens (Olympus, Tokyo, Japan) was used. Excitation dichroic mirrors DM405/ 473/559, beam splitter SDM560 for GFP and mirror for RFP, and variable barrier filters (VBF) of 485 nm–545 nm for GFP and 570 nm–670 nm for RFP were used for the detection of fluorescent signals. In experiments for visualizing dual fluorescence, images were taken in a sequential mode to minimize fluorescent signal leakage. Images were stacks composed of optical sections taken at 1–2 μm intervals or single section taken at a cortical region of a plant cell. In time lapse imaging analyses, images were taken at every 1–10 s. All images were processed using Image J/Fiji (ver. 1.52p) (https://imagej.net/software/fiji/) (Schindelin *et al*., 2012).

The spread of mScarlet-i fluorescence was observed using Zeiss Axio Observer 7 fluorescence microscope using the imaging program ZEN 3.1 pro (Carl Zeiss, Oberkochen, Germany).

Northern blot analysis

Total RNA extraction from wt *N. benthamiana* or B2-GFP plant leaves and northern blot analysis were performed as described previously (Mizumoto *et al*., 2003). Probes used for detection of positive-strand RCNMV RNA1 and RNA2 were as described by Mizumoto *et al*. (2002). The luminescence signal was detected by using a WES-6100 Lumino Graph (ATTO, Osaka, Japan) and the signal intensity was calculated by using Image J/Fiji (ver. 1.52p).

Inhibitor treatment of plants

Half leaf of 5- or 6-week-old plants was infiltrated with 5 μM Latrunculin B (Lat B; Sigma-Aldrich, St. Louis, U. S. A.) in 0.2% dimethyl sulfoxide (DMSO; FUJIFILM Wako Pure Chemical, Osaka, Japan) 6 h in advance of RCNMV inoculation. Plants were inoculated with *in vitro* transcripts of RCNMV and incubated at 17 ◦C. The other half leaf was infiltrated with 0.2% DMSO as a control treatment.

Staining of nucleus

5-week-old B2-GFP plants were infiltrated with 4′–6′-Diamidino-2- phenylindole (DAPI; Tocris bioscience, Bristol, U.K.) in phosphate-buffered saline buffer (PBS; Takara Bio) 20 min before observation and incubated at room temperature.

Agroinfiltration of plants

5- or 6-week-old B2-GFP plants were infiltrated with *Agrobacterium tumefaciens* GV3101 strain (pMP90) containing plasmids given the prefix ‘pBIC’. In the localization analysis experiment of p27-mSi, plants were incubated in a moist chamber at 22 ◦C for 2 days. In the localization analysis experiment of ER-mSi, plants were incubated in a moist chamber at 22 ◦C for 1 day and rub-inoculated with a mixture of *in vitro* RCNMV transcripts. After inoculation, plants were incubated in a moist chamber at 17 ◦C for 20–28 h.

Image analysis

Number and size

After the images were taken and acquired in TIFF format using CLSM, only the

infected cells were trimmed using GNU Image Manipulation Program (GIMP; ver. 2.10.20) (https://www.gimpo.org/) and used for image analysis. Three images were used to create a classifier using Trainable Weka Segmentation (TWS) plug-in (https://imagej.net /plugins/tws/) (Arganda-Carreras *et al*., 2017) for Image J/Fiji. To confirm its effectiveness, the three test images were segmented by each classifier. The same classifier was applied to all images taken at the same experiment. After identifying dsRNA structures, inverting images into 8-bit type and binarizing them to generate binary images, fill hole and analyze particle plug-in for Image J/Fiji were performed to measure the number and size of dsRNA structures.

Velocity

Sequential images were taken at three infected sites and subjected to image analysis. After randomly selecting 10 structures per site, I calculated the mean velocity of each structure using MTrack J plug-in (https://imagej.net/plugins/mtrackj) (Meijering *et al*., 2012) for Image J/Fiji.

RGB intensity

Relative intensities of red and green fluorescent signal were calculated using the RGB profiler plug-in (https://imagej.nih.gov/ij/plugin s/rgb-profiler.html).

RESULTS

I define subcellular structures containing fluorescent proteins as follows. Granules and punctates are fluorescent structures smaller than 1.0 μm^2. Spot-like structures are between 1.0 μm^2 and 20 μm^2 in size. The aggregates represent fluorescent structures larger than 20 μm^2 in size.

B2-GFP based-live imaging revealed the subcellular dynamics of RCNMV dsRNA granules

A previous report showed that B2-GFP localized to larger cytoplasmic aggregates or smaller granules formed only during viral infection (Monsion *et al*., 2018). First, I ascertained whether similar structures could be observed during RCNMV infection using CLSM. In mock-inoculated leaves, B2-GFP localized to the nucleus and spread uniformly throughout the cytoplasm in the epidermal cells (Figure I-2, left panel and Figure I-3A). On the other hand, cytoplasmic small granular structures and large aggregates were observed in the leaves inoculated with wild type RCNMV RNA transcripts (RNA1 + RNA2) at 24 h post inoculation (hpi) (Figure I-2, right panel). Interestingly, nuclear GFP signal in the cells with those aggregates tended to be much weaker than that in mock-inoculated leaves (Figure I-2 and Figure I-3). In the virus-infected cells, B2-GFP might re-localize from nucleus to the cytoplasmic aggregates. Cytoplasmic aggregates and nucleus are easily distinguishable on the basis of their shapes and brightness (Figure I-3). These structures, which are formed specifically during viral infection, are thought to be the sites where dsRNA, a component of VRCs, is synthesized. Since B2-GFP binds to the dsRNA, which is a viral replication intermediate, it is possible that B2-GFP affects viral multiplication. To assess this possibility, I compared the accumulation of RCNMV RNA

in wt *N. benthamiana* plants with that in B2-GFP plants at 2 days post inoculation (dpi; inoculated leaves) and 7 dpi (systemic leaves). Similar amounts of positive-stranded viral RNA accumulated in both plants (Figure I-4). These results suggest that B2-GFP neither inhibited nor promoted viral replication and that B2-GFP plants are favorable for monitoring the dynamics of RCNMV dsRNA structures.

The dynamics of viral dsRNA were monitored in the RCNMV-inoculated leaves of B2-GFP plants over time using CLSM. Numerous dsRNA granules started to appear in the cortical region on the upper wall of epidermal cells at 5 hpi. Later, at 9 hpi and 15 hpi, larger spot-like structures of dsRNA were observed (Figure I-5, left panels). These observations suggest that dsRNA structures grow in size during viral infection. Some of the dsRNA structures were located along the outer edge of the epidermal cells (Figure I-5).

The dynamics of RCNMV dsRNA granules are uncoupled from the functions of MPs

Previous reports have shown that several viral MPs, including RCNMV MPs, colocalize with viral replicase or replication complexes (Heinlein, 2015; Tilsner and Oparka, 2012). To test whether RCNMV MPs are involved in the formation of dsRNA structures and the increase in their size, I inoculated B2-GFP plants with *in vitro*-synthesized transcripts of mutant RCNMV, which does not express MP (RNA1 + RNA2 fsMP). At 5 hpi, small dsRNA granules appeared on the inner surface of epidermal cells, and later, larger structures were detected (Figure I-5, right panels). There was little difference in the localization of the dsRNA compared with that in wt RCNMV-inoculated leaves.

The number and size of dsRNA structures were assessed by using the trainable weka segmentation (TWS) program. The number of dsRNA structures gradually increased over

time (Figure I-6A). Larger dsRNA structures appeared over time. The Steel–Dwass multiple-comparison test detected significant differences in the size of dsRNA structures between at 5 and 9 hpi for wt or fsMP mutant RCNMV (Figure I-6B, left panel). The median value remained almost the same, but the mean value gradually increased. This suggests that over the course of infection, small new dsRNA granules are continuously formed and existing dsRNA granules are gradually enlarged (Figure I-6B, right panel). Since a few conspicuous larger structures than 5 μm^2 in size were found to be formed in infected cells, I focused on the largest structures in each cell and compared them between each time point. The mean size of the largest structures in infected cells increased significantly every 4–5 h (Figure I-6C). I confirmed that there was no significant difference between the size of dsRNA structures in the wt RCNMV- and fsMP mutant-infected cells. These results indicate that the formation of VRCs and the increase in their size are independent of RCNMV MPs.

An actin antagonist inhibited the intracellular transport and aggregation of dsRNA granules

To examine how dsRNA granules grow in size, I performed the time-lapse tracking of dsRNA granules under high magnification. B2-GFP plants were inoculated with wt RCNMV and subjected to time-lapse imaging analysis at 5 hpi. I observed the active movement of dsRNA granules smaller than 1.0 μm^2 in size and sometimes larger dsRNA spot-like structures as well. Notably, small punctate granules were observed to move and coalesce with the larger ones (Figure I-7). This suggests that some dsRNA granules are highly mobile and that the larger aggregates may be formed as small granules coalesce each other and grow in size over time. These small granules looked to move with the ER

streaming (Figure I-8).

Latrunculin B (Lat B), an inhibitor of actin polymerization, prevented the intracellular transport of TMV VRCs (Liu *et al*., 2005). To ascertain the involvement of the acto–myosin system in the intracellular transport of RCNMV dsRNA granules, I treated the leaves with Lat B and observed the subcellular localization of dsRNA structures. In the negative control, i.e., dimethyl sulfoxide (DMSO)-treated leaves, dsRNA structures of various sizes, such as small punctates and larger aggregates, were observed at 12 hpi (Figure I-9A, left panel). Meanwhile, in Lat B-treated leaves, the size of the aggregates appeared to be much smaller than those in DMSO-treated leaves (Figure I-9A, right panel). Image analysis detected no significant difference between the number of dsRNA granules in the DMSO-treated and Lat B-treated leaves (Figure I-9B). However, a significant difference in the size of dsRNA granules was detected between the two treatments. Few aggregates larger than 10 μm^2 in size were detected after the Lat B treatment (Figure I-9C). In addition, the mean size of the largest dsRNA structures was reduced to 30% in the Lat B-treated leaves compared with that in the DMSO-treated leaves (Figure I-9D).

Next, to investigate whether Lat B affects the intracellular transport of dsRNA granules, I performed time-lapse imaging analysis. The dsRNA granules moved actively in DMSO-treated leaves (Figure I-10A, left panel); little intracellular movement was observed in the Lat B-treated leaves (Figure I-10A, right panel). The velocity of dsRNA granules was calculated using Mtrack J. The average velocity after Lat B treatment was reduced to 17.0% of that after DMSO treatment (Figure I-10B). These results suggest that the acto–myosin system is involved in the intracellular transport of dsRNA granules and their subsequent aggregation. Lat B treatment in this experimental condition did not affect

the accumulation level of RCNMV RNAs in the inoculated leaves (Figure I-11). The result suggests that the formation of large dsRNA aggregates is not a prerequisite for the higher accumulation of viral RNA accumulation of RCNMV. Spot-like structures shown in the right panel of Figure I-10A are probably large enough to recruit the MPs and can support cell-to-cell movement of the virus. Higher concentration of Lat B to inhibit the formation of spot-like structures or even granular structures of dsRNA might inhibit the multiplication of RCNMV.

dsRNA structures localize at the sites of viral replication

Thus far, I successfully monitored the subcellular dynamics of RCNMV dsRNA granules; however, whether viral replication occurs within dsRNA granules, especially small cortical punctates (~1 μm^2 in size), formed during RCNMV infection remains unclear, i.e., whether RCNMV dsRNA granules are components of VRCs remains unclear. Thus, I tested whether dsRNA granules colocalize with p27, the localization of which has widely been used as a marker of the RCNMV replication site (Kusumanegara *et al*., 2012; Hyodo *et al*., 2013, 2015, 2017, 2019). First, B2-GFP plants were infiltrated with a mixture of two *Agrobacterium* strains that express a fusion of p27 with an RFP, mScarlet-i (p27-mSi), and another viral replication protein, p88. No cortical dsRNA granules were observed and p27-mSi was observed as a large inclusion (Figure I-12, panels A–C). This observation is similar to the localization of p27-GFP when it is expressed alone (Kusumanegara *et al*., 2012). Next, B2-GFP plants were infiltrated with a mixture of three *Agrobacterium* strains that expressed p27-mSi and p88 and RNA2 as the template for viral RNA replication. Infiltration of this combination of *Agrobacterium r*esulted in the accumulation of lower but substantial amount of RNA2 compared with those expressed

wild type p27 and p88 and RNA2 (Figure I-13A), showing that p27-mSi is functional. The fluorescence of p27-mSi was observed as small punctates or slightly large spot-like structures (Figure I-12, panel E), or large nuclear-sized aggregates (Figure I-12, panel H). Importantly, these red signals coincided with the green dsRNA signals (Figure I-12, panels D–I). At a high magnification, larger aggregates, as well as most tiny granules smaller than 1 μm^2 in size also showed signals of both p27-mSi and B2-GFP (Figure I-12, panels J–L). I calculated the relative intensities of GFP and RFP signals by using an RGB profiler. The green signals of B2-GFP and red signals of p27-mSi were found to overlap in both the tiny dsRNA granules and aggregates (Figure I-14). These results indicate that the cortical punctates detected by B2-GFP are components of the VRC and localize at the sites where viral replication occurs.

RCNMV replication is associated with the ER membrane (Hyodo and Okuno, 2016, 2020). It is reasonable to assume that dsRNA granules colocalize with the cortical ER. Thus, I expressed the mSi tagged with an ER-targeting peptide (ER-mSi) via *Agrobacterium* infiltration and inoculated the leaves of B2-GFP plants with *in vitro* transcripts of wt RCNMV. In mock-inoculated leaves, the ER-mSi localized at reticulated structures around the cortical region on the upper wall of epidermal cells (Figure I-15A, panels a–c), while in RCNMV-inoculated leaves, ER-mSi also localized at the aggregates and overlapped with B2-GFP (Figure I-15A, panels d–f). At high magnification, a large aggregate (approximately 20 μm^2 in size) that merged well with the proliferated ER was observed (Figure I-15A, panels g–i). On the other hand, interestingly, tiny punctates (approximately 0.5 μm^2 in size) did not colocalize with, but rather, localized adjacent to, intact ER tubules (Figure I-15A, panels j–l). I then calculated the relative intensities of GFP and RFP using an RGB profiler. The GFP signals of the dsRNA aggregates almost

overlapped with the RFP signals, while the GFP signals of the tiny dsRNA granules hardly overlapped with the RFP signals (Figure I-15B). These results suggest that punctate dsRNA granules formed at an early infection stage localize adjacent to the ER membrane, and later, they grow larger, involving the ER membrane, to form relatively larger aggregates.

MPs preferentially colocalized with larger VRCs

Using an immunofluorescent labeling method, it was reported that RCNMV MPs colocalized with cortical VRCs containing viral dsRNA; this colocalization is essential for efficient viral cell-to-cell movement (Kaido *et al*., 2014). To assess the colocalization of the MPs with dsRNA in living cells within B2-GFP plants, I used *in vitro* transcripts of the recombinant RCNMV (RNA1-MmSi + RNA2fsMP), which expressed the fusion protein of MP and mScarlet-i (MP-mSi). I also used *in vitro* transcripts of the recombinant RCNMV (RNA1-mSi + RNA2fsMP) that expressed free mSi as the negative control (Figure I-1B). In contrast to the negative control-inoculated leaves, the RFP signal spread to multiple cells by 42 h after inoculation in the leaves inoculated with RNA1-MmSi + RNA2fsMP, confirming that MP-mSi retains the ability to transport viral RNA to adjacent cells (Figure I-13B).

In the negative control-inoculated leaves, B2-GFP localized at both the small punctates and larger aggregates. Free mSi localized at the nucleus and widely distributed in the cytoplasm, but did not colocalize with dsRNA structures (Figure I-16, panels A–C). Per the observation of the leaves inoculated with RNA1-MmSi + RNA2fsMP at 60 × magnification for objective lens, cortical dsRNA structures were observed as both the small punctates and large aggregates. The RFP signals of MP-mSi overlapped almost

perfectly with those of the spot-like structures and the large aggregates (>5 μm^2 in size) of B2-GFP (Figure I-16, panels D–F). Interestingly, however, when the image was enlarged for observation, many tiny dsRNA granules that did not colocalize with MP-mSi were detected (Figure I-16, panels G–I). Observation at 300 × magnification more clearly confirmed the presence of many tiny dsRNA granules (approximately 0.5 μm^2 in size) that did not colocalize with MP-mSi. I also observed tiny granular structures containing only the red signals of MP-mSi; these signals did not overlap with the green signals of the dsRNA structures (Figure I-16, panels J–L). Analysis using the RGB profiler confirmed the presence of three types of granular structures: those containing only GFP signals (Figure I-17B), those containing both GFP and RFP signals (Figure I-17C), and those containing only RFP signals (Figure I-17D). I counted granules smaller than 0.5 μm^2 in size and found that yellow granules that are supposed to contain both dsRNA and MP-mSi accounted for less than 50% of the total granules (data not shown).

These observations suggest that MP-mSi can form tiny granule structures by itself and that MP-mSi has a weak association with tiny dsRNA granules, while MP-mSi colocalizes more frequently with larger spot-like structures and dsRNA aggregates.

DISCUSSION

In this study, I tried to reveal the subcellular dynamics of VRCs. I judged that RCNMV VRCs can be monitored via dsRNA granules based on the following two points: First, RCNMV infected both B2-GFP and wt *N. benthamiana* plants similarly. Second, the replication protein p27 colocalized with the dsRNA granules (Figure I-12); this showed that dsRNA granules are components of VRCs. dsRNA granules were formed in the close vicinity of cortical ER tubules at an early stage of infection and were transported through the cytoplasm; this led to the coalescence of small dsRNA granules, and thus, the dsRNA granules grew in size over time to form aggregates (Figures I-5–7, 15). The formation of such aggregates may have depended on the acto–myosin system (Figures I-9 and 10). Thus, I presented an example of the detailed process of VRC formation and maturation.

I detected the fusion of dsRNA structures (Figures I-7). It should be noted that these results do not exclude other possibilities. For example, it is possible that tiny granular VRCs recruit VRC component proteins to grow larger. However, considering that only one or a few nuclear-sized aggregate VRCs were finally formed in an infected cell (Figure I-12, Kaido *et al*., 2014, data not shown), it seems likely that the fusion of granular VRCs substantially contributes to the growth of VRCs. Thus, larger aggregated VRCs formed in the late stage of infection contained ER (Figures I-15). p27 interacts with the host phospholipase D, which has an ability to modify the lipid composition of the ER membrane and enhances the affinity of p27 for the ER membrane (Hyodo *et al*., 2015). This would help the VRCs to be incorporated into the ER in the later infection stage.

The results obtained in this study suggest that the acto–myosin system drives the intracellular movement of VRCs containing dsRNA, and the VRCs grow in size by fusing with one other. TMV VRCs, which contain replication enzymes and viral RNA, have been

also reported to increase during viral infection. Actin and class XI myosin are involved in the intracellular transport of VRCs in TMV (Amari *et al*., 2014; Liu *et al*., 2005). In addition, the intracellular movement of granular structures derived from the nucleocapsid protein of fig mosaic virus (FMV) and the P6 of cauliflower mosaic virus (CaMV), both of which are probably components of VRCs, is also inhibited by Lat B infiltration. These results suggest that the VRCs of these viruses also move by using the acto–myosin system (Alers-Velazquez *et al*., 2021; Ishikawa *et al*., 2015; Luo *et al*., 2020; Schoelz and Leisner, 2017). Given that FMV and CaMV are negative-sense RNA and dsDNA viruses, respectively, while TMV and RCNMV are positive-sense RNA viruses, the mechanism underlying the intracellular trafficking of VRCs may be widely conserved among plant viruses.

TGBp1, a PVX MP, is indispensable for the formation of large aggregate structures called X-bodies, and infection with the recombinant PVX that does not express TGBp1 induced the formation of smaller-sized VRCs (Tilsner *et al*., 2012). On the contrary, my results showed that RCNMV MPs are neither involved in the formation of VRCs, nor in their enlargement (Figures I-5 and I-6). Given that the levels of viral RNAs accumulated in the presence or absence of RCNMV MPs in *N. benthamiana* protoplasts were comparable (Kaido *et al*., 2009), these results seem to be reasonable. In addition, RCNMV MP-GFP expressed alone from *A. tumefaciens* did not remain in the cytoplasm and was transported to the PD (Kaido *et al*., 2009). This result shows that RCNMV MPs have a low affinity for the ER membrane. Such intrinsic characteristics of RCNMV MP may have led to their independence from VRC formation.

In this study, I observed that MPs preferentially colocalized with relatively large structures, rather than with tiny dsRNA granules (Figures I-16). In other words, larger

VRCs have greater affinity for MPs. So how do MPs colocalize with large VRCs? I observed tiny granular structures of MPs that did not colocalize with dsRNA structures (Figures I-16). This result suggests that newly translated MPs interact with each other to form MP granules and are later recruited to large VRCs. I assume two hypotheses regarding the colocalization of MPs with large VRCs: 1) MP-granular structures may move along the actin–ER network into large VRCs, which contain aggregated ER (Figures I-15). Experiments involving the inhibition of myosin function by using motor domain-deficient myosins suggest that class XI and VIII myosins are involved in the subcellular movement of TMV MP punctates (Amari *et al*., 2014). Like TMV MPs, RCNMV MPs may be also transported through the cytoplasm via the host myosin motor protein. Aggregation of the actin–ER network may increase the frequency of encounters between VRCs and MPs. 2) MP granules may interact and colocalize with host proteins preferentially present in larger VRCs. As the VRCs mature, the accumulation of host proteins required for viral cell-to-cell movement may increase in the VRCs. This may give rise to a strong affinity between the MPs and host proteins, which may lead to the recruitment of MPs to relatively larger VRCs. MPs and VRCs may be colocalized either via the mechanisms described in points 1) or 2) or via both these mechanisms.

Results from previous studies showed that ectopically expressed RCNMV MP-GFP colocalized with the VRCs that replicate RNA1 (Kaido *et al*., 2009) and that their colocalization is essential for the cell-to-cell movement of the virus (Kaido *et al*., 2011, 2014). Considering these results and the results of the present study, this colocalization is assumed to be important in that the MPs capture viral genomic RNAs, especially, RNA1 that does not encode MPs, for their transportation to the neighboring cells. However, how MPs transport the viral genomic RNA to the PD remains unknown. As RCNMV moves

to the neighboring cell without the CP, MP-RNA complexes or components of the VRC are supposed to be transported to the PD. The VRCs of several viruses, including tobamoviruses, PVX, and TuMV, are formed at the entrance of the PD (Chai *et al*., 2020; Levy *et al*., 2015; Szecsi *et al*., 1999; Tilsner *et al*., 2013). These may function towards the co-replicational movement of the viral genome (Levy and Tilsner, 2020; Wu and Chen, 2020). I also detected some RCNMV VRCs that were formed along the outer edge of epidermal cells (they might be in close proximity to PD), while most VRCs were distributed around the cortical region on the upper wall of epidermal cells (Figure I-5). My data do not support or deny the co-replicational movement of viruses. To prove the substantial contribution of VRCs at the entrance of the PD towards the cell-to-cell movement of the virus, I need to identify the conditions in which both the formation of VRCs at the entrance of the PD and the viral cell-to-cell movement are inhibited.

Finally, the varying subcellular localizations of viral proteins and dsRNA raise new questions about how dsRNA and MP granules are formed. Liquid–liquid phase separation (LLPS) is a phenomenon in which a homogeneous mixture of molecules changes from a one-phase liquid state to a two-phase distinguishable liquid state (Alberti and Dormann, 2019; Hyman *et al*., 2014). In addition to some studies showing that LLPS is involved in the multiplication of animal viruses (Guseva *et al*., 2020; Heinrich *et al*., 2018; Nikolic *et al*., 2017), a recent study revealed that the p26 MP of the pea enation mosaic virus 2 (PEMV2) shows phase separation into droplets in vivo, and may lead to viral movement (Brown *et al*., 2021). These findings suggest that LLPS may be a crucial phenomenon associated with the infection of plant viruses. Amino acid sequence analysis using PrDOS (Protein DisOrder prediction system), a natively disordered site-prediction web server, suggests that RCNMV MP, p27, and p88 have putative disordered domains (Takata and

Kaido, unpublished data). Therefore, it is possible that the formation of RCNMV MP granules and dsRNA granules is driven by LLPS. Further efforts are needed to clarify these possibilities and the importance of LLPS in the RCNMV infection process.

REFERENCES

Alers-Velazquez, R., Jacques, S., Muller, C., Boldt, J., Schoelz, J., Leisner, S. (2021). Cauliflower mosaic virus P6 inclusion body formation: A dynamic and intricate process. Virology, 553, 9–22.

Alberti, S., Dormann, D. (2019). Liquid-liquid phase separation in disease. Ann. Rev. Genetics, 53, 171–194.

Amari, K., Di Donato, M., Dolja, V. V., Heinlein, M. (2014). Myosins VIII and XI play distinct roles in reproduction and transport of tobacco mosaic virus. PLoS Pathog., 10(10), e1004448.

Arganda-Carreras, I., Kaynig, V., Rueden, C., Eliceiri, K. W., Schindelin, J., Cardona, A., Seung, H. S. (2017). Trainable Weka Segmentation: a machine learning tool for microscopy pixel classification. Bioinformatics, 33(15), 2424–2426.

Bamunusinghe, D., Hemenway, C. L., Nelson, R. S., Sanderfoot, A. A., Ye, C. M., Silva, M. A. T., Payton, M., Verchot-Lubicz, J. (2009). Analysis of potato virus X replicase and TGBp3 subcellular locations. Virology, 393(2), 272–285.

Benitez-Alfonso, Y., Faulkner, C., Ritzenthaler, C., Maule, A. J. (2010). Plasmodesmata: gateways to local and systemic virus infection. Mol. Plant Microbe Interact., 23(11), 1403–1412.

Brown, S. L., Garrison, D. J., May, J. P. (2021). Phase separation of a plant virus movement protein and cellular factors support virus-host interactions. PLoS Pathog., 17(9), e1009622.

Carette, J. E., Cuhl, K., Wellink, J., van Kammen, A. (2002). Coalescence of the sites of cowpea mosaic virus RNA replication into a cytopathic structure. J. Virol., 76(12), 6235–6243.

Chai, M., Wu, X., Liu, J., Fang, Y., Luan, Y., Cui, X., Zhou, X., Wang, A., Cheng, X. (2020). P3N-PIPO Interacts with P3 via the shared N-terminal domain to recruit viral replication vesicles for cell-to-cell movement. J. Virol., 94(8), e01898-19.

Christensen, N., Tilsner, J., Bell, K., Hammann, P., Parton, R., Lacomme, C., Oparka, K. (2009). The 5' Cap of tobacco mosaic virus (TMV) is required for virion attachment to the actin / endoplasmic reticulum network during early infection. Traffic, 10(5), 536–551.

Cui. X., Yaghmaiean, H., Wu, G., Wu, X., Chen, X., Thorn, G., Wang, A. (2017). The C-terminal region of the Turnip mosaic virus P3 protein is essential for viral infection via targeting P3 to the viral replication complex. Virology, 510, 147-155.

den Boon, J. A., Ahlquist, P. (2010). Organelle-like membrane compartmentalization of positive-strand RNA virus replication factories. Annu. Rev. Microbiol., 64, 241–256.

den Boon, J. A., Diaz, A., Ahlquist, P. (2010). Cytoplasmic viral replication complexes. Cell Host Microbe, 8(1), 77–85.

Diaz, A., Zhang, J., Ollwerther, A., Wang, X., Ahlquist, P. (2015). Host ESCRT proteins are required for bromovirus RNA replication compartment assembly and function. PLoS Pathog., 11(3), e1004742.

Diaz, A., Wang, X., Ahlquist, P. (2010). Membrane-shaping host reticulon proteins play crucial roles in viral RNA replication compartment formation and function. Proc. Natl. Acad. Sci. U. S. A., 107(37), 16291–16296.

Fujiwara, T., Giesman-Cookmeyer, D., Ding, B., Lommel, S. A., Lucas, W. J. (1993). Cell-to-cell Trafficking of macromolecules through plasmodesmata potentiated by the red clover necrotic mosaic virus movement protein. Plant Cell, 5(12), 1783–1794.

Guseva, S., Milles, S., Jensen, M. R., Salvi, N., Kleman, J. P., Maurin, D., Ruigrok, R. W. H., Blackledge, M. (2020). Measles virus nucleo- and phosphoproteins form liquid-like phase-separated compartments that promote nucleocapsid assembly. Sci. Adv., 6(14), eaaz7095.

Heinlein, M., Padgett, H. S., Gens, J. S., Pickard, B. G., Casper, S. J., Epel, B. L., Beachy, R. N. (1998). Changing patterns of localization of the tobacco mosaic virus movement protein and replicase to the endoplasmic reticulum and microtubules during infection. Plant Cell, 10(7), 1107–1120.

Heinlein, M. (2015). Plant virus replication and movement. Virology, 479-480, 657–671.

Heinrich, B. S., Maliga, Z., Stein, D. A., Hyman, A. A., Whelan, S. P. J. (2018). Phase transitions drive the formation of vesicular stomatitis virus replication compartments. mBio, 9(5), e022290-17.

Hyman, A. A., Weber, C. A., Jülicher, F. (2014). Liquid-liquid phase separation in biology. Annu. Rev. Cell Dev. Biol., 30, 39–58.

Hyodo, K., Hashimoto, K., Kuchitsu, K., Suzuki, N., Okuno, T. (2017). Harnessing host ROS-generating machinery for the robust genome replication of a plant RNA virus. Proc. Natl. Acad. Sci. U. S. A., 114(7), E1282–E1290.

Hyodo, K., Mine, A., Taniguchi, T., Kaido, M., Mise, K., Taniguchi, H., Okuno, T. (2013). ADP ribosylation factor 1 plays an essential role in the replication of a plant RNA virus. 87(1), 163–176.

Hyodo, K., Okuno, T. (2014). Host factors used by positive-strand RNA plant viruses for genome replication. J. Gen. Plant Pathol., 80, 123–135.

Hyodo, K., Okuno, T. (2016). Pathogenesis mediated by proviral host factors involved in translation and replication of plant positive-strand RNA viruses. Curr. Opin. Virol., 17, 11–18.

Hyodo, K., Okuno, T. (2020). Hijacking of host cellular components as proviral factors by plant-infecting viruses. Adv. Virus Res., 107, 37–86.

Hyodo, K., Suzuki, N., Okuno, T. (2019). Hijacking a host scaffold protein, RACK1, for replication of a plant RNA virus. New Phytol., 221(2), 935–945.

Hyodo, K., Taniguchi, T., Manabe, Y., Kaido, M., Mise, K., Sugawara, T., Taniguchi, H., Okuno, T. (2015). Phosphatidic acid produced by phospholipase D promotes RNA replication of a plant RNA virus. PLoS Pathog., 11(5), e1004909.

Ishikawa, K., Miura, C., Maejima, K., Komatsu, K., Hashimoto, M., Tomomitsu, T., Fukuoka, M., Yusa, A., Yamaji, Y., Namba, S. (2015). Nucleocapsid protein from fig mosaic virus forms cytoplasmic agglomerates that are hauled by endoplasmic reticulum streaming. J. Virol., 89(1), 480–491.

Jiang, Z., Zhang, K., Li, Z., Li, Z., Yang, M., Jin, X., Cao, Q., Wang, X., Yue, N., Li, D., Zhang, Y. (2020). The Barley stripe mosaic virus γb protein promotes viral cell-to-cell movement by enhancing ATPase-mediated assembly of ribonucleoprotein movement complexes. PLoS Pathog 16(7), e1008709.

Kaido, M., Abe, K., Mine, A., Hyodo, K., Taniguchi, T., Taniguchi, H., Mise, K., Okuno, T. (2014). GAPDH-A recruits a plant virus movement protein to cortical virus replication complexes to facilitate viral cell-to-cell movement. PLoS Pathog., 10(11), e1004505.

Kaido, M., Funatsu, N., Tsuno, Y., Mise, K., Okuno, T. (2011). Viral cell-to-cell movement requires formation of cortical punctate structures containing Red clover necrotic mosaic virus movement protein. Virology, 413(2), 205–215.

Kaido, M., Tsuno, Y., Mise, K., Okuno, T. (2009). Endoplasmic reticulum targeting of the Red clover necrotic mosaic virus movement protein is associated with the replication of viral RNA1 but not that of RNA2. Virology, 395(2), 232–242.

Kumar, G., Dasgupta, I. (2021). Variability, functions and interactions of plant virus movement proteins: What do we know so far? Microorganisms, 9(4), 695.

Kusumanegara, K., Mine, A., Hyodo, K., Kaido, M., Mise, K., Okuno, T. (2012). Identification of domains in p27 auxiliary replicase protein essential for its association with the endoplasmic reticulum membranes in red clover necrotic mosaic virus. Virology, 433(1), 131–141.

Laliberté, J-F., Sanfaçon, H. (2010). Cellular remodeling during plant virus infection. Ann. Rev. Phytopathol. 48, 69–91.

Laliberté, J-F., Zheng, H. (2014). Viral manipulation of plant host membranes. Ann. Rev. Virol. 1(1), 237–259.

Levy, A., Tilsner, J. (2020). Creating contacts between replication and movement at plasmodesmata-A role for membrane contact sites in plant virus infections? Front. Plant Sci., 11, 862.

Levy, A., Zheng, J. Y., Lazarowitz, S. G. (2015). Synaptotagmin SYTA forms ER-plasma membrane junctions that are recruited to plasmodesmata for plant virus movement. Curr. Biol., 25, 2018-2025.

Linnik, O., Liesche, J., Tilsner, J., Oparka, K. (2013). Unraveling the structure of viral replication complexes at super-resolution. Front. Plant Sci., 4, 6.

Liu, J., Blancaflor, E. B., Nelson, R. S. (2005). The tobacco mosaic virus 126-kilodalton protein, a constituent of the virus replication complex, alone or within the complex aligns with and traffics along microfilaments. Plant Phyiol., 138(4), 1853–1865.

Lucas, W. J. (2006). Plant viral movement proteins: agents for cell-to-cell trafficking of viral genomes. Virology, 344(1), 169–184.

Luo, M., Terrell, J. R., Mcmanus, S. A. (2020). Nucleocapsid Structure of Negative Strand RNA Virus. Viruses, 12(8), 835.

Meijering, E., Dzyubachyk, O., Smal, I. (2012). Methods for Cell and Particle Tracking. Meth. Enzymol., 504, 183–200.

Mine, A., Okuno, T. (2012). Composition of plant virus RNA replicase complexes. Curr. Opin. Virol., 2(6), 669–675.

Mizumoto, H., Hikichi, Y., Okuno, T. (2002). The 3'-untranslated region of RNA1 as a primary determinant of temperature sensitivity of red clover necrotic mosaic virus Canadian strain. Virology, 293(2), 320–327.

Mizumoto, H., Tatsuta, M., Kaido, M., Mise, K., Okuno, T. (2003). Cap-independent translational enhancement by the 3' untranslated region of red clover necrotic mosaic virus RNA1. J. Virol., 77(22), 12113–12121.

Monsion, B., Incarbone, M., Hleibieh, K., Poignavent, V., Ghannam, A., Dunoyer, P., Daeffler, L., Tilsner, J., Ritzenthaler, C. (2018). Efficient detection of long dsRNA in vitro and in vivo using the dsRNA binding domain from FHV B2 protein. Front. Plant Sci., 9, 1–16.

Mori, M., Mise, K., Kobayashi, K., Okuno, T., Furusawa, I. (1991). Infectivity of plasmids containing brome mosaic virus cDNA linked to the cauliflower mosaic virus 35S RNA promoter. J. Gen. Virol., 72, 243–246.

Nagy, P. D., Feng, Z. (2021). Tombusviruses orchestrate the host endomembrane system to create elaborate membranous replication organelles. Curr. Opin. Virol., 48, 30–41.

Nikolic, J., Bars, R. L., Lama, Z., Scrima, N., Lagaudrière-Gesbert, C., Gaudin, Y., Blondel, D. (2017). Negri bodies are viral factories with properties of liquid organelles. Nat. Commun., 8(1), 58.

Reagan, B. C., Burch-Smith, T. M. (2020). Viruses reveal the secrets of plasmodesmal cell biology. Mol. Plant Microbe Interact., 33(1), 26–39.

Sambade, A., Brandner, K., Hofmann, C., Seemanpillai, M., Mutterer, J., Heinlein, M. (2008). Transport of TMV movement protein particles associated with the targeting of RNA to plasmodesmata. Traffic, 9(12), 2073–2088.

Schindelin, J., Arganda-Carreras, I., Frise, E., Kaynig, V., Longair, M., Pietzsch, T., Preibisch, S., Rueden, C., Saalfeld, S., Schmid, B., Tinevez, J. Y., White, D. J., Hartenstein, V., Eliceiri, K., Tomancak, P., Cardona, A. (2012). Fiji: an open-source platform for biological-image analysis. Nat. Methods., 9(7), 676–682.

Schoelz, J. E., Leisner, S. (2017). Setting up shop: the formation and function of the viral factories of Cauliflower mosaic virus. Front. Plant Sci., 8, 1832.

Schwartz, M., Chen, J., Janda, M., Sullivan, M., den Boon, J., Ahlquist, P. (2002). A positive-strand RNA virus replication complex parallels form and function of retrovirus capsids. Mol. Cell, 9(3), 505–514.

Schwartz, M., Chen, J., Lee, W., Janda, M., Ahlquist, P. (2004). Alternate, virus-induced membrane rearrangements support positive-strand RNA virus genome replication. Proc. Natl. Acad. Sci. U. S. A., 101(31), 11263–11268.

Szécsi, J., Ding, X. S., Lim, C. O., Bendahmane, M., Cho, M. J., Nelson, R. S., Beachy, R. N. (1999). Development of tobacco mosaic virus infection sites in Nicotiana benthamiana. Mol. Plant Microbe Interact., 12, 143–152.

Takeda, A., Tsukuda, M., Mizumoto, H., Okamoto, K., Kaido, M., Mise, K., Okuno, T. (2005). A plant RNA virus suppresses RNA silencing through viral RNA replication. EMBO J., 24(17), 3147–3157.

Tatsuta, M., Mizumoto, H., Kaido, M., Mise, K., Okuno, T. (2005). The red clover necrotic mosaic virus RNA2 trans-activator is also a cis-acting RNA2 replication element. J. Virol., 79(2), 978–986.

Tilsner, J., Linnik, O., Louveaux, M., Roberts, I. M., Chapman, S. N., Oparka, K. J. (2013). Replication and trafficking of a plant virus are coupled at the entrances of plasmodesmata. J. Cell Biol., 201(7), 981-995.

Tilsner, J., Linnik, O., Wright, K. M., Bell, K., Roberts, A. G., Lacomme, C., Cruz, S. S., Oparka, K. J. (2012). The TGB1 movement protein of potato virus X reorganizes actin and endomembranes into the X-body, a viral replication factory. Plant Physiol., 158(3), 1359–1370.

Tilsner, J., Oparka, K. J. (2012). Missing links? - The connection between replication and movement of plant RNA viruses. Curr. Opin. Virol., 2(6), 705–711.

Tilsner, J., Taliansky, M. E., Torrance, L. (2014). Plant Virus Movement. eLS, 1–12.

Tremblay, D., Vaewhongs, A. A., Turner, K. A., Sit, T. L., Lommel, S. A. (2005). Cell wall localization of red clover necrotic mosaic virus movement protein is required for cell-to-cell movement. Virology, 333(1), 10–21.

Turner, K. A., Sit, T. L., Callaway, A. S., Allen, N. S., Lommel, S. A. (2004). Red clover necrotic mosaic virus replication proteins accumulate at the endoplasmic reticulum. Virology, 320(2), 276–290.

Waigmann, E., Ueki, S., Trutnyeva, K., Citovsky, V. (2004). The ins and outs of nondestructive cell-to-cell and systemic movement of plant viruses. Crit. Rev. Plant Sci., 23, 195–250.

Wang, A. (2021). Cell-to-cell movement of plant viruses via plasmodesmata: a current perspective on potyviruses. Curr. Opin. Virol., 48, 10–16.

Wu, X., Cheng, X. (2020). Intercellular movement of plant RNA viruses: Targeting replication complexes to the plasmodesma for both accuracy and efficiency. Traffic, 21(12), 725–736.

Xiong, Z., Kim, K. H., Giesman-Cookmeyer, D., Lommel, S. A. (1993a). The roles of the red clover necrotic mosaic virus capsid and cell-to-cell movement proteins in systemic infection. Virology. 192(1), 27–32.

Xiong, Z., Kim, K. H., Kendall, T. L., Lommel, S. A. (1993b). Synthesis of the putative red clover necrotic mosaic virus RNA polymerase by ribosomal frameshifting in vitro. Virology, 193(1), 213–221.

Xiong, Z., Lommel, S. A. (1989). The complete nucleotide sequence and genome organization of red clover necrotic mosaic virus RNA-1. Virology, 171(2), 543–554.

Xiong, Z., Lommel, S. A. (1991). Red clover necrotic mosaic virus infectious transcripts synthesized in vitro. Virology, 182(1), 388–392.

Yang, X., Li, Y., Wang, A. (2021). Research advances in potyviruses: From the laboratory bench to the field. Ann. Rev. Phytopath. 59, 1–29.

Zavriev, S. K., Hickey, C. M., Lommel, S. A. (1996). Mapping of the red clover necrotic mosaic virus subgenomic RNA. Virology, 216(2), 407–410.

Table I-1. Primers used in this study.

Name		Sequence (5' → 3')
primer 1	35S/P(-)106R	GTTCCAACCACGTCTTCAAAGC
primer 2	mS-ER-Rev	GCCCTTGCTCACCATGAATTCGGCCGAGGATAA
primer 3	ER-mS-Fw	TCCTCGGCCGAATTCATGGTGAGCAAGGGCGAG
primer 4	Kpn-mS-Rev	CGGGGTACCTTAAAGCTCATCATGCTTGTACAGCTCGTCCATGC
primer 5	Kpn-mSi-Rev	GGGGTACCTACTTGTACAGCTCGTCCATG
primer 6	H6-mSi-Fw	GGGCATGCATCATCATCATCATCATATGGTGAGCAAGGGCGAGG
primer 7	H4G2p27-Rev	ATGATGATGATGCATGCCCCCAAAATCCTCAAGGGATTTGA
primer 8	Bamp27-Fw	CGGGGATCCGGATGGGTTTTATAAATCTTTCGC
primer 9	Mlu-mS Rev	TGCACGCGTTACTTGTACAGCTCGTCCAT
primer 10	Cla-mS Fw	GCATCGATGCATCATCATCATCATCATATGGTGAGCAAGGGCGAGGCAGT
primer 11	SmaI/R2-3'-2	GACCCCGGGGTGCCTAGCCGTTATAC
primer 12	EcoRI/T7	CGGGAATTCTAATACGACTCACTATAG
primer 13	SmaI/R2-3'	GACCCCGGGGGGGTGCCTAGCCGTTATAC

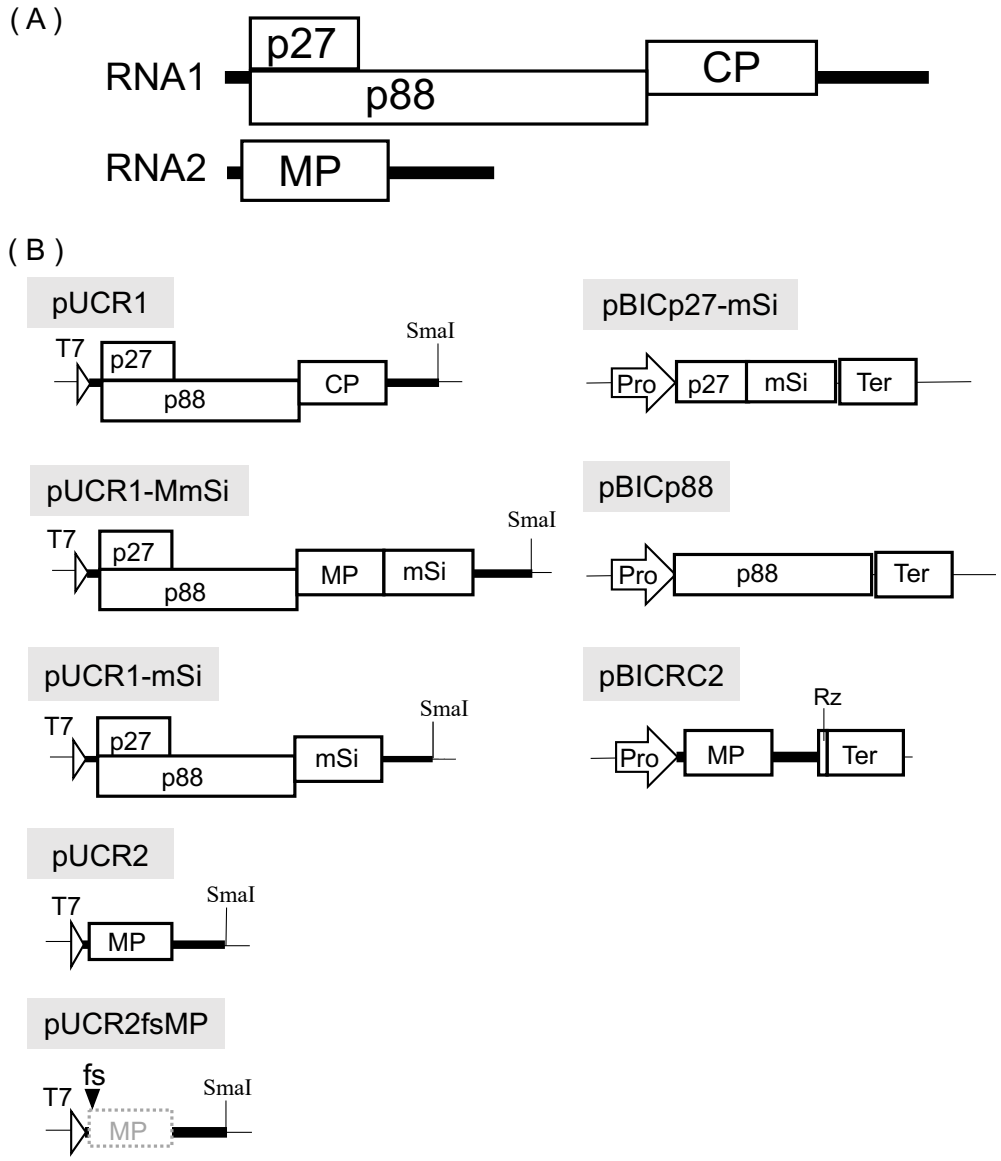

Figure I-1. Schematic diagrams of red clover necrotic mosaic virus (RCNMV) genome organization and various derivative constructs. (A) Genome map of RCNMV. RNA1 encodes two N-terminal overlapping nonstructural proteins (p27 and p88) and coat protein (CP), which is expressed from subgenomic RNA. RNA2 encodes 35 kDa movement protein (MP). Four open boxes show viral proteins encoded on genomic RNAs and bold horizontal lines show viral noncoding sequences. (B) Genome map of the plasmids used in this study. Plasmids containing the prefix 'pUC' were cut with Sma I and used as the templates for *in vitro* transcription. Plasmids containing the prefix 'pBIC' were used for inoculation via Agrobacterium. Key: T7, T7 promoter; Pro, cauliflower mosaic virus (CaMV) 35S promoter; Ter, CaMV terminator; Rz, ribozyme sequence; Sma I, Sma I recognition sequence; mSi, mScarlet-i.

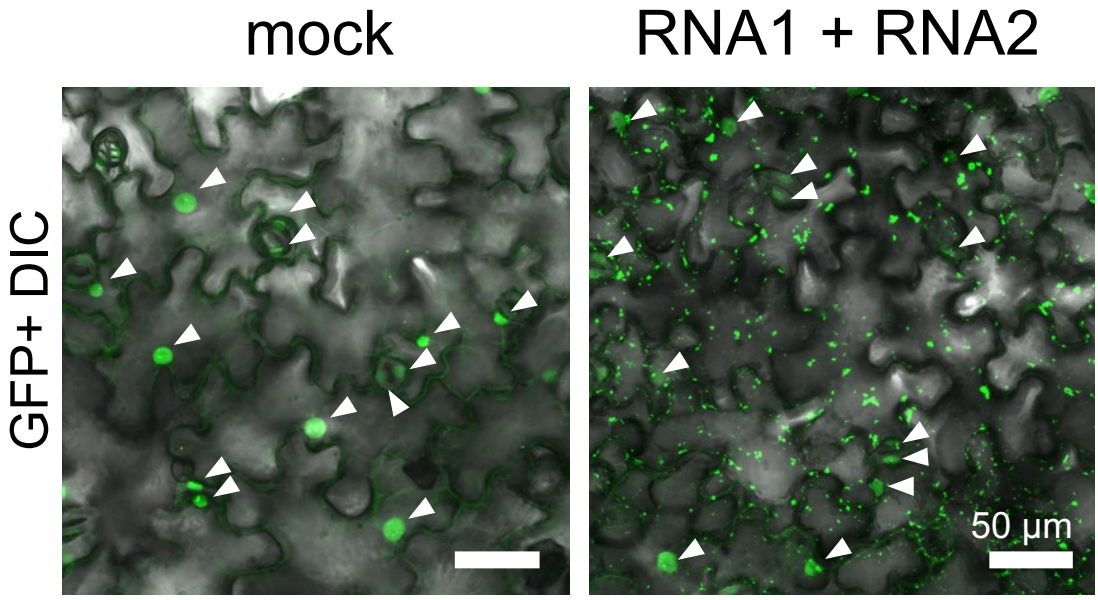

Figure I-2. Confocal imaging of dsRNA reporter *N. benthamiana* (B2-GFP plant). B2-GFP plants were inoculated with mock (DEPC-treated water; DDW) or *in vitro* transcripts of pUCR1 and pUCR2 (RNA1 and RNA2 of RCNMV). All images are confocal projections composed of about 10 consecutive optical sections taken at 1.5 μm intervals, which cover from the surface to the middle of epidermal cells. Observation of mock-infected leaves (left panel) and RCNMV-infected leaves (right panel) at 24 hours post inoculation (hpi). DIC, differential interference contrast. Arrowheads, nucleus. Scale bars = 50 μm.

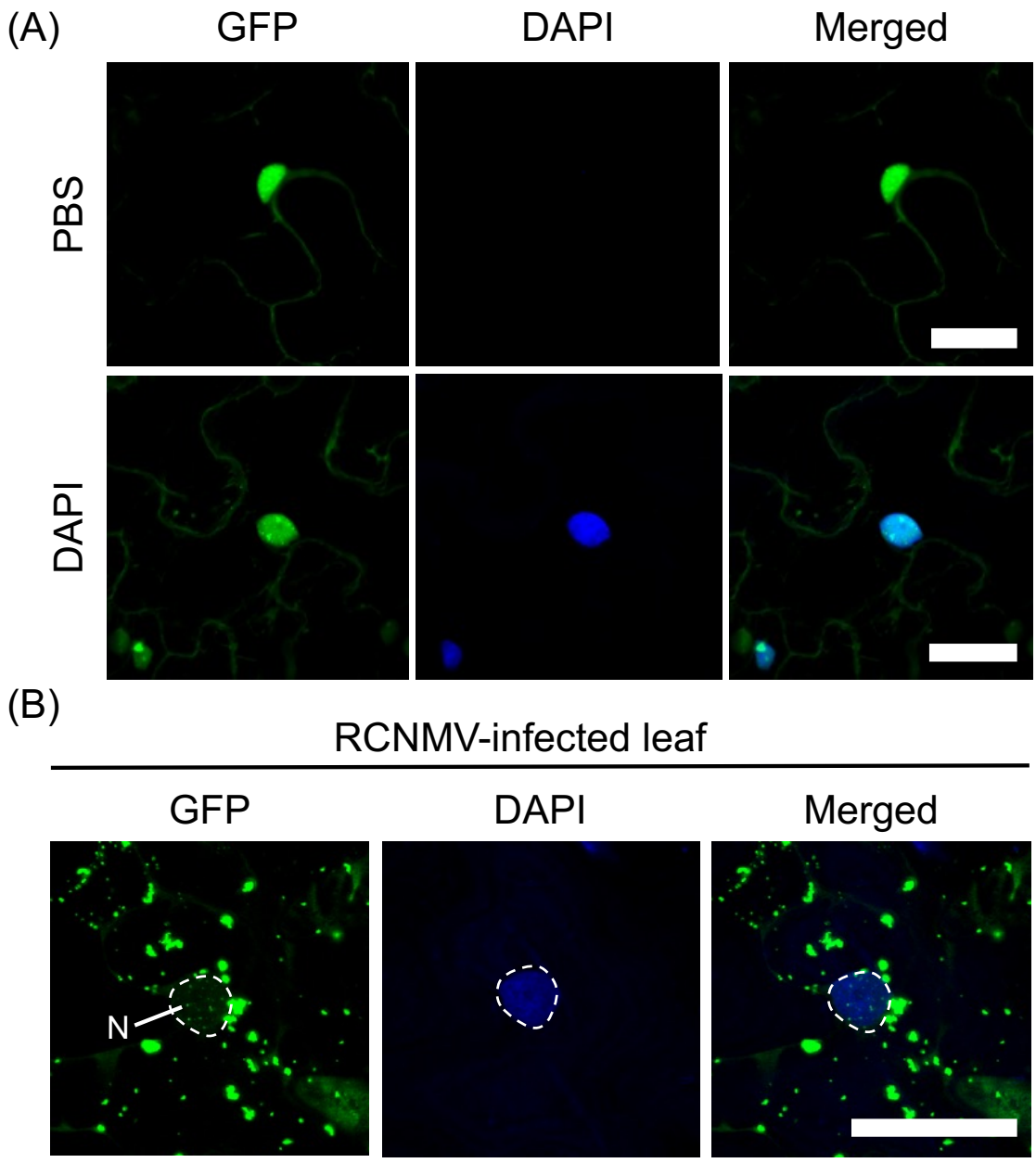

Figure I-3. The signals of DAPI-marked nucleus and dsRNA structures are clearly distinguishable. (A) 5-week-old B2-GFP plants were infiltrated with PBS buffer (upper panels) or DAPI solution (lower panels), and incubated for 20 min. Scale bars = 30 μm. (B) 5-week-old B2-GFP plants were inoculated with a mixture of RNA1 and RNA2, followed by infiltration 19 hours later with DAPI solution. N, nucleus (shown by dashed line). Scale bars = 30 μm.

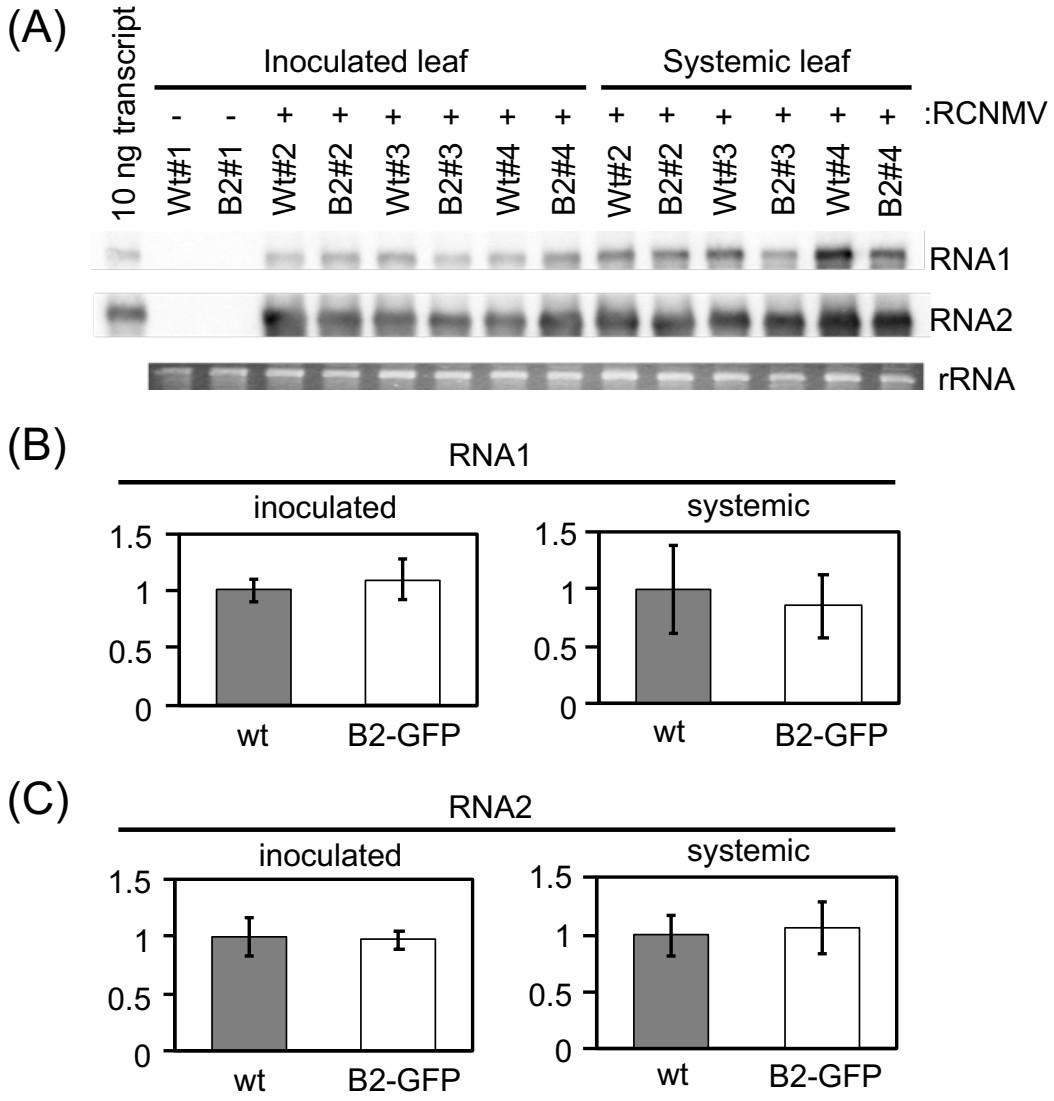

Figure I-4. The accumulation level of viral RNAs in wild type *N. banthamiana* or in B2-GFP plants. Four 4-week-old wild type *N. benthamiana* (Wt#1-Wt#4) and B2-GFP (B2#1-B2#4) were inoculated with a mixture of RNA1 and RNA2 (RCNMV+) or DDW as the negative control (RCNMV-), and incubated at 17 ℃. The total RNA was extracted from the inoculated leaves at 2 dpi or from the systemic leaves at 7 dpi. One microgram each of total RNA was subjected to Northern blotting using DIG-labeled riboprobes specific for the plus-strand RNA1 or RNA2 of RCNMV. Ethidium bromide-stained ribosomal RNA (rRNA) was used as loading control. (A) Images taken by using Lumiograph (ATTO). (B, C) Relative accumulation level of RNA1 (B) and RNA2 (C) in inoculated leaves or systemic leaves was calculated by Image J.

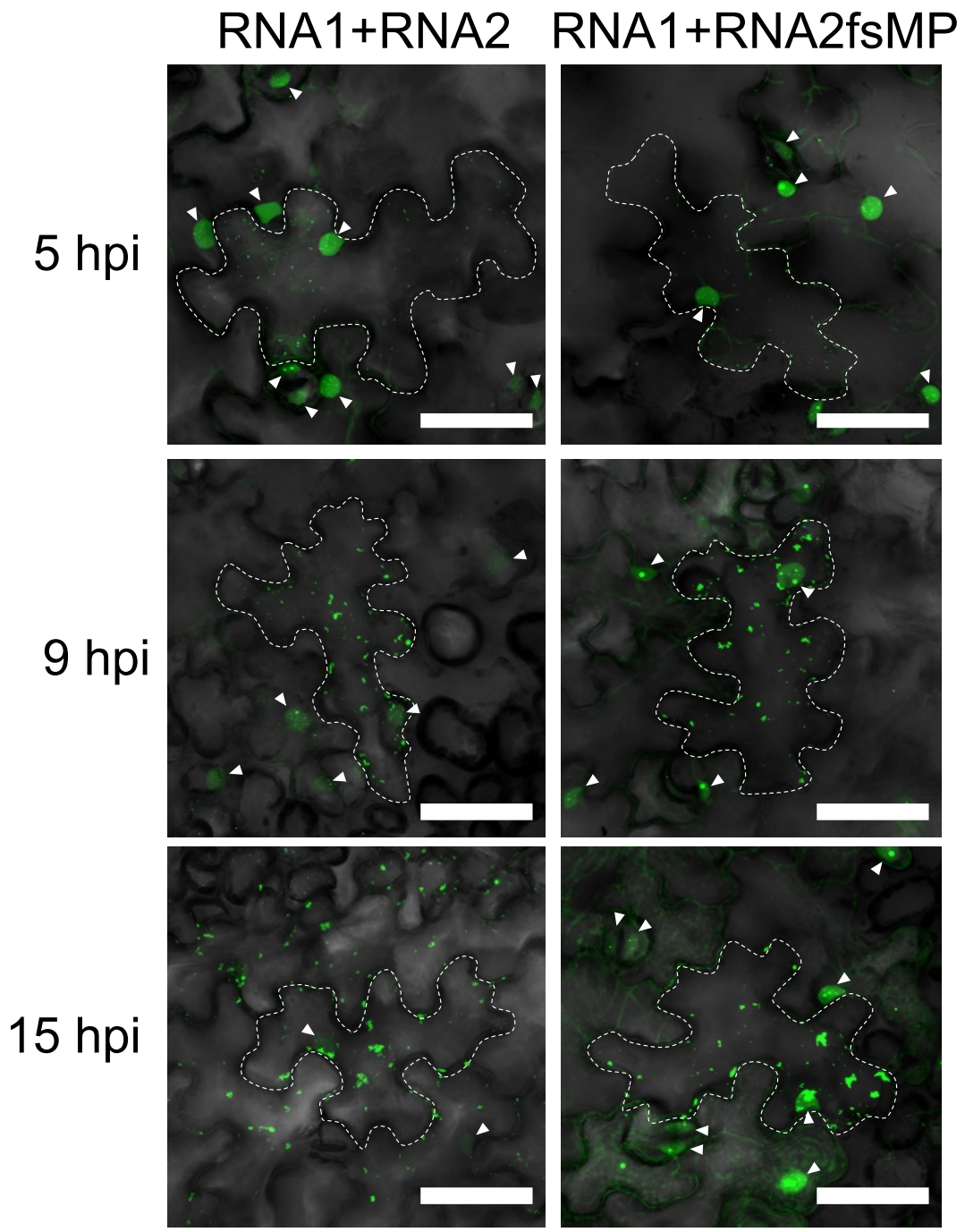

Figure I-5. Time course imaging of dsRNA structures. 5-week-old B2-GFP plants were inoculated with a mixture of RNA1 and RNA2 (left panels) or RNA1 and RNA2fsMP (right panels), and incubated at 17 ℃. Observation at 5 hpi (upper panels), 9 hpi (middle panels), 15 hpi (lower pannels). Arrowheads, nucleus. Scale bars = 50 μm.

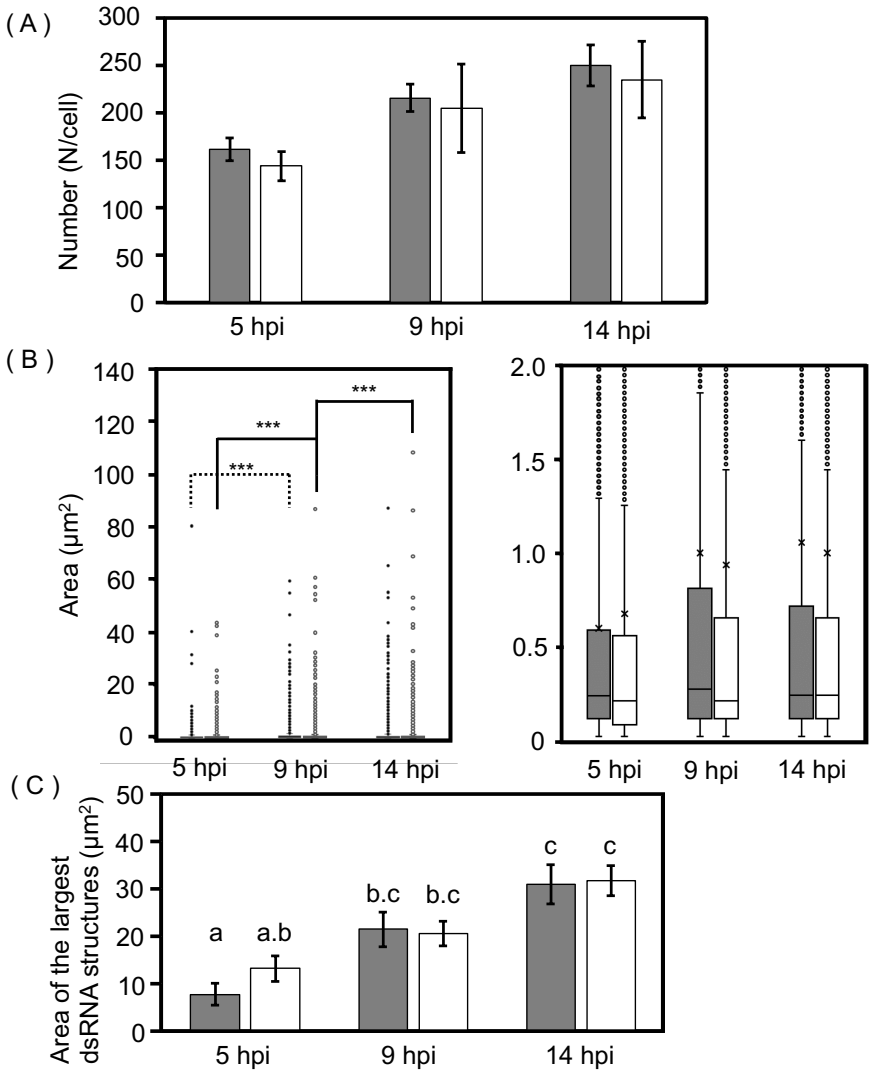

Figure I-6. Number and area of dsRNA structures. 4-week-old B2-GFP plants were inoculated with a mixture of RCNMV RNA1 and RNA2 (gray) or RNA1 and RNA2fsMP (white), and incubated at 17 °C. Confocal microscopy images were taken at 5 hpi, 9 hpi and 14 hpi. Ten images were subjected to image analysis at each time point. The number and size of dsRNA structures were calculated by Trainable Weka Segmentation (TWS), image J plug-in tool. Results were obtained from three independent experiments. (A) The mean number of dsRNA structures per cell. (B) The area of all dsRNA structures (left graph) and dsRNA structures less than 2 µm^2 (right graph) (Steel-Dwass test: ***, $P <$ 0.001). × in the right box plot shows the mean of the size. (C) The mean area of the largest structures in infected cells. Significantly different statistical groups indicated by two-way ANOVA with post-hoc Tukey‘s honest significance test were shown with different capital letters ($P < 0.05$).

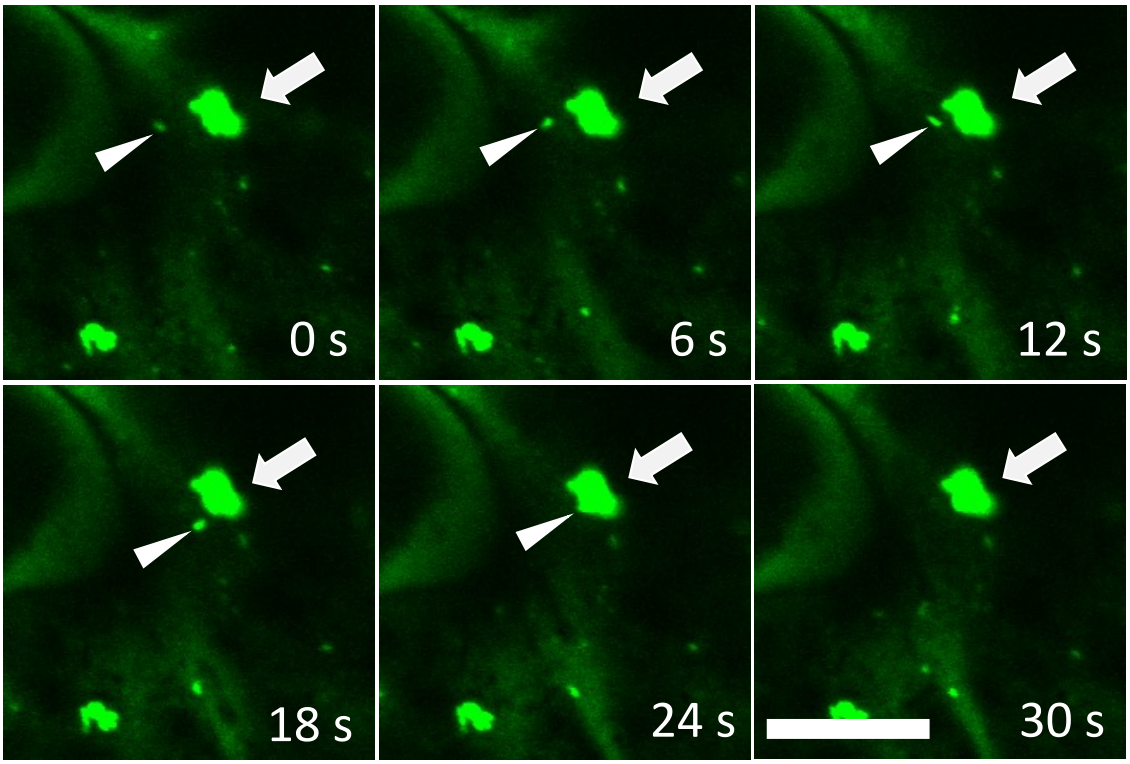

Figure I-7. Time lapse imaging showing dsRNA structures and fusion event. 4-week-old B2-GFP plants were inoculated with a mixture of RCNMV RNA1 and RNA2 and incubated at 17 ℃. Sequential images of the same focus were taken every 6 seconds at 5 hpi. A small dsRNA granule (arrowheads) moved and fused with bigger one (arrows). Scale bar = 10 μm.

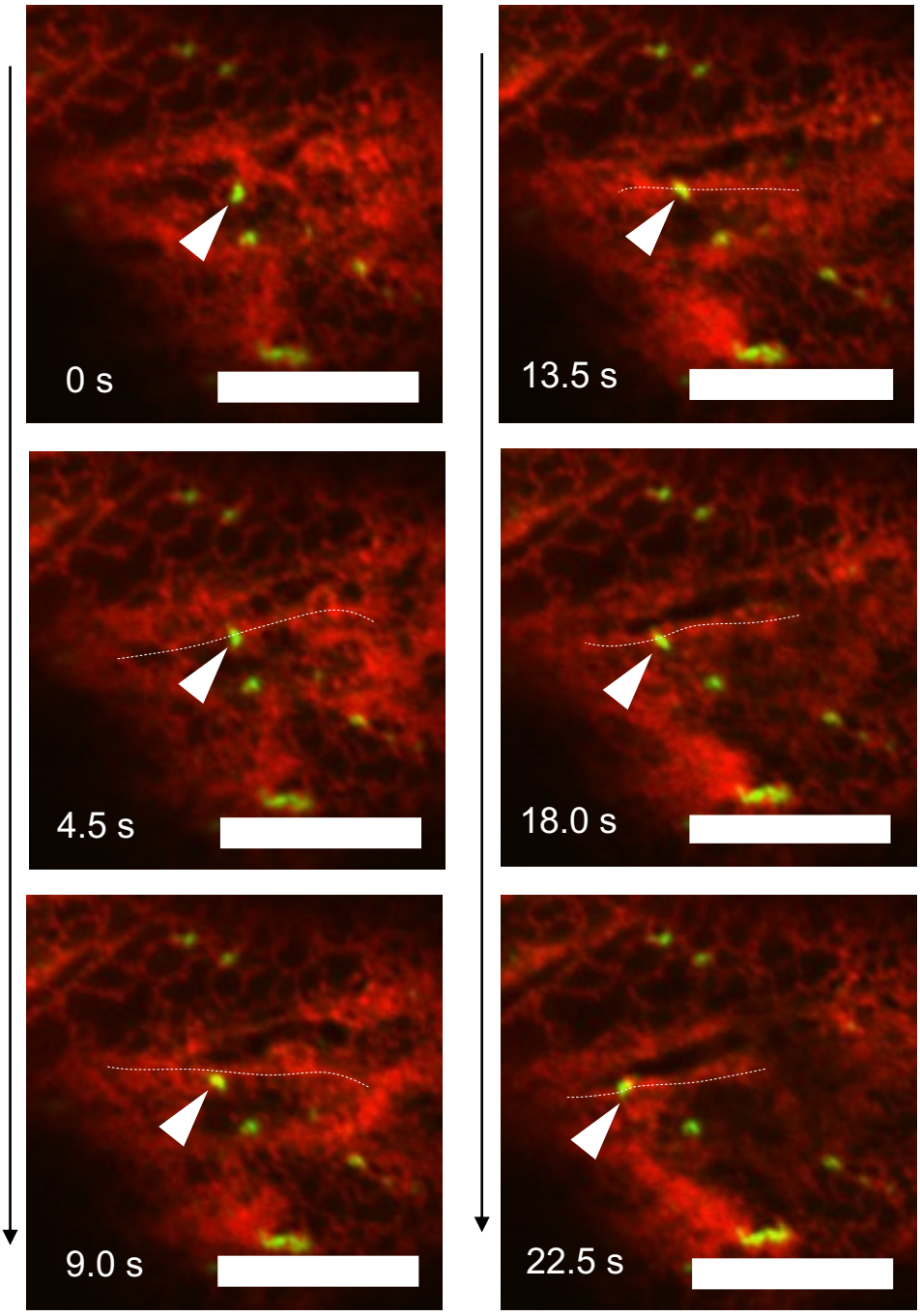

Figure I-8. dsRNA granules moved with the streaming of ER. Agrobacterium that contains pBICER-mSi (OD_{600} = 0.4) was infiltrated into 5-week-old B2-GFP plants and incubated at 22 ℃. 1 day later, plants ware mechanically inoculated with a mixture of RCNMV RNA1 and RNA2, and incubated at 17 ℃. Sequential images were taken every approximately 4.5 second at 19 h post inoculation. Small dsRNA granule (arrow head) moved along ER tubule (white dotted line). Scale bar = 10 μm.

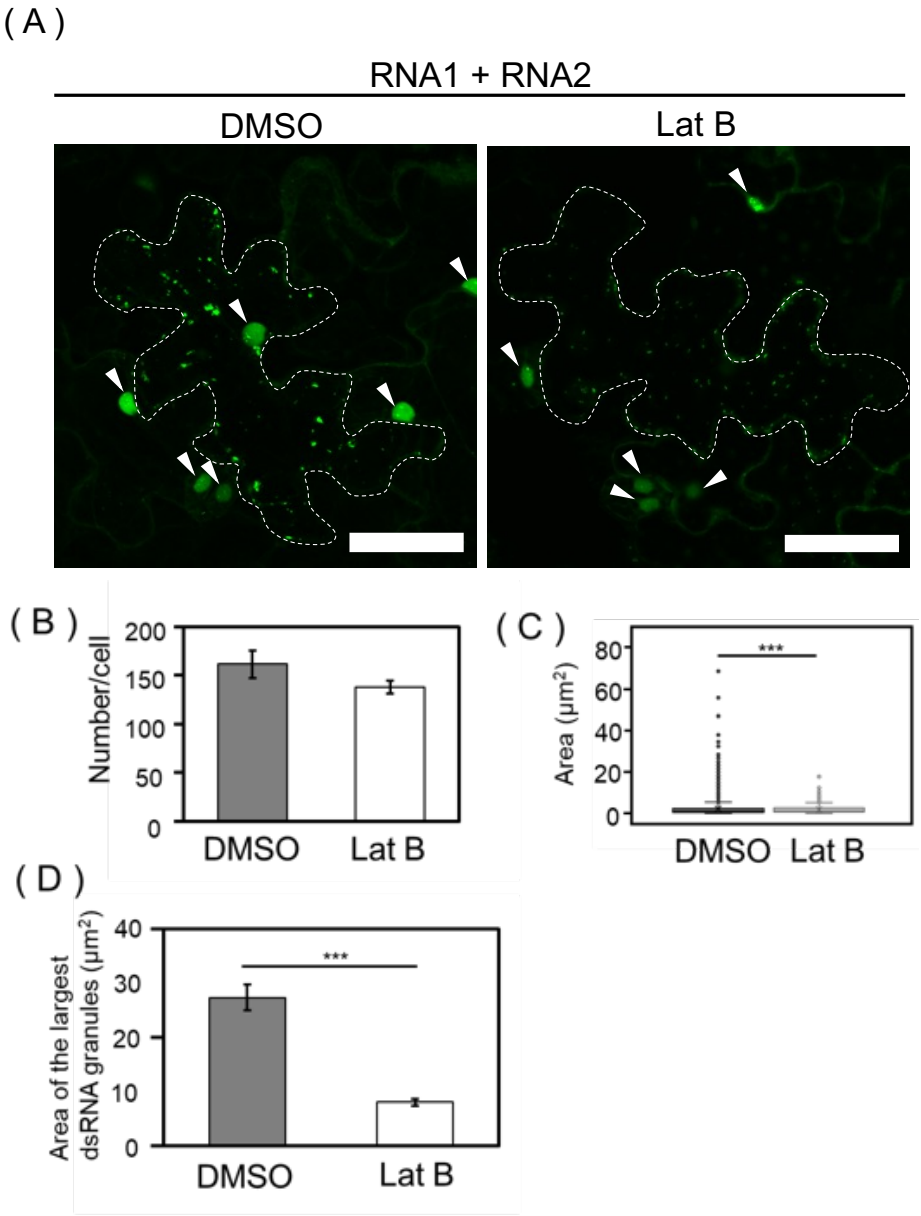

Figure I-9. Effect of Latrunculin B on subcellular localization of dsRNA structures. 5-week-old B2-GFP plants were infiltrated with DMSO solution (0.2 % DMSO/DW) or Latrunculin B (Lat B) solution (5 μM Lat B in 0.2 % DMSO/DW), followed by mechanical inoculation 6 hours later with a mixture of RCNMV RNA1 and RNA2. Ten images were subjected to image analysis using TWS. Results were obtained from three independent experiments. (A) Representative confocal microscopy images of inoculated leaves at 12 h post inoculation. Scale bars = 50 μm. Arrowheads, nucleus. (B) The mean number of dsRNA structures per cell. (C) The area of all dsRNA structures (Wilcoxon rank sum test: ***, $P < 0.001$). (D) The mean size of the largest dsRNA structures (Welch's t-test: ***, $P < 0.001$).

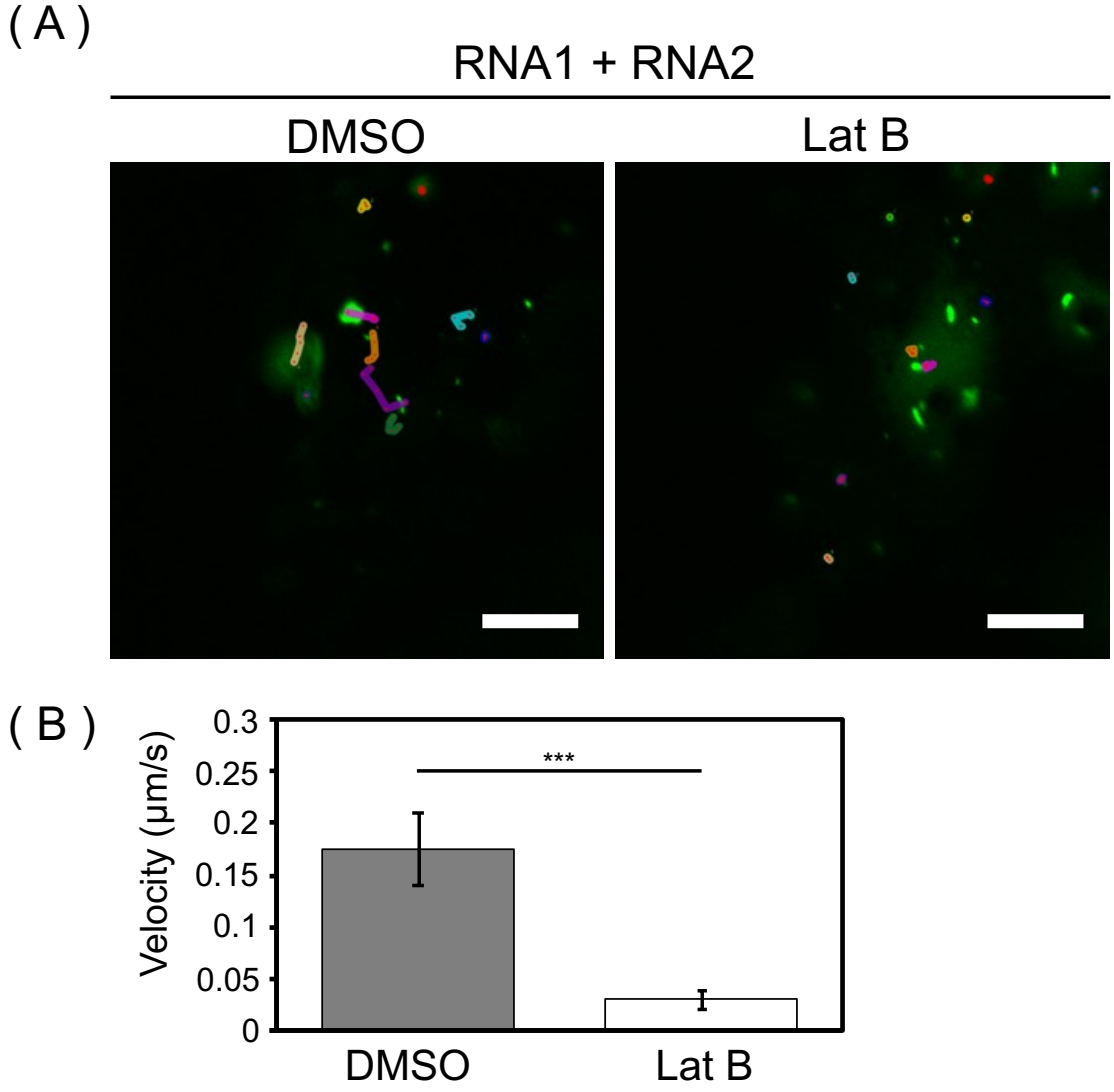

Figure I-10. Effect of Latrunculin B on intracellular movement of dsRNA structures. 5-week-old B2-GFP plants were infiltrated with DMSO solution (0.2 % DMSO/DW) or Latrunculin B (Lat B) solution (5 μM Lat B in 0.2 % DMSO/DW), followed by mechanical inoculation 6 hours later with a mixture of RNA1 and RNA2. (A) Sequential images were taken every 1.6 second for 8.0 s at 13 h post inoculation. Tracks, represented by different colors, of randomly selected 10 dsRNA structures were imaged by using Mtrack J, image J plug-in tool. Scale bars = 10 μm. (B) Sequential images were taken every 3.2 second for 16.0 s at 13 h post inoculation. 3 images of infected cells were taken at each treatment and subjected to image analysis. The average velocity of randomly selected 10 dsRNA structures per each image was calculated by using Mtrack J. Each bar represents the mean velocity of dsRNA structures from three independent experiments (Welch's t-test: ***, $P < 0.001$).

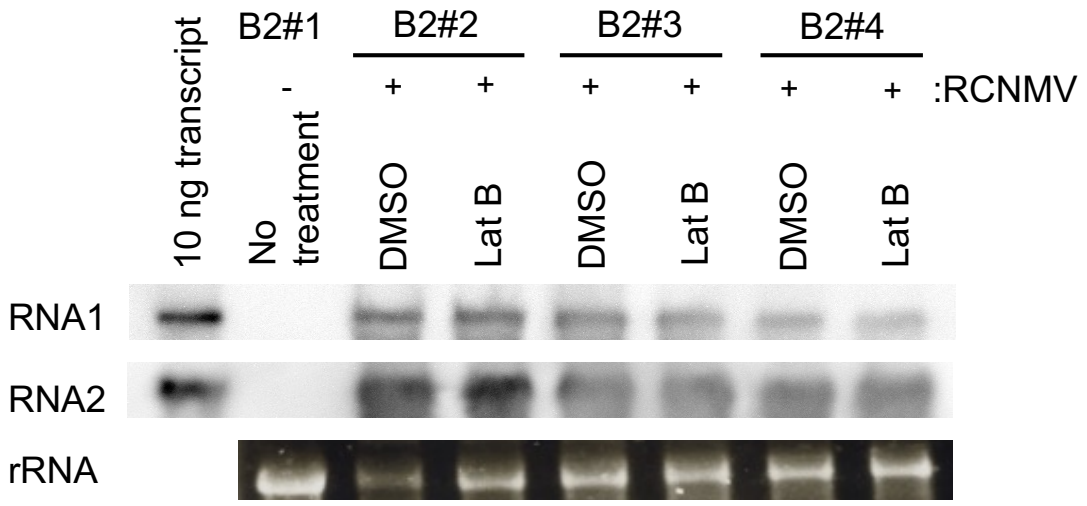

Figure I-11. The effect of Lat B on the accumulation of viral RNAs. Half leaves of 5-week-old B2-GFP plants were infiltrated with DMSO solution (0.2 % DMSO/DW, B2#2-B2#4) or Latrunculin B (Lat B) solution (5 μM Lat B in 0.2 % DMSO/DW, B2#2-B2#4), followed by mechanical inoculation 6 hours later with a mixture of RCNMV RNA1 and RNA2 (RCNMV+). Untreated B2-GFP inoculated with DDW (B2#1) was used as a negative control (RCNMV-). The total RNA was extracted from the inoculated leaves. Each 1 μg total RNA was subjected to Northern blotting using DIG-labeled riboprobes specific for the plus-strand (+) RNA1 or RNA2 of RCNMV. rRNA is an ethidium bromide-stained agarose gel image of total RNA as the loading control. Images taken by using LumioGraph (ATTO).

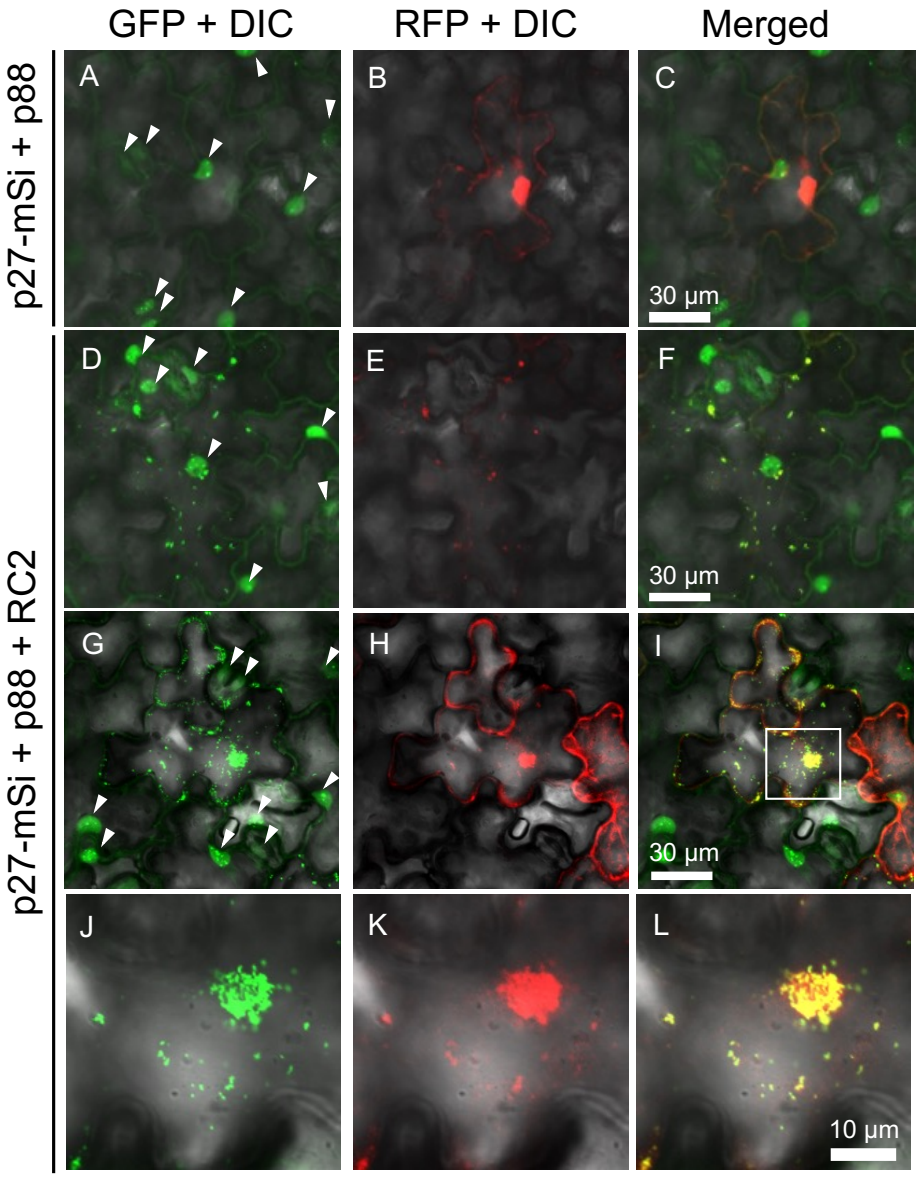

Figure I-12. Subcellular localization of p27-mSi and dsRNA structures. Representative confocal images of p27-mSi and B2-GFP localization in epidermal cells at 2 days post infiltration. An *Agrobacterium* that contains pBICp27-mSi (OD_{600} = 0.1) and pBICp88 (OD_{600} = 0.27) together with or without pBICRC2 (OD_{600} = 0.27), which expresses RNA2, were infiltrated into 5-week-old B2-GFP plants. (A-L) Images of leaves infiltrated with p27-mSi and p88 (A-C) or p27-mSi, p88 and RC2 (D-L). (D-I) Images at low magnification. (J-L) Images of the area surrounded by white line in image (I) at high magnification. In each raw, the right and middle images were taken under GFP and RFP channels for B2-GFP and p27-mSi signals, respectively. The right panels represent merged images of the left and middle images in the same raw. DIC, differential interference contrast. Arrowheads, nucleus.

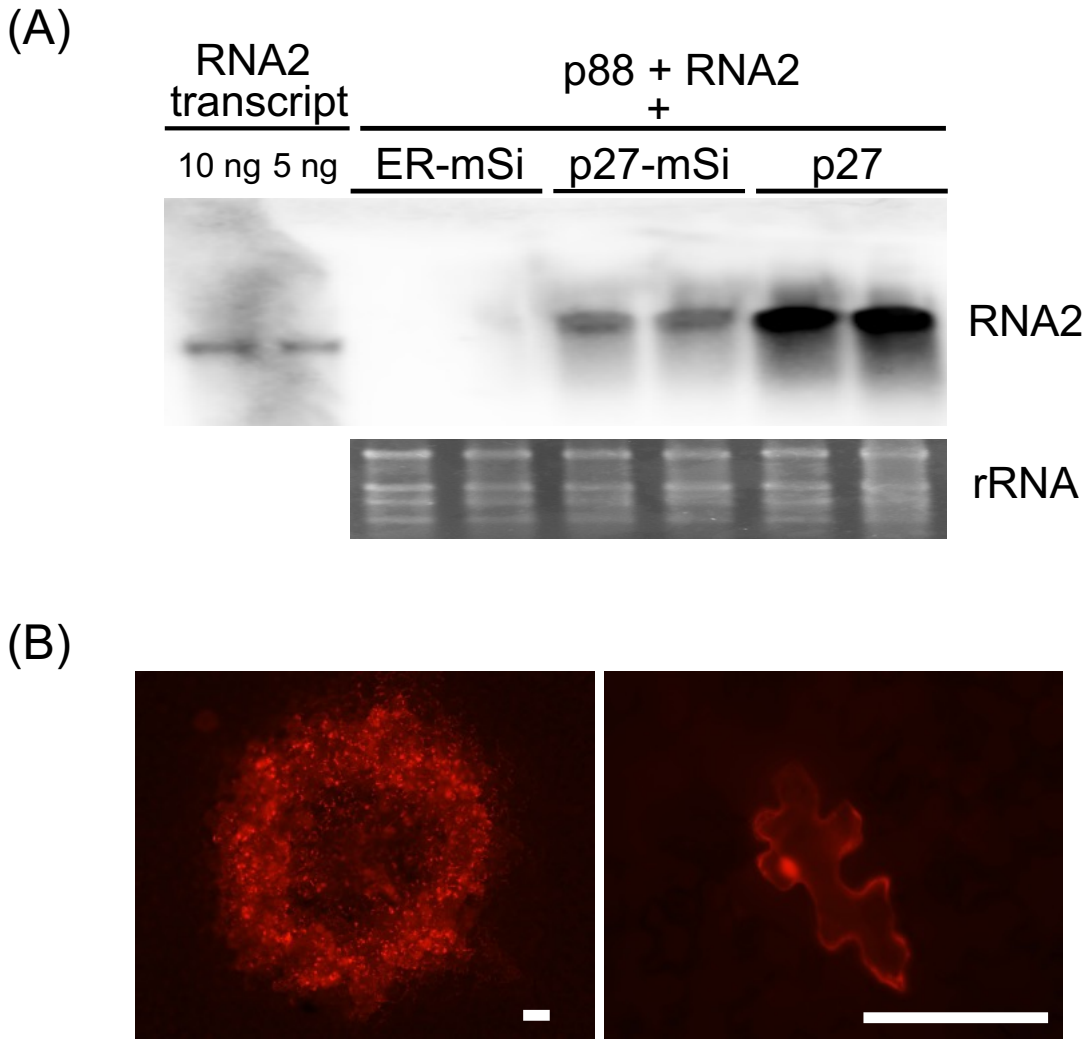

Figure I-13. RCNMV p27 and MP tagged with mScarlet-i are functional. (A) 5-week-old two B2-GFP plants were infiltrated with a mixture of *Agrobacterium* that express p27-mSi, or p27 (positive control), or mScarlet-i tagged with ER localizing signal (ER-mSi, negative control) together with those expressing p88 and RNA2, respectively. The total RNA was extracted from the infiltrated leaves at 48 hpi. Each 1 µg total RNA was subjected to Northern blotting using DIG-labeled riboprobes specific for the plus-strand (+) RNA2 of RCNMV. rRNA is an ethidium bromide-stained agarose gel image of total RNA (1 µg each) as the loading control. Images taken by using ImageQuant 800 (Amersham). (B) Fluorescent microscopy images of 5-week-old B2-GFP leaves mechanically inoculated with *in vitro* transcripts of RNA1-MmSi + RNA2fsMP (left panel) or RNA1-mSi + RNA2fsMP (right panel) at 42 hpi. Images were taken under RFP channel. Scale bars = 100 µm.

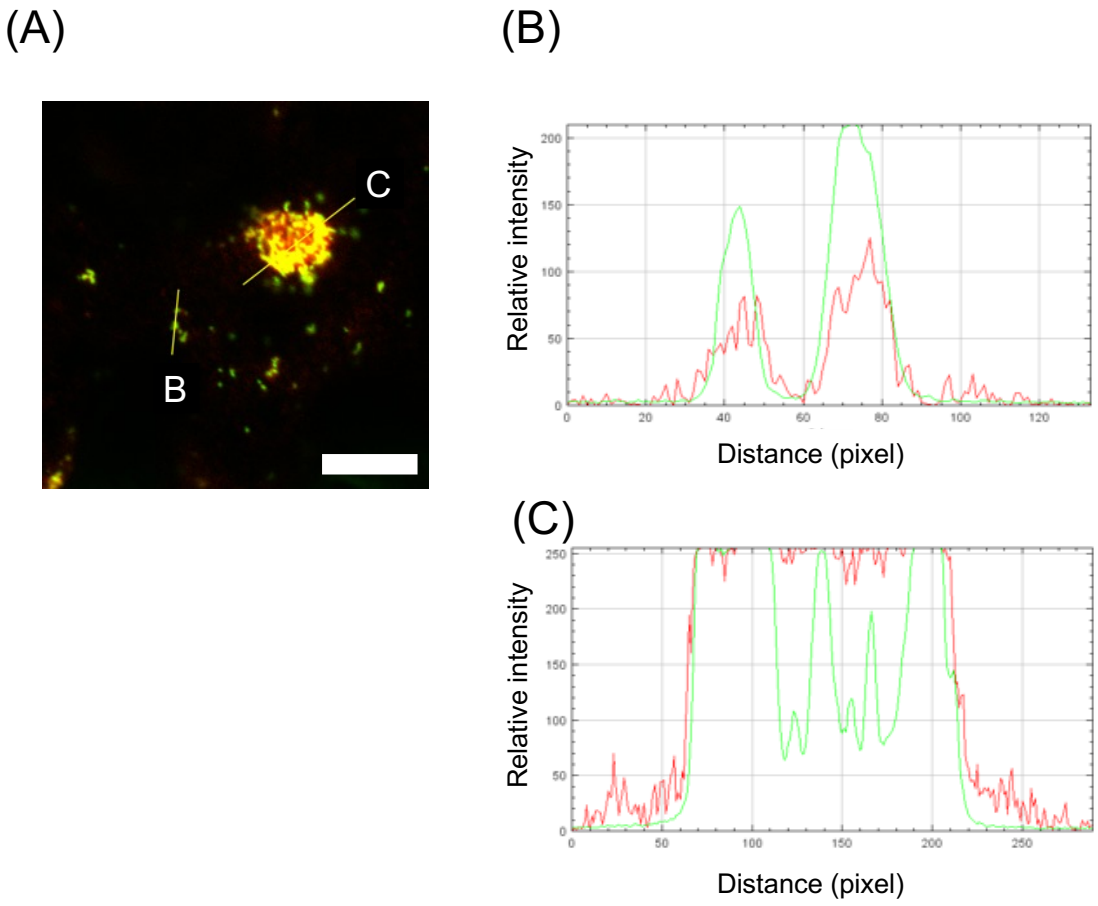

Figure I-14. Relative intensity of B2-GFP and p27-mSi. (A) Same image as Figure 12L without DIC channel. Small granules (line B) and a large aggregate (line C) were analyzed by RGB profiles. Scale bar = 10 μm. (B) RGB profile of small granules. (C) RGB profile of a large aggregate. Green and red represent dsRNA and p27, respectively.

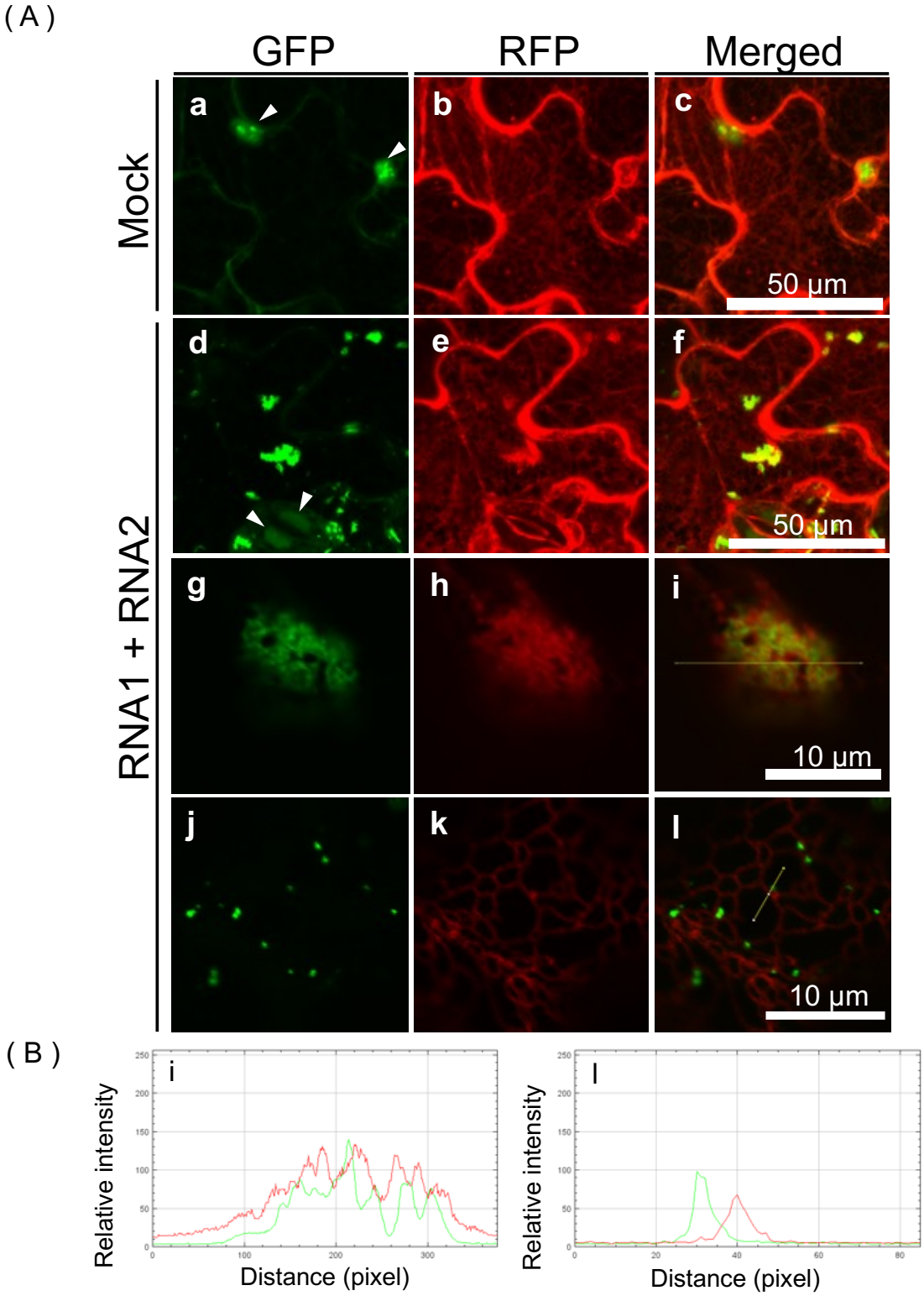
(A)
GFP
RFP
Merged
Mock
RNA1 + RNA2
a
b
c
d
e
f
g
h
i
j
k
l
50 μm
50 μm
10 μm
10 μm
(B)
i
l
Relative intensity
Distance (pixel)
Relative intensity
Distance (pixel)

Figure I-15. Subcellular localization of ER-mSi and dsRNA structures. (A) An *Agrobacterium* that contains pBICER-mSi (OD_{600} = 0.4) was infiltrated into 5-week-old B2-GFP plants and incubated at 22 ℃. 1 day later, plants ware mechanically inoculated with mock (a-c) or a mixture of RCNMV RNA1 and RNA2 (d-l), and incubated at 17 ℃ for approximately 1 day. Observation of dsRNA structures at low magnification (d-f). Observation of a larger aggregation (g-i) and tiny dsRNA granules (j-l) under high magnification. For others, refer to the legend for Figure I-12. (B) RGB profiles of lines in image (i) and image (l). Arrowheads, nucleus.

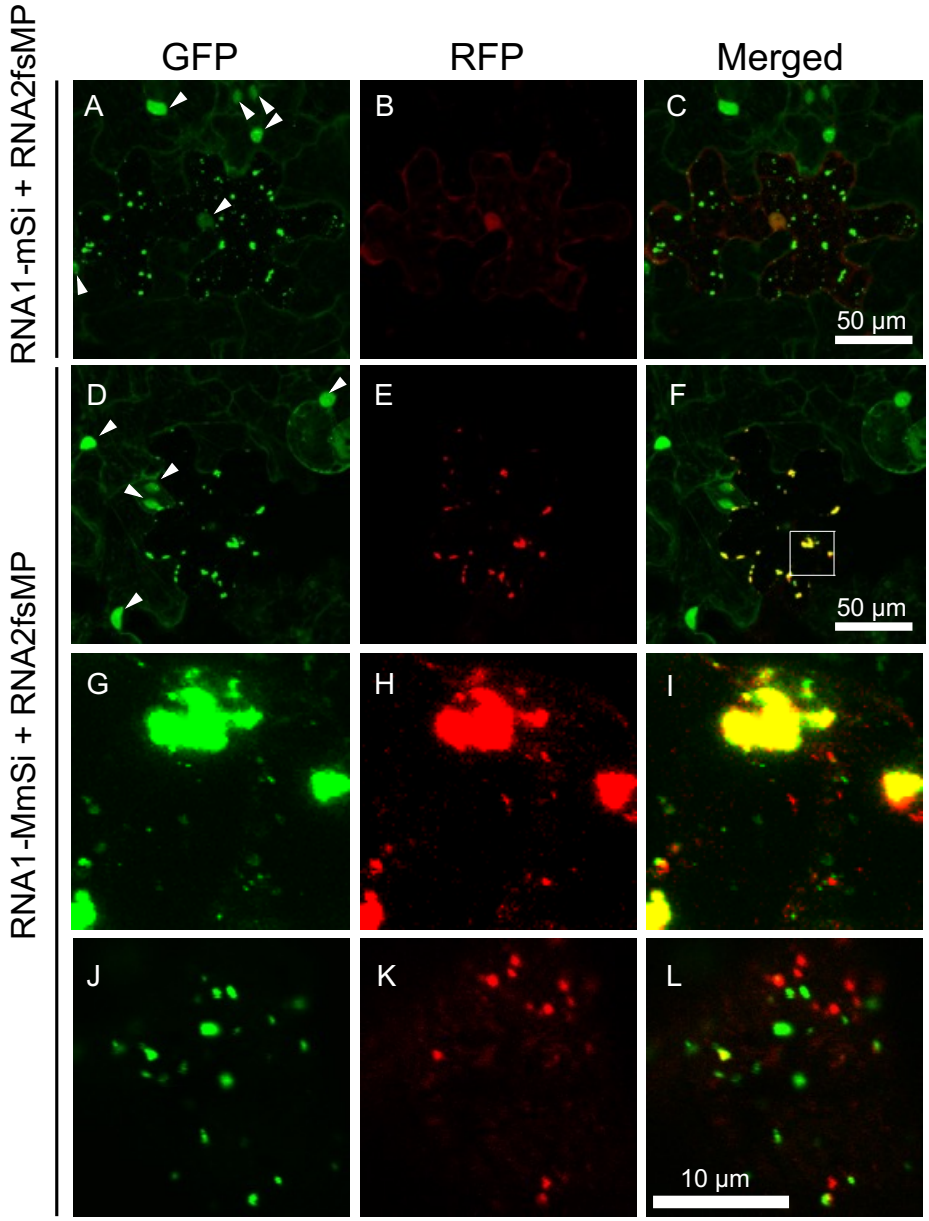

Figure I-16. Subcellular localization of mSi, MP-mSi and dsRNA structures. 4-week-old B2-GFP plants were mechanically inoculated with a mixture of RNA1-mSi and RNA2fsMP or RNA1-MmSi and RNA2fsMP, and incubated at 17 °C for 16 hours. All images are confocal projections composed of about 10 optical sections taken at 1.5 µm intervals, which range from the surface to the middle of epidermal cells. Each panel represents images of leaves inoculated with RNA1-mSi and RNA2fsMP (A-C) and RNA1-MmSi and RNA2fsMP (D-L). (D-F) Observation at low (60x) magnification. (G-I) Enlarged images of the area surrounded by white line in image (F) (0.3 % contrast-enhanced images). (J-L) Observation at high (300x) magnification. Arrowheads, nucleus. For others, refer to the legend for Figure I-12.

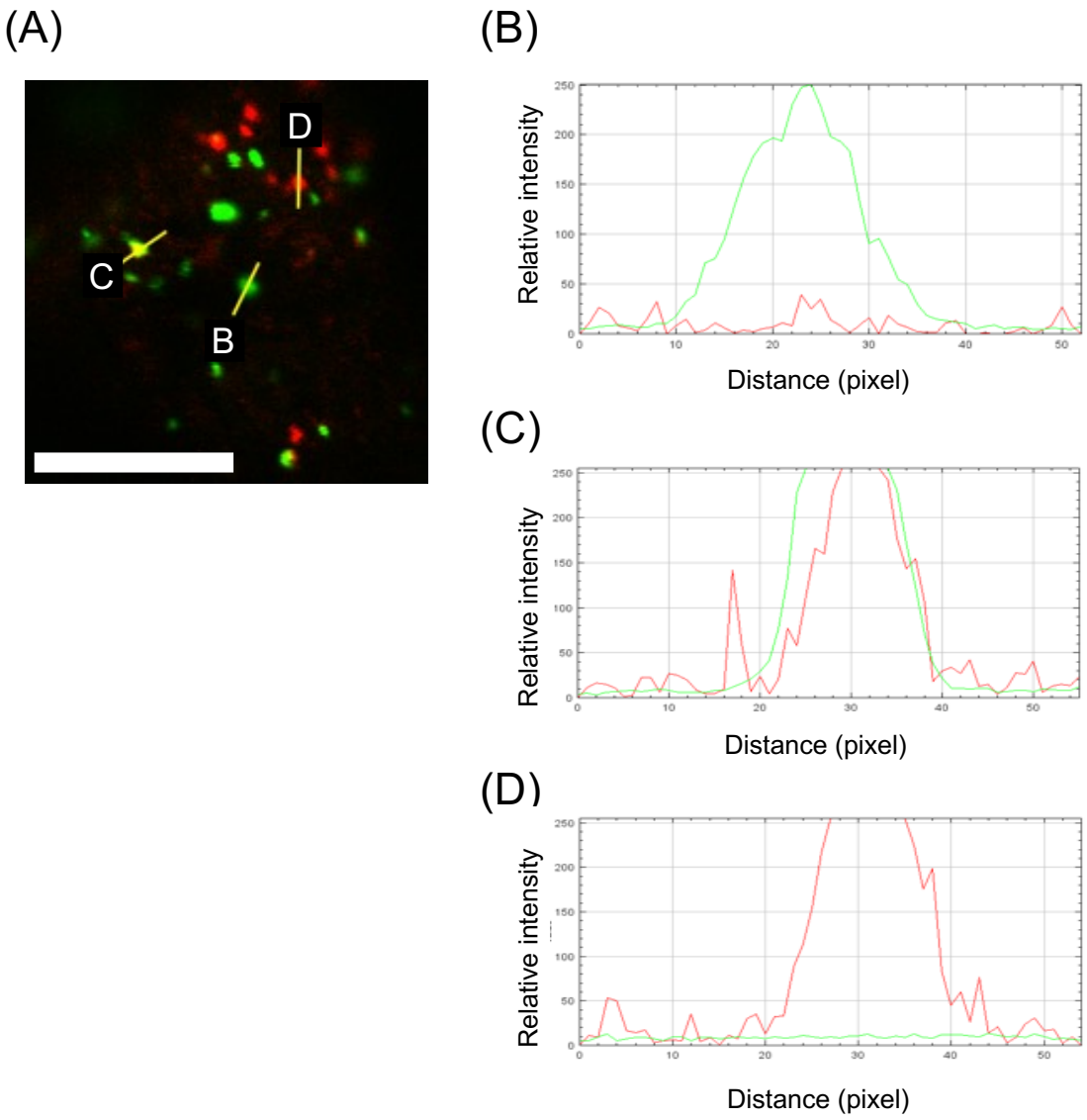

Figure I-17. Relative intensity of B2-GFP and MP-mSi. (A) Same image as Figure I-16L. Three small granules in green (line B), yellow (line C) and red (line D) were analyzed by RGB profiles. Scale bar = 10 μm. (B) RGB profile of a green granule. (C) RGB profile of a yellow granule. (D) RGB profile of a red granule. Green and red represent dsRNA and MP, respectively.

CHAPTER II

Unveiling crucial amino acids in red clover necrotic mosaic movement protein for optimal subcellular localization and viral cell-to-cell movement

INTRODUCTION

Positive-strand RNA viruses replicate their genome within specialized viral replication complexes (VRCs). These VRCs are formed through the remodeling of the host's endomembrane system (den Boon and Ahlquist, 2010; Miller and Krijnse-Locker, 2008; Nagy and Feng, 2021). Following replication, the movement protein (MP) facilitates the transport of viral RNA to adjacent cells via plasmodesmata (PD) (Niehl and Heinlein, 2011). PD are tubular structures that connect neighboring cells, participating in the symplastic transport of small molecules between plant cells (Faulkner, 2018). PD possess a size exclusion limit (SEL), indicating that substances with high molecular weight, such as MP-nucleic acid complexes, cannot freely pass through them (Tucker *et al.*, 1982; Wolf *et al*., 1989; Oparka *et al*., 1999). MPs localize to the PD and expand the SEL, thereby allowing passage of viral RNA complexes or viral particles (Lee and Lu, 2011; Lucas, 2006; Lucas *et al*., 2009; Waigmann *et al*., 2004). The significance of PD localization in viral intercellular movement is emphasized by the observation that specific MP mutants, lacking the ability to localize to PD, lose their capacity for cell-to-cell movement (Berna *et al*., 1991; Sasaki *et al*., 2006). Peptide sequences of MP exhibit a high degree of diversity, with various plant virus species encoding different numbers of MPs and employing distinct strategies for cell-to-cell movement (Scholthof, 2005; Niehl and Heinlein, 2011). Consequently, a comprehensive understanding of viral cell-to-cell movement mechanisms requires the investigation of individual viruses' intercellular

trafficking to elucidate their unique characteristics.

In various transport system inhibitor studies, several MPs are transported to PD through a COP II transport-dependent mechanism or the ER-actin network (Niehl and Heinlein, 2011; Sun *et al*., 2013; Wei *et al*., 2010; Wright *et al*., 2007; Yuan *et al*., 2011). Some viral MPs have been hypothesized to reach PD via endocytosis after their transport to the plasma membrane, while others have been implicated in microtubule-mediated transport to PD (Shemyakina *et al*., 2011; Carluccio *et al*., 2014). Investigations into the MP domains and specific amino acids crucial for PD localization have also been undertaken. TGB3, one of MP from potato mop-top pomovirus (PMTV), requires a transmembrane domain and a membrane-anchored tyrosine-based motif for PD localization (Tilsner *et al*., 2010). In the case of cucumber mosaic virus (CMV) MP, a cysteine-histidine-rich region involved in Zinc binding is required for the PD localization (Sasaki *et al*., 2006). Furthermore, phosphorylation of the N-terminal residues S71 and S79, as well as the C-terminus, plays a pivotal role in targeting the MP of potato leaf roll virus (PLRV) to PD (Link *et al*., 2011). Consequently, knowledge of PD targeting is expanding, although numerous details remain obscure, including the host factors involved in transport of MP and the mechanism by which these host factors recognize MPs.

The analysis of subcellular viral protein localization using electron and fluorescence microscopy has revealed that MPs of several plant viruses colocalize with the components essential for viral replication (Heinlein *et al*., 1998; Dohi *et al*., 2001; Bamunusinghe *et al*. 2009; Kaido *et al*. 2009). This observation indicates that MPs specifically accumulate in the VRCs, which serve as the sites for viral replication. In the case of tobacco mosaic virus (TMV), MP colocalizes with VRCs and is subsequently delivered to neighboring cells in the form of a complex consisting of MP, vRNA and replication enzyme.

(Christensen *et al*., 2009; Hirashima and Watanabe, 2003; Kawakami *et al*., 2004). The γb protein encoded by barley stripe mosaic virus (BSMV) is involved in recruiting the movement proteins TGB2 and TGB3 to chloroplasts, the site for virus replication. This recruitment process is essential for enabling efficient cell-to-cell movement of BSMV (Jiang *et al*., 2020). Thus, the localization of MPs to VRCs is considered important event for effective cell-to-cell movement (Heinlein, 2015), but the mechanism of its localization is not well understood.

Red clover necrotic mosaic virus (RCNMV) is a positive-strand RNA virus with two RNA segments. The MP encoded by RNA2 belongs to the 30K superfamily and is essential for viral cell-to-cell movement and systemic infection. Although some viruses require coat protein (CP) for intracellular movement, RCNMV does not require CP (Niehl and Heinlein, 2011; Xiong *et al*., 1993). The RCNMV MP has ability to bind to single-stranded nucleic acids (Giesman-Cookmeyer and Lommel, 1993; Fujiwara *et al*., 1993). When MP is microinjected alone into cowpea leaves, it can increase the SEL of PD and transport co-injected viral RNA (vRNA) to adjacent cells (Fujiwara *et al*., 1993). Analysis of MP using alanine scanning mutants revealed that amino acids 27-31, 122-123, 128-129, 144-145, 161-163, 204-205, 242-243, 280-281, 291-292, 305-306 are involved in RNA binding. Additionally, amino acids 122-123, 128-129, and 161-163 are implicated in pericellular localization and are required for viral cell-to-cell movement (Fujiwara *et al*., 1993; Tremblay *et al*., 2005).

The subcellular localization of RCNMV MP, combined with sGFP fusion proteins, has been documented in several studies. When expressed from recombinant viruses, MP:sGFP localizes to the PD during the early stages of infection, eventually forming aggregated structures (Kaido *et al*., 2009). These aggregates colocalize with the

components of VRCs, including the endoplasmic reticulum (ER) membrane, p27 protein and double-stranded RNA (Kaido *et al*., 2009, 2011, 2014). Notably, MP:sGFP transiently expressed via *Agrobacterium* localizes exclusively to the PD, indicating that other viral factors are not required for MP transport to PD (Kaido *et al*., 2009). Furthermore, under RNA1 replication conditions, transiently expressed MP:sGFP is observed at the cortical VRCs along the ER, but this is not the case under RNA2 replication (Kaido *et al*., 2009). The C-terminal 70 amino acids of MP are important for the localization to VRCs (Kaido *et al*., 2011), and the host protein NbGAPDH-A acts as a bridge between MP and VRCs (Kaido *et al*., 2014). These results suggest that MP is recruited to the surface ER by viral replication complexes containing RNA1 through the C-terminal 70 amino acid sequence. MP may capture newly synthesized RNA1 through such a recruitment mechanism, efficiently transferring RNA1 to adjacent cells. These findings underscore the importance of proper localization of RCNMV MP to PD and VRCs for efficient cell-to-cell movement. However, the detailed transport mechanisms and crucial host factors for this localization remain elusive.

In this study, I explored the intracellular transport pathways and analyzed the functional domains of RCNMV MP involved in subcellular localization to elucidate the intracellular transport mechanisms of RCNMV MP. Concerning the intracellular transport pathway of RCNMV MP, I investigated the cytoskeleton and the ER-Golgi membrane transport system, which may be involved in the transport of MP and RNA-MP complexes. The results suggest that these cytoskeletal and membrane transport systems are not involved in the transport of RCNMV MP to PD. For functional domain analysis, I focused on the α-helix structure, which is the fundamental structure of the protein. Five α-helix structures within RCNMV MP were predicted by protein secondary structure prediction

software. Analysis of mutants deficient in the predicted α-helix and alanine-substituted mutants of the constitutive amino acids identified the specific amino acids required for proper localization to the PD and VRCs.

MATERIALS AND METHODS

Plasmid construction

Plasmids given the prefix “pBIC” were used for agroinfiltration, and those labeled “pUC” were used for *in vitro* transcription. The ligation mix (Takara Bio, Shiga, Japan) or the NEBBuilder HiFi DNA assembly (New England BioLabs, Ipswich, USA) was used to introduce insert fragments into vector plasmids. Details of the plasmids and primers utilized in this research are listed in Table II-3 and 4, respectively.

For the construction of the vectors intended for *in vitro* transcription, the MP coding region was amplified by PCR using pUCR1-MsG (Kaido *et al*., 2009) as template. Subsequently, the PCR products were then introduced into the XhoI/ClaI site of pUCR1-MsG, resulting in mutants of pUCR1-MsG.

Similarly, for the construction of vectors intended for assessing PD localization, the MP coding region was amplified by PCR using pUCR1-MsG (Kaido *et al*., 2009) as template. The PCR products were then inserted into the BamHI/ClaI site of pBICRMsG (Kaido *et al*., 2009), resulting in mutants of pBICRMsG.

To construct the vectors for expression of mutant MP in *Echerichia coli* (*E. coli*), the coding region of MP with an α-helix deletion was amplified by PCR using pUCR1Mdhel(1 to 5)sG (Kawano, 2016, master’s thesis) as template. The PCR products were introduced into the NheI/BamHI site of pRAMPd70-15b (Kaido *et al*., 2011) via ligation, resulting in mutants of pRAMP-15b.

Plant growth conditions

N. benthamiana were cultivated in commercial soil (Sumirin-Ryokka, Tokyo, Japan) under controlled conditions at 25 ± 2℃ with a photoperiod of 16 hours of illumination

per day. Plants aged between 4 to 5 weeks were used for viral RNA inoculation, while those at 5 to 6 weeks of age were utilized for agroinfiltration or inhibitor treatment.

Inoculation of plants with viral RNA

RCNMV RNA was synthesized *in vitro* from plasmids bearing the prefix 'pUC' as described by Mizumoto *et al*. (2003) with minor modifications. Plasmids digested by FastDigest SmaI (Thermo fisher scientific, Waltham, U. S. A.) or BamHI (Takara Bio, Shiga, Japan) were transcribed using T7 RNA polymerase (Takara Bio). Following incubation for two hours, samples were treated with DNase (Qiagen, Tokyo, Japan). The enzyme was then inactivated with Phenol/Chloroform/Isoamyl alcohol (FUJIFILM Wako Pure Chemical, Osaka, Japan), and samples were centrifuged. The supernatant was purified with a Sephadex G-50 fine column (GE Healthcare, Chicago, U. S. A.). After ethanol precipitation, ultrapure water (Thermo fisher scientific) was added to samples to adjust the final concentration of RNA to 1.0 μg/μl. Four-week-old *N. benthamiana* was rub-inoculated with a mixture of *in vitro*-transcribed RCNMV RNA, and then incubated at 17 ℃ under long-day conditions with 16 hours illumination per day.

Microscopy

Proteins labeled with fluorescent proteins were visualized for their subcellular localization using an Olympus FluoView FV1200 confocal laser scanning microscope (CLSM). Imaging was performed with either a 40× Plan Apo objective lens (numerical aperture 0.95) or a 60× Plan Apo (numerical aperture 1.35) oil immersion objective lens (Olympus, Tokyo, Japan). Excitation dichroic mirrors DM405/473/559, beam splitter SDM560 for GFP and mirror for RFP were employed, along with variable barrier filters

(VBF) set to 485 nm to 545 nm for GFP and 570 nm to 670 nm for RFP to capture the fluorescent signals. In experiments involving the visualization of dual fluorescence, images were acquired in a sequential mode to minimize fluorescent signal leakage. The images were stacks consisting of optical sections captured at 2 μm intervals or single section taken at a cortical region of a plant cell. All images were processed using Image J/Fiji (2.3.0/ver. 1.53q) (https://imagej.net/software/fiji/) (Schindelin *et al*., 2012).

For quantifying fluorescent foci that comprised multiple cells, a BX53 fluorescence microscope (Olympus) equipped with a DP72 camera was employed. Cell sense software (Olympus) was utilized for image observation.

Electrophoretic mobility shift assay (EMSA)

The expression of RCNMV MP and α-helix-deleted mutant was carried out in the BL21(DE3) strain of *E. coli* using the pET-15b vector (Novagen). The purification of MP followed the protocol outlined by Kaido *et al.* (2011). After MP purification, gel shift assay was performed using the LightShift™ Chemiluminescent RNA EMSA Kit (Thermo fisher scientific, Waltham, U. S. A.). The RNA used in these assays was transcribed from BamHI-digested pUCR2-200/5' (Kaido *et al.,* 2011) and subsequently end-labelled with biotin at the 3'-terminus.

Western blot analysis

SDS polyacrylamide gel electrophoresis of protein samples, transfer to PVDF membrane (Immobilion-P, Millipore), and blocking were performed according to Tatsuta *et al*. (2005). A GFP antibody B-2 (Santa cruz biotechnology, Dallas, U. S. A.) was used for the first antibody, and an HRP-conjugated anti-mouse IgG antibody (Funakoshi,

Tokyo, Japan) was used for the secondary antibody. The luminescence signal was detected using ChemiDoC™ XRS+ with Image Lab™ Software (Bio-rad, Hercules, U. S. A.).

Inhibitor treatment of plants

Inhibitor studies were conducted following the protocol described by Sun *et al*. (2013) and Yuan *et al.* (2011) with minor modification. 10 μM or 100 μM Latrunculin B (Lat B; abcam, Cambridge, U. K.) in 0.4% or 4% dimethyl sulfoxide (DMSO; FUJIFILM Wako Pure Chemical, Osaka, Japan) was infiltrated into 5- or 6-week-old plants twice: at the time of agroinfiltration and again 12 hours prior to observation. Observation was conducted at 36 hours post-infiltration of *Agrobacterium*. 100 μM Oryzalin (Sigma-Aldrich, St. Louis, U. S. A.) in 0.5% DMSO was infiltrated 20 hours after agroinfiltration, and observation was conducted at 48 hours post-infiltration of *Agrobacterium.*

Plasmolysis

Plasmolysis treatment was performed as described by Yuan *et al*. (2016) with minor modification. 10% (w/v) NaCl was dropped on a part of leaf samples just before observation while water was used for negative control.

Agroinfiltration of plants

Agroinfiltration assay was carried out as described by Kaido *et al*. (2009). 5- or 6-week-old *N. benthamiana* was infiltrated with *Agrobacterium* (*Agrobacterium tumefaciens*) GV3101 strain (pMP90) containing plasmids given the prefix ‘pBIC’. Plants were incubated at 25℃ for 36-48 hours.

RESULTS

Inhibitors of ER-secretory pathway and cytoskeleton do not interfere with the PD localization of MP

Previous studies have reported that for several MPs from different viruses, PD targeting depends on the ER-Golgi secretory system and/or the cytoskeleton (Genovés *et al*., 2010; Niehl and Heinlein, 2011; Sun *et al*., 2013; Wei *et al*., 2010; Wright *et al*., 2007; Yuan *et al*., 2011). Given that interfering with the ER-Golgi secretory system and the cytoskeleton also hinders the PD targeting of PDLP1a, I utilized PDLP1a as a positive control (Di Donato and Amari, 2015; Thomas *et al*., 2008; Wei *et al*., 2010). Sar1[H74L], a dominant-negative form of Sar1, is known to interfere with the ER-Golgi vesicular transport pathway (daSilva *et al*., 2004; Takeuchi *et al*., 2000). PDLP1a:mRuby and RCNMV MP:sGFP were co-expressed with Sar1[H74] or intact Sar1 as negative control using the agroinfiltration method. Observation was conducted using CLSM at 48 hours post-infiltration. Co-expression of Sar1 did not affect the PD targeting of either PDLP1a:mRuby or MP:sGFP (Figure II-1, panel A). Subsequently, plasmolysis was performed to distinguish the accumulation of proteins in the PD and cytoplasm (Yuan *et al*., 2016). In plasmolyzed cells, both PDLP1a:mRuby and MP:sGFP were retained at the cell wall (Figure II-1, panel B). Conversely, when Sar1[H74L] was expressed, the targeting of PDLP1a:mRuby to the PD was inhibited, and retention in an ER-like network structure was observed. In contrast, MP:sGFP still localizes to the PD (Figure II-1, panel C). Following plasmolysis, MP:sGFP retained its position at the cell wall, whereas PDLP1a:mRuby detached from the cell wall (Figure II-1, panel D). These results suggest that the ER-golgi secretory pathway is not involved in the PD targeting of MP:sGFP.

I further explored the role of the cytoskeleton in PD localization. Leaves expressing

MP:sGFP and PDLP1a:mRuby were infiltrated with either 10 μM Lat B solution or diluted DMSO solution. In the cells treated with DMSO, the fluorescence signals of PDLP1a:mRuby and MP:sGFP overlapped at the cell wall, regardless of whether plasmolysis was induced (Figure II-2, panels A and B). In contrast, Lat B treatment inhibited the PD targeting of PDLP1a:mRuby, resulting in relocation of PDLP1a:mRuby to vesicle-like structures and cytoplasm. MP:sGFP still retained its PD localization (Figure II-2, panel C). Plasmolysis treatment made the differences in the localization of the two proteins more apparent, with MPs localizing to the PD and PDLPs moving away from the cell wall (Figure II-2, panel D). These findings suggest that while actin plays a role in PDLP1a:mRuby trafficking, it does not influence the transport of MP:sGFP to PD.

ER is a crucial component of PD, and the movement of molecules into and through the PD is also closely related to the ER (Wright and Oparka, 2006). Thus, I hypothesized that the ER might play a role in the transport of MP to PD. Since the ER forms a network along the actin, it has been reported that the injection of high concentrations of the actin polymerization inhibitor Lat B (100 μM) disrupts the network structure of the ER (Nakano *et al*., 2009). To investigate whether the ER is involved in the PD transport of MP, 100 μM Lat B was applied. In leaves treated with DMSO solution, a web-like structure of the ER was observed, and the PD localization of MP was also evident. However, in leaves treated with 100 μM Lat B, the network structure of the ER disintegrated, forming spots or aggregate structures. Notably, the signal of MP:sGFP remained at the PD (Figure II-3), suggesting that MP is not transported to the PD via ER tubules.

Subsequently, I investigated the functional redundancy of the ER-actin network and the secretory pathway in transporting MPs to the PD. The samples were treated with both

Sar1[H74L] and 100 μM Lat B. The localization of PDLP1a was markedly altered, and its association with PD was inhibited. However, MP remained in the PD (Figure II-4A). Additionally, upon quantification of the spots on cell wall structures, the number of PDLP1a was significantly reduced, whereas the count for MP remained unchanged (Figure II-4B). This suggests that these pathways do not function redundantly and are not responsible for MP's transport to the PD.

To investigate the involvement of microtubules with PD targeting of MP, I examined the effect of oryzalin, an inhibitor of microtubule polymerization, to the PD localization of MP. Tua:GFP, a marker of microtubules, showed a fibrous localization pattern in DMSO-treated leaves, whereas the fibrous structure of tua:GFP was disrupted in oryzalin-treated leaves. However, the PD localization of MP was not impaired (Figure II-5). These results suggest that PD targeting of MP is not dependent on microtubules.

Thus, these data suggest that PD targeting of RCNMV MP does not require the secretory pathway and the cytoskeleton.

Deletion of predicted α-helices affects intracellular localization of the mutant MP and the cell-to-cell movement of recombinant viruses

In this study, recombinant viruses encoding MP:sGFP in place of CP were employed to investigate viral cell-to-cell movement and the localization of MP. Co-inoculation of *in vitro* transcripts from pUCR1-MsG and pUCR2fsMP facilitated the observation of MP dynamics and infection progression via the the expression of MP:sGFP from RNA1 (Kaido *et al*., 2009).

I tried to identify functional regions within MP crucial for its localization to PD and viral replication sites. Neither the transmembrane domain nor the signal peptide was

predicted to be present in RCNMV MP (data not shown). Consequently, I turned my attention to the α-helix, a fundamental protein structure that is thought to be involved in protein-protein interactions (Azzarito *et al*., 2013). To predict α-helices, PsiPred ver.3 (http://bioinf.cs.ucl.ac.uk/psipred/), a secondary structure prediction tool, was used. From this analysis, five α-helices were predicted. Deletion mutants for each helix were constructed and labeled as Δα1 to Δα5 mutants (Figure II-6). I inoculated *N. benthamiana* with recombinant viruses expressing MP or its mutant derivative from the CP coding region of RNA1. In leaves inoculated with virus expressing wt MP, fluorescent foci containing multiple cells were observed at 24 hours post-inoculation (hpi). Cortical cytoplasmic punctate and aggregate structures, as previously characterized by Kaido *et al*. (2011 and 2014), were also detected (Figure II-7A). These structures likely colocalize with viral replication complexes (VRCs). I then investigated the effect of the deletion of the α-helices on viral cell-to-cell movement and the localization of MP. Except for the fifth mutant (Δα5), the distribution of fluorescence was mainly confined to one or two cells (Figure II-7A). Furthermore, certain α-helix deletions affected the localization. Δα1 and Δα3 failed to form cortical punctate structures, while Δα2 showed aggregate structure formation without cell wall localization (Fig. II-7A). The percentage of infected sites containing multiple fluorescent cells was quantified using epifluorescence microscopy (Fig. II-7B). Quantitative analysis showed that, aside from the fifth mutant at 70%, fewer than 10% of fluorescent foci consisted of multiple fluorescent cells. This indicates a significant inhibition of cell-to-cell movement (Figure II-7C). These results suggest the significance of α-helices, with exception of the fifth, in efficient viral cell-to-cell movement and appropriate MP localization.

Deletion mutants retains its RNA binding ability

The α-helix structure has been identified as a crucial element for RNA binding in several proteins (Law *et al*., 2013; Tan *et al*., 1993; Vilar *et al*., 2005). Therefore, the compromised RNA-binding capacity of the α-helix deletion mutants could contribute to the low efficiency of cell-to-cell movement. To evaluate the RNA-binding affinity of the wt and mutant MP, I conducted an electrophoretic mobility shift assay (EMSA). I used purified 6× histidine-tagged wt MP and α-helix deletion mutants along with biotin-labeled viral RNA2 fragment. The results showed that all mutants exhibited a concentration-dependent band shift comparable to WT, suggesting that they retained their RNA-binding ability (Figure II-8). In a previous study, the accumulation of α-helix mutant in protoplasts was investigated. Recombinant viruses expressing wt or mutant MPs tagged with GFP from the CP coding region of RNA1 were used to infect protoplasts. The protein accumulation of mutant MP with deletion of the first and third alpha helix (Δα1 and Δα3) was found to be comparable to that of WT, whereas Δα2 was reduced to about 50% and Δα4 to about 25% (Kawano, 2016, master's thesis). Given that there were not obvious alterations in the localization or RNA-binding capability of the Δα4 protein, the attenuated cell-to-cell movement of Δα4 is hypothesized to stem from protein destabilization in plants. As a result, Δα4 was excluded from further analysis.

Deletion mutants retain the plasmodesmata-targeting ability, except for the second α-helix

Plasmodesmata localization of MP is postulated to be a requisite for viral cell-to-cell movement (Berna *et al*., 1991; Sáray *et al*., 2021; Sasaki *et al*., 2006). It was hypothesized that mutants with α-helix deletions lack PD localization, which leads to the loss of their

ability for viral cell-to-cell movement. Since the transient expression of wt MP via agroinfiltration clearly shows the accumulation of wt MP in cell walls (Kaido *et al*., 2009), I utilized this transient expression system to investigate the localization of the various mutants. The subsequent expression of the deletion mutants showed that Δα1 and Δα3 colocalized with the PD marker, whereas the Δα2 mutant primarily localized to the cytoplasm and did not colocalize with the PD marker (Figure II-9). This observation is consistent with the finding that the Δα2 mutant failed to localize near the cell wall when expressed from the viral genome (Figure II-7). These results suggest that the loss of PD localization reduces the cell-to-cell movement ability of the virus with Δα2 mutant and that this region is essential for PD trafficking.

I then sought to identify the essential amino acids for the PD localization of MP. Initially, three mutants were constructed by dividing the second α-helix into three parts, each with an alanine substitution, and they were named α2L, α2M, and α2R (Figure II-10A). Transiently expressed α2L and α2M mutants did not localize at PD, unlike the α2R mutant (Figure II-10B). Subsequent individual alanine substitutions of amino acids in α2L all showed the PD localization (Figure II-11A). However, the three alanine substitutions, S43/M44/M45A, led to a loss of the PD localization (Figure II-11B). Further alanine substitutions of amino acids in the α2M region revealed that the alanine substitution at the 50th aspartic acid resulted in a loss of the PD localization (Figure II-12A). Given that protein accumulation in single cells of mutants lacking the second α-helix has been found to be reduced to 50% (Kawano, 2016, master's thesis), I hypothesized that the inability of mutant MPs with S43/M44/M45A and D50A to localize to PD could be due to an MP accumulation issue. Therefore, I extracted proteins from leaves of *N. benthamiana* transiently expressing these mutant MPs and confirmed their

accumulation by Western blotting. The results showed that the amount of accumulation was comparable to or higher than that of the WT. Thus, the loss of PD localization was not due to protein destabilization (Figure II-12B).

Next, the alanine-substituted mutant MPs were introduced into the viral genome, and their effects on intercellular movement were assessed. Mutant MPs with S43/M44/M45A and D50A localized to aggregate structures on the cell surface. However, the spread of fluorescence was strongly limited (Figure II-13A). Quantitative analysis revealed that the spread rate of the mutant virus with T49A, which retains the ability to localize to PD, was comparable to WT. Conversely, no fluorescent foci in the mutant with S43/M44/M45A and 0.7 % fluorescent foci in the mutant with D50A comprised multiple fluorescent cells. This indicates a significant reduction in the ability of cell-to-cell movement for these mutants (Figure II-13B, Table II-1). These results suggest that the residues S43/M44/M45 and D50, embedded within the second putative α-helix, play crucial roles in PD localization and in the intercellular movement of the virus. Furthermore, the findings emphasize the crucial role of PD localization of MP in cell-to-cell movement of RCNMV.

Substituting alanine for leucine in the first α-helix significantly impairs viral cell-to-cell movement

Deletion mutations in the first and third α-helices hindered the formation of cortical punctate and aggregated structures, underscoring the importance of these regions in the proper localization of MP and subsequent viral cell-to-cell movement (Figure II-7). To identify the essential amino acids within these α-helices, I designed several alanine-substituted mutants. The α1(6A) mutant was developed by replacing all six residues in the first α-helix with alanine. Microscopic analysis showed a widespread cytoplasmic

distribution of the GFP signal of the α1(6A) mutant (Figure II-14A). Furthermore, the efficiency of cell-to-cell movement of this mutant was significantly reduced compared to the WT, with a barely discernible difference between Δα1 and α1(6A) (Figure II-14B, Table II-1). These findings provided further evidence for the importance of this putative α-helix region in both subcellular localization and cell-to-cell movement.

Subsequently, I produced and evaluated single alanine-substituted mutants of the first α-helix. CLSM observation revealed that the L11A mutant, which has the 11th leucine replaced by alanine, demonstrated compromised formation of cortical aggregated structures, akin to the α1(6A) mutant (Figure II-15A). Quantitative data showed a significant reduction in the percentage of infection sites with fluorescence spanning multiple cells: 26.0% for the L11A mutant, in contrast to 71.6% for the WT. This percentage closely resembled that of the α1(6A) mutant, which was 26.2% (Figure II-15B, C, Table II-1). These results suggest that the 11th leucine residue within the α-helix plays a crucial role in proper subcellular localization and cell-to-cell movement.

Substituting alanine for threonine in the third α-helix significantly impairs viral cell-to-cell movement

I then moved on to examine the third α-helix. The α3(4A) mutant was constructed by replacing all amino acids in the helix with alanine. When *in vitro* transcripts of recombinant virus with α3(4A) mutation was inoculated, this mutant displayed an inhibited formation of granule structures on the cell surface, similar to the Δα3 mutant (Figure II-16A). Additionally, its efficiency in cell-to-cell movement was also significantly reduced (Figure II-16B, Table II-1). These results further support the importance of the third putative α-helix region for subcellular localization and cell-to-cell

movement. To delve deeper, I generated mutants with a single alanine substitution and evaluated their behavior. Microscopy revealed that the mutant with alanine substitution of 182nd threonine lacked the formation of aggregate structures on the cell surface and exhibited a similar localization pattern as α3(4A) (Figure II-17A). Quantitative analysis also showed that the virus with alanine substitution of the 182nd threonine exhibited a markedly reduced cell-to-cell movement efficiency compared to the WT, which was comparable to that of α3(4A) (Figure II-17B, Table II-1). These results pinpoint the 182nd threonine as crucial for the efficient cell-to-cell movement and appropriate MP localization at the viral replication site.

Phosphorylation mimic mutant retains the ability of localization to aggregated structures and viral cell-to-cell movement

Phosphorylation of threonine is one of the common protein modifications in plant viruses (Zhuang *et al*., 2022). The MP of tomato mosaic virus is phosphorylated, leading to a change in subcellular localization (Kawakami *et al*., 1999). I hypothesized that the phosphorylation of the 182nd threonine might be important for subcellular localization and cell-to-cell movement. Aspartic acid substitution for threonine confers a negative charge and could mimic phosphorylated threonine (Waigmann *et al*., 2000). Therefore, I constructed an aspartic acid-substituted mutant for threonine and tested its effect. Confocal microscopy observations revealed that the formation of aggregated structures and cell-to-cell movement were inhibited in the mutant with T182A. In contrast, the mutant with T182D had the ability to form aggregation and facilitate cell-to-cell movement, albeit to a lesser degree than the WT (Figure II-18, Table II-1). At 24 hpi, cells at the center of infection were observed with an epifluorescence microscope and classified

into three types based on the localization pattern of MP. Specifically, the localization of MP was categorized into type I, in which MPs were spread throughout the cytoplasm, type II, in which small granular structures were observed on the cell surface, and type III, in which aggregate structures of approximately 20 μm^2 or more were observed. The percentage of each type was determined quantitatively. The average percentage of type III was 45.3%, 6.0%, and 22.6% for WT, T182A, and T182D, respectively (Figure II-19, Table II-2). This indicates that the percentage of aggregated structures in leaves infected with the virus carrying T182D mutation decreased compared to WT but increased compared to T182A. Furthermore, the pattern of type III percentage and cell-to-cell movement ability coincided, suggesting that the ability to form aggregation is linked to cell-to-cell movement capability (Figure II-18). These results suggest that the phosphorylation of the 182^{nd} threonine is important for aggregation of MP at the viral replication site and for viral cell-to-cell movement.

DISCUSSION

The detailed mechanism underlying the localization of MP to PD and VRCs, the site of viral replication, remains elusive. In this study, I delved into the trafficking pathway to PD and identified crucial amino acids of MP required for the proper localization.

Neither the actin polymerization inhibitor Lat B, the microtubule polymerization inhibitor Oryzalin, nor the vesicular transport system inhibitor Sar1[H74L] affected the PD localization of RCNMV MP. Thus, these results suggest these transport systems are not involved in PD targeting of MP. TMV MPs are transported to PD via the ER-actin transport system. When transiently expressed, TMV MP establishes granular structures and interact with the ER-actin network (Wright *et al*., 2007; Hak *et al*., 2023). In contrast, RCNMV MP, upon transient expression, was observed to localize exclusively to the PD, supporting that PD targeting is carried out independently of the ER (Figure II-9, Kaido *et al*., 2009). It is thought that CaMV MP colocalize with vesicles labeled with endocytosis markers and are transported to PD by endocytosis (Carluccio *et al*., 2014). However, the finding that transient expression of RCNMV MP does not localize to vesicle-like structures suggests that endocytosis is also not involved in PD transport of RCNMV MP. While the inhibitor treatments do not eliminate the possibility that RCNMV MPs are transported to the PD using a residual amount of cytoskeleton or vesicular transport—or that they might reach the PD through diffusion without any pathway—they raise the prospect that RCNMV MP might utilize a previously unidentified transport mechanism. The PD localization of TGBp3 from poa semilatent virus is reported to remain unaffected by various inhibitors, pointing toward the potential existence of a yet-unknown transport system (Schepetilnikov *et al*., 2008). The findings in my research further bolster the hypothesis of such an undiscovered transport mechanism and emphasize the need for

continued exploration.

I further used mutational analysis to identify amino acids important for PD localization. S43/M44/M45 and D50 alanine substitutions within the second putative α-helix completely abolished PD localization (Figure II-11B, Figure II-12A). Furthermore, recombinant viruses with these mutations lacked cell-to-cell movement ability, strongly supporting the importance of these amino acids for both PD localization and cell-to-cell movement (Figure II-13). There are two possible reasons for the loss of PD localization in these mutants. The first is that MPs are transported toward PD but fail to interact with acceptors on the PD, resulting in loss of PD localization. As for host factors that anchor MPs to the PD, there have been reports of synaptotagmin localized at the ER-PM contact sites near PD and PDLP proteins believed to control the accumulation of callose localized at the PD (Amari *et al*., 2010; Liu *et al*., 2020; Yuan *et al*., 2018). The second possibility is that the mutants fail to interact with host factors required for transport to the PD and thus cannot localize to the PD. When recombinant viruses carrying these mutations were infected, the granular structures in the cytoplasm appeared to be larger and more aggregated than in the WT. This suggested that although the mutant MPs accumulated at sites on the cell surface that are thought to be VRCs, they failed to export to the PD and accumulated as an aggregated structure (Figure II-13). If so, this would suggest that the second hypothesis, that mutant MP fails the interaction with host factors involved in export to the PD, has not been achieved. In any case, future comparisons of interacting factors between wt and mutant MPs may reveal the presence of an acceptor or an unknown transport system.

I also used mutational analysis to identify amino acids important for localization to aggregates that may be associated with VRCs. I found that alanine substitutions at L11

and T182 markedly impaired the efficiency of cell-to-cell movement and localization to aggregation structures, with the T182A mutant showing a more pronounced degree of inhibition (Figure II-15, Figure II-17). Furthermore, aspartic acid substitutions, which mimic the phosphorylation of threonine, partially enhanced intracellular movement and aggregation (Figure II-18). This suggests that phosphorylation of MP is important for its accumulation in aggregated structures. However, the presence or absence of phosphorylation should be investigated using mass spectrometry or phosphorylated threonine-specific antibodies. Phosphorylation of several MPs and their functions have been reported (Zhuang *et al*., 2022). For instance, the phosphorylation of TGB1, one of the MPs of BSMV, enhances its interaction with TGB3 and promotes intercellular movement (Hu *et al*., 2015). Phosphorylation of MP from Potato leaf roll virus promotes the PD localization of MP (Link *et al*., 2011). Thus, the phosphorylation of MP regulates a wide variety of MP functions. The results obtained in this study suggest a new function for phosphorylation in which it regulates MP's localization to viral replication sites.

This study revealed that different functional regions within the MP are involved in the various localizations of the MP, i.e., localization to the replication complex and localization to the PD. How these localizations are regulated remains to be elucidated. In general, MPs are thought to have multifunctional properties such as RNA binding, PD opening and closing ability, and localization to different locations (Lucas, 2006; Heinlein, 2015). Therefore, MPs likely bind and utilize a variety of host factors, but this property has made the identification of host factors difficult. In the future, a comparative analysis of interacting factors between mutants lacking localization to specific sites and wt MP will enable the identification of host factors utilized by the MP.

REFERENCES

Amari, K., Boutant, E., Hofmann, C., Schmitt-Keichinger, C., Fernandez-Calvino, L., Didier, P., Lerich, A., Mutterer, J., Thomas, C. L., Heinlein, M., Mély, Y., Maule, A. J., Ritzenthaler, C. (2010). A family of plasmodesmal proteins with receptor-like properties for plant viral movement proteins. PLoS Pathog., 6(9), e1001119.

Azzarito, V., Long, K., Murphy, N. S., Wilson, A. J. (2013). Inhibition of α-helix-mediated protein-protein interactions using designed molecules. Nat. Chem., 5(3), 161-173.

Bamunusinghe, D., Hemenway, C. L., Nelson, R. S., Sanderfoot, A. A., Ye, C. M., Silva, M. A. T., Payton, M., Verchot-Lubicz, J. (2009). Analysis of potato virus X replicase and TGBp3 subcellular locations. Virology, 393(2), 272-285.

Berna, A., Gafny, R., Wolf, S., Lucas, W. J., Holt, C. A., Beachy, R. N. (1991). The TMV movement protein: role of the C-terminal 73 amino acids in subcellular localization and function. Virology, 182(2), 682-689.

Carluccio, A. V., Zicca, S., Stavolone, L. (2014). Hitching a ride on vesicles: cauliflower mosaic virus movement protein trafficking in the endomembrane system. Plant Physiol., 164(3), 1261-1270.

Christensen, N., Tilsner, J., Bell, K., Hammann, P., Parton, R., Lacomme, C., Oparka, K. (2009). The 5' cap of tobacco mosaic virus (TMV) is required for virion

attachment to the actin/endoplasmic reticulum network during early infection. Traffic, 10(5), 536-51.

daSilva, L. L., Snapp, E. L., Denecke, J., Lippincott-Schwartz, J., Hawes, C., Brandizzi, F. (2004). Endoplasmic reticulum export sites and Golgi bodies behave as single mobile secretory units in plant cells. Plant Cell, 16(7), 1753-1771.

den Boon, J. A., Ahlquist, P. (2010). Organelle-like membrane compartmentalization of positive-strand RNA virus replication factories. Annu. Rev. Microbiol., 64, 241-256.

Di Donato, M., Amari, K. (2015). Analysis of the role of myosins in targeting proteins to plasmodesmata. Methods Mol. Biol., 1217, 283-293.

Dohi, K., Mori, M., Furusawa, I., Mise, K., Okuno, T. (2001). Brome mosaic virus replicase proteins localize with the movement protein at infection-specific cytoplasmic inclusions in infected barley leaf cells. Arch. Virol., 146(8), 1607-1615.

Faulkner, C. (2018). Plasmodesmata and the symplast. Curr. Biol., 28(24), R1374-R1378.

Fujiwara, T., Giesman-Cookmeyer, D., Ding Biao, Lommel, S. A., Lucas, W. J. (1993). Cell-to-cell Trafficking of macromolecules through plasmodesmata potentiated by the red clover necrotic mosaic virus movement protein. Plant Cell, 5(12), 1783-1794.

Genovés, A., Navarro, J. A., Pallás, V. (2010). The intra- and intercellular movement of melon necrotic spot virus (MNSV) depends on an active secretory pathway. Mol. Plant Microbe Interact., 23(3), 263-272.

Giesman-Cookmeyer, D., Lommel, S. A. (1993). Alanine scanning mutagenesis of a plant virus movement protein identifies three functional domains. Plant Cell. 5(8), 973-982.

Hak, H., Raanan, H., Schwarz, S., Sherman, Y., Dinesh-Kumar, S. P., Spiegelman, Z. (2023). Activation of Tm-22 resistance is mediated by a conserved cysteine essential for tobacco mosaic virus movement. Mol. Plant Pathol., 24(8), 838-848.

Heinlein, M. (2015). Plant virus replication and movement. Virology, 479-480, 657-671.

Heinlein, M., Padgett, H. S., Gens, J. S., Pickard, B. G., Casper, S. J., Epel, B. L., Beachy, R. N. (1998). Changing patterns of localization of the tobacco mosaic virus movement protein and replicase to the endoplasmic reticulum and microtubules during infection. Plant Cell, 10(7), 1107-1120.

Hirashima, K., Watanabe, Y. (2003). RNA helicase domain of tobamovirus replicase executes cell-to-cell movement possibly through collaboration with its nonconserved region. J. Virol., 77(22), 12357-12362.

Hu, Y., Li, Z., Yuan, C., Jin, X., Yan, L., Zhao, X., Zhang, Y., Jackson, A. O., Wang, X., Han, C., Yu, J., Li, D. (2015). Phosphorylation of TGB1 by protein kinase CK2 promotes barley stripe mosaic virus movement in monocots and dicots. J. Exp. Bot., 66(15), 4733-4747.

Jiang, Z., Zhang, K., Li, Z., Li, Z., Yang, M., Jin, X., Cao, Q., Wang, X., Yue, N., Li, D., Zhang, Y. (2020). The Barley stripe mosaic virus γb protein promotes viral cell-to-cell movement by enhancing ATPase-mediated assembly of ribonucleoprotein movement complexes. PLoS Pathog., 16 (7), e1008709.

Kaido, M., Abe, K., Mine, A., Hyodo, K., Taniguchi, T., Taniguchi, H., Mise, K., Okuno, T. (2014). GAPDH-A recruits a plant virus movement protein to cortical virus replication complexes to facilitate viral cell-to-cell movement. PLoS Pathog., 10 (11), e1004505.

Kaido, M., Funatsu, N., Tsuno, Y., Mise, K., Okuno, T. (2011). Viral cell-to-cell movement requires formation of cortical punctate structures containing red clover necrotic mosaic virus movement protein. Virology, 413(2), 205-215.

Kaido, M., Tsuno, Y., Mise, K., Okuno, T. (2009). Endoplasmic reticulum targeting of the Red clover necrotic mosaic virus movement protein is associated with the replication of viral RNA1 but not that of RNA2. Virology, 395 (2), 232–242.

Kawakami, S., Padgett, H. S., Hosokawa, D., Okada, Y., Beachy, R. N., Watanabe, Y. (1999). Phosphorylation and/or presence of serine 37 in the movement protein of tomato mosaic tobamovirus is essential for intracellular localization and stability in vivo. J. Virol., 73(8), 6831-6840.

Kawakami, S., Watanabe, Y., Beachy, R. N. (2004). Tobacco mosaic virus infection spreads cell to cell as intact replication complexes. Proc. Natl. Acad. Sci. U. S. A., 101(16), 6291-6296.

河野早帆 (2016). Red clover necrotic mosaic virus 移行タンパク質の細胞内輸送に関する研究. 京都大学修士論文.

Law, M. J., Lee, D. S., Lee, C. S., Anglim, P. P., Haworth, I. S., Laird-Offringa, I. A. (2013). The role of the C-terminal helix of U1A protein in the interaction with U1hpII RNA. Nucleic Acids Res., 41(14), 7092-7100.

Lee, J. Y., Lu, H. (2011). Plasmodesmata: the battleground against intruders. Trends Plant Sci., 16(4), 201-210.

Link, K., Vogel, F., Sonnewald, U. (2011). PD Trafficking of Potato leaf roll virus movement protein in Arabidopsis depends on site-specific protein phosphorylation. Front. Plant Sci., 2, 18.

Liu, Y., Huang, C., Zeng, J., Yu, H., Li, Y., Yuan. C. (2020). Identification of two additional plasmodesmata localization domains in the tobacco mosaic virus cell-to-cell-movement protein. Biochem. Biophys. Res. Commun., 521(1), 145-151.

Lucas, W. J. (2006). Plant viral movement proteins: agents for cell-to-cell trafficking of viral genomes. Virology, 344(1), 169-184.

Lucas, W. J., Ham, B. K., Kim, J. Y. (2009). Plasmodesmata - bridging the gap between neighboring plant cells. Trends Cell Biol., 19(10), 495-503.

Miller, S., Krijnse-Locker, J. (2008). Modification of intracellular membrane structures for virus replication. Nat. Rev. Microbiol., 6(5), 363-374.

Mizumoto, H., Tatsuta, M., Kaido, M., Mise, K., Okuno, T. (2003). Cap-independent translational enhancement by the 3' untranslated region of red clover necrotic mosaic virus RNA1. J. Virol., 277(22), 12113-12121.

Nagy, P. D., Feng, Z. (2021). Tombusviruses orchestrate the host endomembrane system to create elaborate membranous replication organelles. Curr. Opin. Virol., 48, 30-41.

Nakano, R. T., Matsushima, R., Ueda, H., Tamura, K., Shimada, T., Li, L., Hayashi, Y., Kondo, M., Nishimura, M., Hara-Nishimura, I. (2009). GNOM-LIKE1/ERMO1 and SEC24a/ERMO2 are required for maintenance of endoplasmic reticulum morphology in Arabidopsis thaliana. Plant Cell, 21(11), 3672-3685.

Niehl, A., Heinlein, M. (2011). Cellular pathways for viral transport through plasmodesmata. Protoplasma, 248(1), 75-99.

Oparka, K. J., Roberts, A. G., Boevink, P., Santa, Cruz, S., Roberts, I., Pradel, K. S., Imlau, A., Kotlizky, G., Sauer, N., Epel, B. (1999). Simple, but not branched, plasmodesmata allow the nonspecific trafficking of proteins in developing tobacco leaves. Cell, 97(6), 743-54.

Sáray, R., Fábián, A., Palkovics, L., Salánki, K. (2021). The 28 Ser amino acid of Cucumber mosaic virus movement protein has a role in symptom formation and plasmodesmata localization. Viruses, 13(2), 222.

Sasaki, N., Park, J. W., Maule, A. J., Nelson, R. S. (2006). The cysteine-histidine-rich region of the movement protein of cucumber mosaic virus contributes to plasmodesmal targeting, zinc binding and pathogenesis. Virology, 349(2), 396-408.

Schepetilnikov, M. V., Solovyev, A. G., Gorshkova, E. N., Schiemann, J., Prokhnevsky, A. I., Dolja, V. V., Morozov, S. Y. (2008). Intracellular targeting of a hordeiviral membrane-spanning movement protein: sequence requirements and involvement of an unconventional mechanism. J. Virol., 82(3), 1284-1293.

Schindelin, J., Arganda-Carreras, I., Frise, E., Kaynig, V., Longair, M., Pietzsch, T., Preibisch, S., Rueden, C., Saalfeld, S., Schmid, B., Tinevez, J. Y., White, D. J.,

Scholthof, H. B. (2005). Plant virus transport: motions of functional equivalence. Trends Plant Sci., 10(8), 376-382.

Shemyakina, E. A., Solovyev, A. G., Leonova, O. G., Popenko, V, I., Schiemann, J., Morozov, S. Y. (2011). The role of microtubule association in plasmodesmal targeting of Potato mop-top virus movement protein TGBp1. Open Virol. J., 5, 1-11.

Sun, Z., Zhang, S., Xie, L., Zhu, Q., Tan, Z., Bian, J., Sun, L., Chen, J. (2013). The secretory pathway and the actomyosin motility system are required for plasmodesmatal localization of the P7-1 of rice black-streaked dwarf virus. Arch. Virol., 158(5), 1055-1064.

Takeuchi, M., Ueda, T., Sato, K., Abe, H., Nagata, T., Nakano, A. (2000). A dominant negative mutant of sar1 GTPase inhibits protein transport from the endoplasmic reticulum to the Golgi apparatus in tobacco and Arabidopsis cultured cells. Plant J., 23(4), 517-525.

Tan, R., Chen, L., Buettner, J. A., Hudson, D., Frankel, A. D. (1993). RNA recognition by an isolated alpha helix. Cell. 73(5), 1031-1040.

Tatsuta, M., Mizumoto, H., Kaido, M., Mise, K., Okuno, T. (2005). The red clover necrotic mosaic virus RNA2 trans-activator is also a cis-acting RNA2 replication element. J. Virol., 79 (2), 978–986.

Thomas, C. L., Bayer, E. M., Ritzenthaler, C., Fernandez-Calvino, L., Maule, A. J. (2008). Specific targeting of a plasmodesmal protein affecting cell-to-cell communication. PLoS Biol., 6(1), e7.

Tilsner, J., Cowan, G. H., Roberts, A. G., Chapman, S. N., Ziegler, A., Savenkov, E., Torrance, L. (2010). Plasmodesmal targeting and intercellular movement of potato mop-top pomovirus is mediated by a membrane anchored tyrosine-based motif on the lumenal side of the endoplasmic reticulum and the C-terminal transmembrane domain in the TGB3 movement protein. Virology, 402(1), 41-51.

Tremblay, D., Vaewhongs, A. A., Turner, K. A., Sit, T. L., Lommel, S. A. (2005). Cell wall localization of Red clover necrotic mosaic virus movement protein is required for cell-to-cell movement. Virology, 333(1), 10-21.

Tucker, E. B. (1982). Translocation in the stamina hairs of Setcreasea purpuerea. 1. A study of cell ultrastructur and cell-to-cell passage of molecular probes. Protoplasma, 113, 193-201.

Vilar, M., Saurí, A., Marcos, J. F., Mingarro, I., Pérez-Payá, E. (2005). Transient structural ordering of the RNA-binding domain of carnation mottle virus p7 movement protein modulates nucleic acid binding. Chembiochem., 6(8), 1391-1396.

Waigmann, E., Chen, M. H., Bachmaier, R., Ghoshroy, S., Citovsky. V. (2000). Regulation of plasmodesmal transport by phosphorylation of tobacco mosaic virus cell-to-cell movement protein. EMBO J., 19(18), 4875-4884.

Waigmann, E., Ueki, S., Trutnyeva, K., Citovsky, V. (2004). The ins and outs of nondestructive cell-to-cell and systemic movement of plant viruses. Crit. Rev. Plant Sci., 23, 195-250.

Wei, T., Zhang, C., Hong, J., Xiong, R., Kasschau, K. D., Zhou, X., Carrington, J. C., Wang, A. (2010). Formation of complexes at plasmodesmata for potyvirus intercellular movement is mediated by the viral protein P3N-PIPO. PLoS Pathog., 6(6), e1000962.

Wolf, S., Deom, C. M., Beachy, R. N., Lucas, W. J. (1989). Movement protein of tobacco mosaic virus modifies plasmodesmatal size exclusion limit. Science, 246(4928), 377-379.

Wright, K. M., Oparka, K. J. (2006). The ER within plasmodesmata. The Plant Endoplasmic Reticulum, 4, 279-308.

Wright, K. M., Wood, N, T., Roberts, A. G., Chapman, S., Boevink, P., Mackenzie, K. M., Oparka, K. J. (2007). Targeting of TMV movement protein to plasmodesmata requires the actin/ER network: evidence from FRAP. Traffic, 8(1), 21-31.

Xiong, Z., Kim, K. H., Giesman-Cookmeyer, D., Lommel, S. A. (1993). The roles of the red clover necrotic mosaic virus capsid and cell-to-cell movement proteins in systemic infection. Virology. 192(1), 27-32.

Yuan, Z., Chen, H., Chen, Q., Omura, T., Xie, L., Wu, Z., Wei, T. (2011). The early secretory pathway and an actin-myosin VIII motility system are required for plasmodesmatal localization of the NSvc4 protein of rice stripe virus. Virus Res., 159(1), 62-68.

Yuan, C., Lazarowitz, S. G., Citovsky, V. (2016). Identification of a functional plasmodesmal localization signal in a plant viral cell-to-cell-movement protein. mBio. 7(1), e02052-15.

Yuan, C., Lazarowitz, S. G., Citovsky, V. (2018). The plasmodesmal localization signal of TMV MP is recognized by plant synaptotagmin SYTA. mBio, 9(4), e01314-01318.

Zhuang, X., Guo, X., Gu, T., Xu, X., Qin, L., Xu, K., He, Z., Zhang, K. (2022). Phosphorylation of plant virus proteins: Analysis methods and biological functions. Front. Microbiol., 13, 935735.

Table II-1. Detailed result of quantification for cell-to-cell movement.

Type	Trial	number		
		1	2	3>
WT	1st	1	1	8
	2nd	0	2	8
	3rd	3	1	6
Δα1	1st	9	0	1
	2nd	10	0	0
	3rd	9	0	1
Δα2	1st	9	1	0
	2nd	10	0	0
	3rd	10	0	0
Δα3	1st	10	0	0
	2nd	10	0	0
	3rd	10	0	0
Δα4	1st	10	0	0
	2nd	10	0	0
	3rd	10	0	0
Δα5	1st	2	0	8
	2nd	3	0	7
	3rd	4	1	5

Type	Trial	number		
		1	2	3>
WT	1st	18	16	80
	2nd	45	17	53
	3rd	47	18	41
Δα1	1st	75	14	18
	2nd	85	16	7
	3rd	66	11	1
α1(6A)	1st	83	16	5
	2nd	63	16	29
	3rd	89	10	4

Type	Trial	number		
		1	2	3>
WT	1st	58	18	30
	2nd	46	20	37
	3rd	28	14	71
	4th	43	26	33
α1(6A)	1st	92	9	2
	2nd	72	20	14
	3rd	83	23	6
	4th	112	9	0
L8A	1st	43	22	38
	2nd	54	17	37
	3rd	31	17	59
	4th	52	7	17
S9A	1st	53	20	30
	2nd	39	24	45
	3rd	36	11	58
	4th	39	18	48
D10A	1st	68	19	16
	2nd	59	10	34
	3rd	32	14	67
	4th	57	14	33

Type	Trial	number		
		1	2	3>
WT	1st	38	10	56
	2nd	26	19	59
	3rd	25	25	55
α1(6A)	1st	70	20	15
	2nd	82	13	7
	3rd	78	14	13
L11A	1st	78	17	10
	2nd	80	20	7
	3rd	80	21	9
K13A	1st	47	16	41
	2nd	38	14	49
	3rd	33	10	60

Type	Trial	number		
		1	2	3>
WT	1st	3	0	7
	2nd	5	1	4
	3rd	1	3	6
Δα3	1st	0	0	0
	2nd	9	1	0
	3rd	10	0	0
α3(4A)	1st	8	2	0
	2nd	10	0	0
	3rd	10	0	0

Type	Trial	number		
		1	2	3>
WT	1st	6	4	32
	2nd	9	6	40
	3rd	7	9	47
α3(4A)	1st	35	6	2
	2nd	52	1	0
	3rd	55	6	7
Q180A	1st	8	3	52
	2nd	14	6	32
	3rd	21	19	19
R181A	1st	14	7	19
	2nd	22	12	18
	3rd	15	11	37
T182A	1st	31	5	6
	2nd	47	10	9
	3rd	44	5	10
L183A	1st	37	12	7
	2nd	24	5	21
	3rd	35	10	17

Type	Trial	number		
		1	2	3>
WT	1st	31	15	63
	2nd	43	10	45
	3rd	55	21	33
T182A	1st	81	14	9
	2nd	96	2	0
	3rd	89	12	4
T182D	1st	58	20	33
	2nd	67	15	21
	3rd	75	14	16

Type	Trial	number		
		1	2	3>
WT	1st	11	4	35
	2nd	18	6	27
	3rd	18	10	25
S43/M44/M45	1st	51	0	0
	2nd	53	0	0
	3rd	53	0	0
T49A	1st	9	2	40
	2nd	16	10	27
	3rd	19	12	23
D50A	1st	50	1	0
	2nd	52	0	0
	3rd	53	0	0

Table II-2. Detailed result of quantification for localization type.

Type	Trial	Type		
		I	II	III
WT	1st	5	52	42
	2nd	8	41	46
	3rd	18	37	45
T182A	1st	55	28	11
	2nd	61	34	0
	3rd	55	33	6
T182D	1st	32	38	31
	2nd	30	60	9
	3rd	24	48	28

Table II-3. Primers used in this study.

Name	Sequence (5' > 3')
p88_Xho1_Fw	AACCTGTCGATGTACTCGAG
linker_Cla_Rev	ATGATGATGATGCATCGATGC
4A_Fw	TTATGCGGCGGCGGCGCTGTCGAGCATCAAGGCAG
4A_Rev	AGCGCCGCCGCCGCATAACCTACTTCCAACTC
Q180A_Fw	GGTTATGCGCGGACGTTACTGTCGAGCAT
Q180A_Rev	CGTCCGCGCATAACCTACTTCCAACTCAA
R181A_Fw	TATCAGGCGACGTTACTGTCGAGCATCAA
R181A_Rev	TAACGTCGCCTGATAACCTACTTCCAACT
T182A_Fw	CAGCGGGCGTTACTGTCGAGCATCAAGG
T182A_Rev	CAGTAACGCCCGCTGATAACCTACTTCCA
T182D_Fw	CAGCGGGACTTACTGTCGAGCATCAAGG
T182D_Rev	CAGTAAGTCCCGCTGATAACCTACTTCC
L183A_Fw	CGGACGGCGCTGTCGAGCATCAAGGCAG
L183A_Rev	CGACAGCGCCGTCCGCTGATAACCTAC
6A_Fw	AAATGCGGCGGCGGCGGCGGCGACAAATGATGGAATAGCAG
6A_Rev	TTGTCGCCGCCGCCGCCGCCGCATTTTCCACATGAACAGCC
L8A_Fw	GAAAATGCGAGTGATTTGGCAAAGACAAA
L8A_Rev	ATCACTCGCATTTTCCACATGAACAGCC
S9A_Fw	AATTTAGCGGATTTGGCAAAGACAAATG
S9A_Rev	CAAATCCGCTAAATTTTCCACATGAACAG
D10A_Fw	TTAAGTGCGTTGGCAAAGACAAATGATGG
D10A_Rev	TGCCAACGCACTTAAATTTTCCACATGAAC
L11A_Fw	AGTGATGCGGCAAAGACAAATGATGGAAT
L11A_Rev	CTTTGCCGCATCACTTAAATTTTCCACATG
K13A_Fw	TTGGCAGCGACAAATGATGGAATAGCAG
K13A_Rev	ATTTGTCGCTGCCAAATCACTTAAATTTTC
NdeI-RAMP5Fw	CAGCCATATGGCTGTTCATGTGGAAAAT
Bam-RAMP3Rev	GGGGGATCCCTAGAGTCTTTCCGGATTTGGGTC

Table II-3. (continued)

Name	Sequence (5' > 3')
BamH1_MP_Fw	GGAGAGGCCTACGGGGATCCCGATGGCTGTTCATGTGGAAAA
Cla_MP_Rev	ATGATGATGATGCATCGATGCGAGTCTTTCCGGAT
2L_Fw	GCCGCGGCGGCGGCGAAGATCACTGACTACGCTAAAAC
2L_Rev	CGCCGCCGCCGCGGCAGGTATAAGAGGAGCTTC
2M_Fw	GCGGCGGCGGCGGCGGCTAAAACTACTGCTAAAGG
2M_Rev	CGCCGCCGCCGCCGCACTCATCATACTGGCAGGTA
2R_Fw	GCTGCGGCGGCGGCTAAAGGAAACAGTGTTGC
2R_Rev	AGCCGCCGCCGCAGCGTAGTCAGTGATCTTAC
S43A_Fw	CCTGCCGCGATGATGAGTAAGATCACTGAC
S43A_Rev	CATCATCGCGGCAGGTATAAGAGGAGCTTC
M44A_Fw	GCCAGTGCGATGAGTAAGATCACTGACTAC
M44A_Rev	ACTCATCGCACTGGCAGGTATAAGAGGAG
M45A_Fw	AGTATGGCGAGTAAGATCACTGACTACGC
M45A_Rev	CTTACTCGCCATACTGGCAGGTATAAGAG
S46A_Fw	ATGATGGCGAAGATCACTGACTACGCTAA
S46A_Rev	GATCTTCGCCATCATACTGGCAGGTATAAG
S43/M44A_Fw	CCTGCCGCGGCGATGAGTAAGATCACTGACTAC
S43/M44A_Rev	TCATCGCCGCGGCAGGTATAAGAGGAGCTTC
M44/M45A_Fw	CAGTGCGGCGAGTAAGATCACTGACTACGC
M44/M45A_Rev	TTACTCGCCGCACTGGCAGGTATAAGAGGAG
M45/S46A_Fw	GTATGGCGGCGAAGATCACTGACTACGCTA
M45/S46A_Rev	TCTTCGCCGCCATACTGGCAGGTATAAGAG
S43/M44/M45A_Fw	GCCGCGGCGGCGAGTAAGATCACTGACTACGC
S43/M44/M45A_Rev	ACTCGCCGCCGCGGCAGGTATAAGAGGAGCTTC
M44/M45/S46A_Fw	AGTGCGGCGGCGAAGATCACTGACTACGCTAA
M44/M45/S46A_Rev	CTTCGCCGCCGCACTGGCAGGTATAAGAGGAG
K47A_Fw	ATGAGTGCGATCACTGACTACGCTAAAAC
K47A_Rev	AGTGATCGCACTCATCATACTGGCAGGTA
I48A_Fw	AGTAAGGCGACTGACTACGCTAAAACTAC
I48A_Rev	GTCAGTCGCCTTACTCATCATACTGGCAG
T49A_Fw	AAGATCGCGGACTACGCTAAAACTACTGC
T49A_Rev	GTAGTCCGCGATCTTACTCATCATACTGG
D50A_Fw	ATCACTGCGTACGCTAAAACTACTGCTAA
D50A_Rev	AGCGTACGCAGTGATCTTACTCATCATAC
Y51A_Fw	ACTGACGCGGCTAAAACTACTGCTAAAGG
Y51A_Rev	TTTAGCCGCGTCAGTGATCTTACTCATCA

Table II-4. Plasmids used in this study.

Name	Description	Construction/Reference
Plasmids for transient expression in *N. benthamiana*		
pBIC/AtSar1[H74L]	The vector for expression of AtSar1[H74L]	Kawano, 2016, master's thesis
pBIC/AtSar1	The vector for expression of AtSar1	Kawano, 2016, master's thesis
pPDLP1a:mRuby	The vectorfor expression of AtPDLP1a tagged with mRuby. This vector contains *Lotus japonicus ubiquitine* promoter and *AtHSP* terminator	Otsu, unpublished
pBICER-mSi	The vector for expression of HDEL ER retention signal tagged with mScarlet-I (ER:mSi)	constructed in chapter I
pBICMP-mSi	The vector for expression of RCNMV MP tagged with mScarlet-i (MP:mSi)	Inoue, 2020, master's thesis
pBICGFP	The vector for expression of GFP	Takeda *et al* ., 2002
pBICRMsG	The vector for expression of RCNMV MP tagged with sGFP	Kaido *et al* ., 2009
pBICMPdhel1-sGFP	The vector for expression of MP lacking the first putative α-helix (Δα1)	Kawano, 2016, master's thesis
pBICMPdhel2-sGFP	The vector for expression of MP lacking the second putative α-helix (Δα2)	Kawano, 2016, master's thesis
pBICMPdhel3-sGFP	The vector for expression of MP lacking the third putative α-helix (Δα3)	Kawano, 2016, master's thesis
pBICRM(2L):sGFP	The vector for expression of mutant MP with alanine substitution of amino acids from the 43rd to 46th	The MP coding region was PCR-amplified with primers 2L_Fw/Cla_MP_Rev and 2L_Rev/ BamH1_MP_Fw, respectively. These fragments were inserted the BamHI/ClaI site of pBICRMsG via HiFi DNA assembly.
pBICRM(2M):sGFP	The vector for expression of mutant MP with alanine substitution of amino acids from the 47th to 51st	The primers 2M_Fw/Cla_MP_Rev and 2M_Rev/ BamH1_MP_Fw were used.
pBICRM(2R):sGFP	The vector for expression of mutant MP with alanine substitution of amino acids from the 53rd to 55th	The primers 2R_Fw/Cla_MP_Rev and 2R_Rev/ BamH1_MP_Fw were used.
pBICRM(S43A):sGFP	The vector for expression of mutant MP with alanine substitution of S43	The primers S43A_Fw/Cla_MP_Rev and S44A_Rev/ BamH1_MP_Fw were used.
pBICRM(M44A):sGFP	The vector for expression of mutant MP with alanine substitution of M44	The primers M44A_Fw/Cla_MP_Rev and M44A_Rev/ BamH1_MP_Fw were used.
pBICRM(M45A):sGFP	The vector for expression of mutant MP with alanine substitution of M45	The primers M45A_Fw/Cla_MP_Rev and M45A_Rev/ BamH1_MP_Fw were used.
pBICRM(S46A):sGFP	The vector for expression of mutant MP with alanine substitution of S46	The primers S46A_Fw/Cla_MP_Rev and S46A_Rev/ BamH1_MP_Fw were used.
pBICRM(S43/M44A):sGFP	The vector for expression of mutant MP with alanine substitution of S43 and M44	The primers S43/M44A_Fw/Cla_MP_Rev and S43/M44A_Rev/ BamH1_MP_Fw were used.
pBICRM(M44/M45A):sGFP	The vector for expression of mutant MP with alanine substitution of M44 and M45	The primers M44/M45A_Fw/Cla_MP_Rev and M44/M45A_Rev/ BamH1_MP_Fw were used.
pBICRM(M45/S46A):sGFP	The vector for expression of mutant MP with alanine substitution of M45 and S46	The primers M45/S46A_Fw/Cla_MP_Rev and M45/S46A_Rev/ BamH1_MP_Fw were used.
pBICRM(S43/M44/M45A):sGFP	The vector for expression of mutant MP with alanine substitution of S43, M44 and M45	The primers S43/M44/M45A_Fw/Cla_MP_Rev and S43/M44/M45A_Rev/ BamH1_MP_Fw were used.
pBICRM(M44/M45/S46A):sGFP	The vector for expression of mutant MP with alanine substitution of M44, M45 and S46	The primers M44/M45/S46A_Fw/Cla_MP_Rev and M44/M45/S46A_Rev/ BamH1_MP_Fw were used.
pBICRM(K47A):sGFP	The vector for expression of mutant MP with alanine substitution of K47	The primers K47A_Fw/Cla_MP_Rev and K47A_Rev/ BamH1_MP_Fw were used.
pBICRM(I48A):sGFP	The vector for expression of mutant MP with alanine substitution of I48	The primers I48A_Fw/Cla_MP_Rev and I48A_Rev/ BamH1_MP_Fw were used.
pBICRM(T49A):sGFP	The vector for expression of mutant MP with alanine substitution of T49	The primers T49A_Fw/Cla_MP_Rev and T49A_Rev/ BamH1_MP_Fw were used.
pBICRM(D50A):sGFP	The vector for expression of mutant MP with alanine substitution of D50	The primers D50A_Fw/Cla_MP_Rev and D50A_Rev/ BamH1_MP_Fw were used.
pBICRM(Y51A):sGFP	The vector for expression of mutant MP with alanine substitution of Y51	The primers Y51A_Fw/Cla_MP_Rev and Y51A_Rev/ BamH1_MP_Fw were used.

Table II-4. (continued)

Name	Description	Construction/Reference
Plasmids for *in vitro* transcription		
pUCR1-MsG	The vecor encodes a recombinant RCNMV expressing sGFP-tagged MP from the CP gene region of RNA1	Kaido *et al*., 2009
pUCR1-Mdhel1sG	The vector encodes a recombinant RCNMV expressing mutant MP with deletion of the first putative α-helix (Δα1)	Kawano, 2016, master's thesis
pUCR1-Mdhel2sG	The vector encodes a recombinant RCNMV expressing mutant MP with deletion of the second putative α-helix (Δα2)	Kawano, 2016, master's thesis
pUCR1-Mdhel3sG	The vector encodes a recombinant RCNMV expressing mutant MP with deletion of the third putative α-helix (Δα3)	Kawano, 2016, master's thesis
pUCR1-Mdhel4sG	The vector encodes a recombinant RCNMV expressing mutant MP with deletion of the fourth putative α-helix (Δα4)	Kawano, 2016, master's thesis
pUCR1-Mdhel5sG	The vector encodes a recombinant RCNMV expressing mutant MP with deletion of the fifth putative α-helix (Δα5)	Kawano, 2016, master's thesis
pUCR1-M(S43/M44/M45A):sGFP	The vector encodes a recombinant RCNMV expressing mutant MP with alanine substitution of S43, M44 and M45	A genomic fragment containg part of p88 and MP was PCR-amplified from pUCR1-MsG with primers p88_Xho1_Fw/S43/M44/M45A_Rev and linker_Cla_Rev/S43/M44/M45A_Fw, respectively. These fragments was inserted the XhoI/ClaI site of pUCR1-MsG via HiFi DNA assembly.
pUCR1-M(T49A):sGFP	The vector encodes a recombinant RCNMV expressing mutant MP with alanine substitution of T49	The primers p88_Xho1_Fw/T49A_Rev and linker_Cla_Rev/ T49A_Fw were used.
pUCR1-M(D50A):sGFP	The vector encodes a recombinant RCNMV expressing mutant MP with alanine substitution of D50	The primers p88_Xho1_Fw/D50A_Rev and linker_Cla_Rev/ D50A_Fw were used.
pUCR1-Mα1(6A):sGFP	The vector encodes a recombinant RCNMV expressing mutant MP with alanine substitution of amino acids fro the 8th to 13th	The primers p88_Xho1_Fw/6A_Rev and linker_Cla_Rev/6A_Fw were used.
pUCR1-M(L8A):sGFP	The vector encodes a recombinant RCNMV expressing mutant MP with alanine substitution of L8	The primers p88_Xho1_Fw/L8A_Rev and linker_Cla_Rev/L8A_Fw were used.
pUCR1-M(S9A):sGFP	The vector encodes a recombinant RCNMV expressing mutant MP with alanine substitution of S9	The primers p88_Xho1_Fw/S9A_Rev and linker_Cla_Rev/S9A_Fw were used.
pUCR1-M(D10A):sGFP	The vector encodes a recombinant RCNMV expressing mutant MP with alanine substitution of D10	The primers p88_Xho1_Fw/D10A_Rev and linker_Cla_Rev/D10A_Fw were used.
pUCR1-M(L11A):sGFP	The vector encodes a recombinant RCNMV expressing mutant MP with alanine substitution of L11	The primers p88_Xho1_Fw/L11A_Rev and linker_Cla_Rev/L10A_Fw were used.
pUCR1-M(K13A):sGFP	The vector encodes a recombinant RCNMV expressing mutant MP with alanine substitution of K13	The primers p88_Xho1_Fw/K13A_Rev and linker_Cla_Rev/K10A_Fw were used.
pUCR1-Mα3(4A):sGFP	The vector encodes a recombinant RCNMV expressing mutant MP with alanine substitution of amino acids fro the 180th to 183rd	The primers p88_Xho1_Fw/4A_Rev and linker_Cla_Rev/4A_Fw were used.
pUCR1-M(Q180A):sGFP	The vector encodes a recombinant RCNMV expressing mutant MP with alanine substitution of Q180	The primers p88_Xho1_Fw/Q180A_Rev and linker_Cla_Rev/Q180A_Fw were used.
pUCR1-M(R181A):sGFP	The vector encodes a recombinant RCNMV expressing mutant MP with alanine substitution of R181	The primers p88_Xho1_Fw/R181A_Rev and linker_Cla_Rev/R181A_Fw were used.
pUCR1-M(T182A):sGFP	The vector encodes a recombinant RCNMV expressing mutant MP with alanine substitution of T182	The primers p88_Xho1_Fw/T182A_Rev and linker_Cla_Rev/T182A_Fw were used.
pUCR1-M(L183A):sGFP	The vector encodes a recombinant RCNMV expressing mutant MP with alanine substitution of L183	The primers p88_Xho1_Fw/L183A_Rev and linker_Cla_Rev/L183A_Fw were used.
pUCR1-M(T182D):sGFP	The vector encodes a recombinant RCNMV expressing mutant MP with aspartic acid substitution of T182	The primers p88_Xho1_Fw/T182D_Rev and linker_Cla_Rev/T182D_Fw were used.
pUCR2fsMP	The vector encodes mutant RNA2 lacking MP	Kaido *et al*., 2009
pUCR2-200/5'	The vector encodes 5' terminal 200 nt of RNA2	Kaido *et al*., 2011

Table II-4. (continued)

Name	Description	Construction/Reference
Plasmids for protein expression in *Echerichia coli*		
pRAMP-15b	The vector for expression of wt RCNMV MP in *E. coli*	Kaido *et al* ., 2011
pRAMP(Δα1)-15b	The vector for expression of mutant MP with deletion of the first putative α-helix in *E. coli*	The MP coding region was PCR-amplified from pUCR1-Mdhel1sG with primers NdeI-RAMP5Fw and Bam-RAMP3Rev. This fragment was inserted the NdeI/BamHI site of pRAMPdC70-15b (Kaido *et al* ., 2011) via ligation.
pRAMP(Δα2)-15b	The vector for expression of mutant MP with deletion of the second putative α-helix in *E. coli*	pUCR1-Mdhel2sG was used as template. The PCR fragment was gaind with the primers NdeI-RAMP5Fw and Bam-RAMP3Rev.
pRAMP(Δα3)-15b	The vector for expression of mutant MP with deletion of the third putative α-helix in *E. coli*	pUCR1-Mdhel3sG was used as template. The PCR fragment was gaind with the primers NdeI-RAMP5Fw and Bam-RAMP3Rev.
pRAMP(Δα4)-15b	The vector for expression of mutant MP with deletion of the fourth putative α-helix in *E. coli*	pUCR1-Mdhel4sG was used as template. The PCR fragment was gaind with the primers NdeI-RAMP5Fw and Bam-RAMP3Rev.
pRAMP(Δα5)-15b	The vector for expression of mutant MP with deletion of the fifth putative α-helix in *E. coli*	pUCR1-Mdhel5sG was used as template. The PCR fragment was gaind with the primers NdeI-RAMP5Fw and Bam-RAMP3Rev.

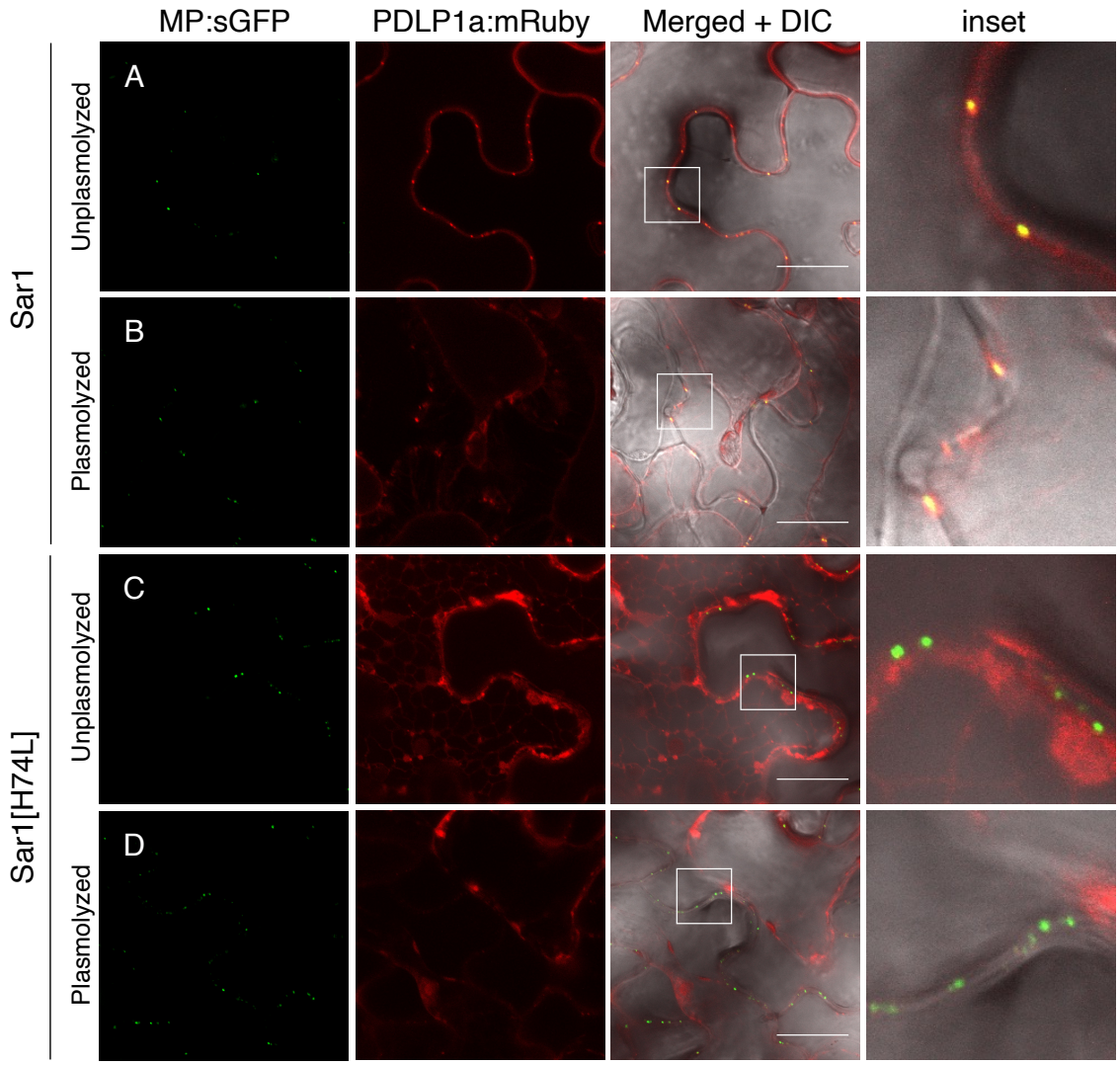

Figure II-1. Sar1[H74L] had no effect on the PD targeting of RCNMV MP. A mixture of *Agrobacterium* harboring a construct encoding RCNMV MP:sGFP and PDLP1a:mRuby, respectively, was infiltrated into *N. benthamiana* together with one harboring a construct encoding AtSar1 or AtSar1[H74L]. OD_{600} of each culture was adjust to 0.4. For plasmolysis, 10% (w/v) NaCl was dropped on a part of leaf samples just before observation while water was used for negative control. Representative confocal microscopy images of RCNMV MP:sGFP and PDLP1a:mRuby localization in *N. benthamiana* epidermal cells at 48 hours post-infiltration. The inset shows an enlarged image of the area surrounded by a white frame in each merged image. All images are confocal projections composed of several sections taken at 2 μm intervals, which range from the surface to the middle of epidermal cells. Scale bars = 20 μm. DIC, differential interference contrast.

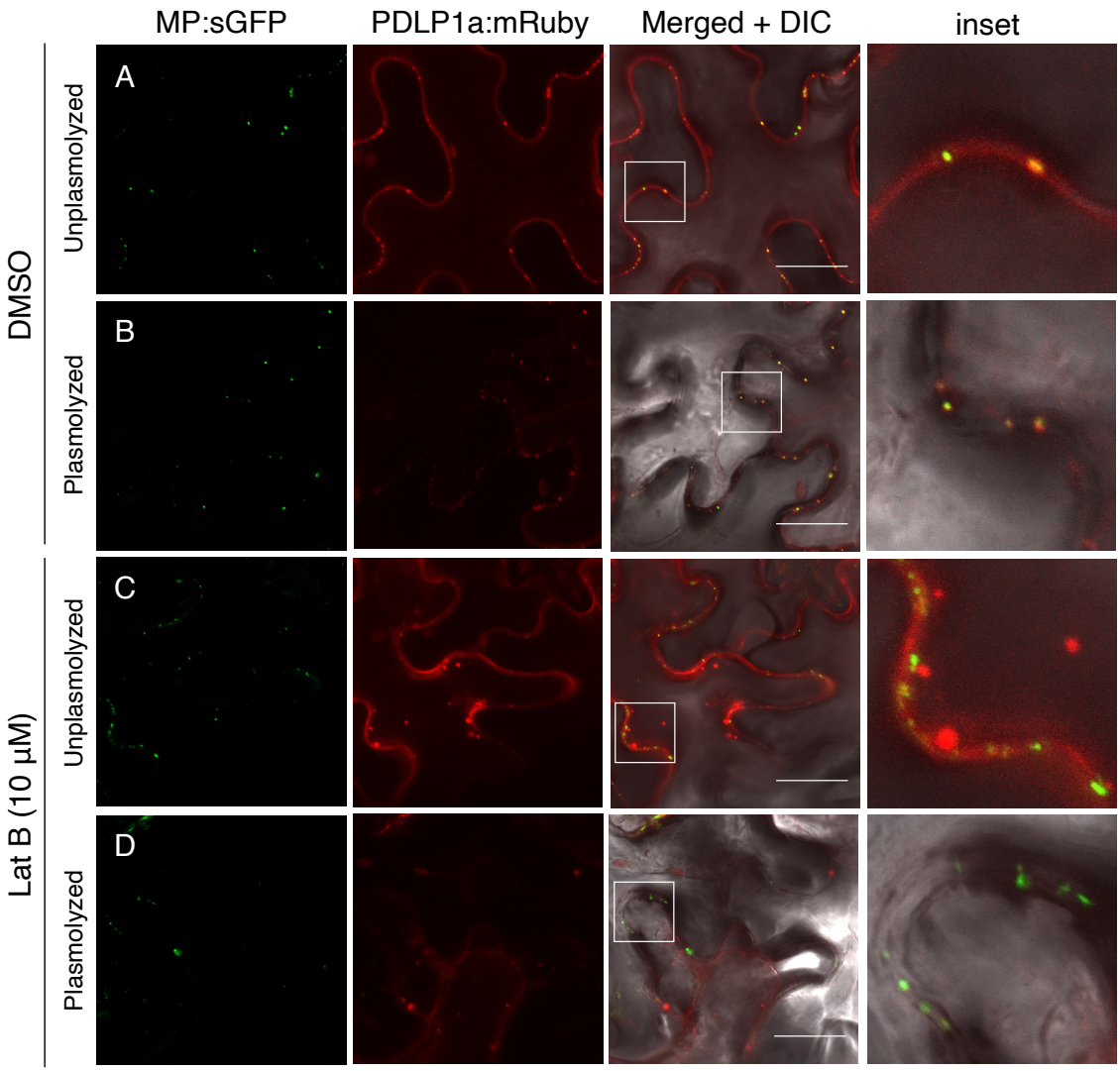

Figure II-2. 10 μM Lat B had no effect on the PD targeting of RCNMV MP. A mixture of *Agrobacterium* harboring a construct encoding RCNMV MP:sGFP and PDLP1a:mRuby, respectively, was infiltrated into *N. benthamiana* together with 10 μM Lat B. OD_{600} of each culture was adjust to 0.4. 10 μM Lat B was infiltrated again 12 hours before observation. Representative confocal microscopy images of RCNMV MP:sGFP and PDLP1a:mRuby localization in *N. benthamiana* epidermal cells at 36 hours post-infiltration. The inset shows an enlarged image of the area surrounded by a white frame in each merged image. All images are confocal projections composed of several sections taken at 2 μm intervals, which range from the surface to the middle of epidermal cells. Scale bars = 20 μm. DIC, differential interference contrast.

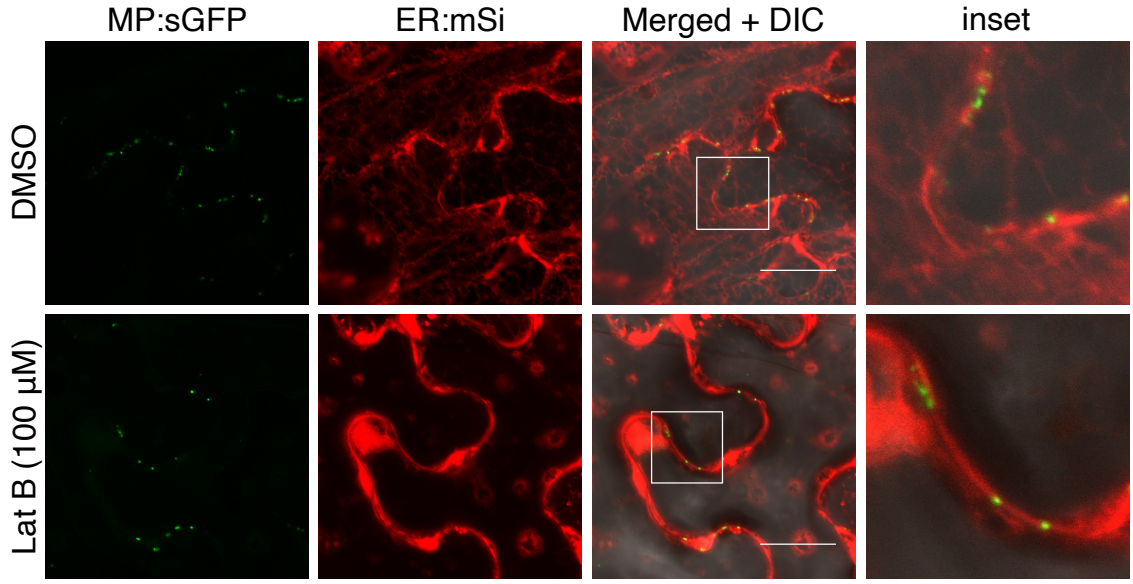

Figure II-3. 100 μM Lat B had no effect on the PD targeting of RCNMV MP. A mixture of *Agrobacterium* harboring a construct encoding RCNMV MP:sGFP and ER:mSi, respectively, was infiltrated into *N. benthamiana* together with 100 μM Lat B. OD_{600} of each culture was adjust to 0.4 for MP:sGFP and 0.2 for ER:mSi. 100 μM Lat B was injected again 12 hours before observation. Representative confocal microscopy images of RCNMV MP:sGFP and ER:mSi localization in *N. benthamiana* epidermal cells at 36 hours post-infiltration. The inset shows an enlarged image of the area surrounded by a white frame in each merged image. All images are confocal projections composed of several sections taken at 2 μm intervals, which range from the surface to the middle of epidermal cells. Scale bars = 20 μm. DIC, differential interference contrast.

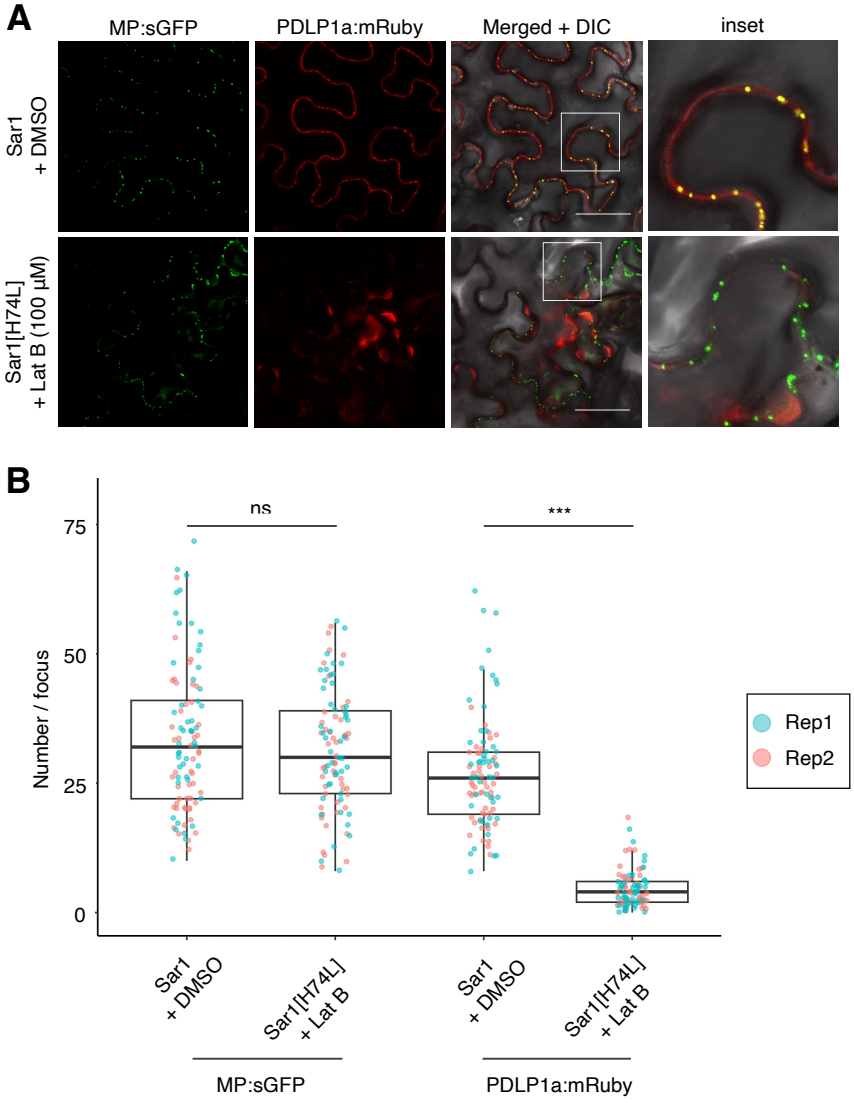

Figure II-4. Treatment of both Sar1[H74L] and 100 µM Lat B had no effect on the PD targeting of RCNMV MP. A mixture of *Agrobacterium* harboring a construct encoding RCNMV MP:sGFP and PDLP1a:mRuby, respectively, was infiltrated into *N. benthamiana* together with one harboring a construct encoding AtSar1 or AtSar1[H74L]. OD_{600} of each culture was adjust to 0.4. 100 µM Lat B or DMSO solution was injected twice: at the time of agroinfiltration and again 12 hours prior to observation. (A) Representative confocal microscopy images of RCNMV MP:sGFP and PDLP1a:mRuby at 36 hours post-infiltration. All images are confocal projections composed of several sections taken at 2 µm intervals, which range from the surface to the middle of epidermal cells. Scale bars = 20 µm. DIC, differential interference contrast. (B) Number of dots at the cell wall per focus. Statistical significance in the difference of the means was assessed using Welch's *t*-test. ***, $P < 0.001$; ns, not significant ($P > 0.05$).

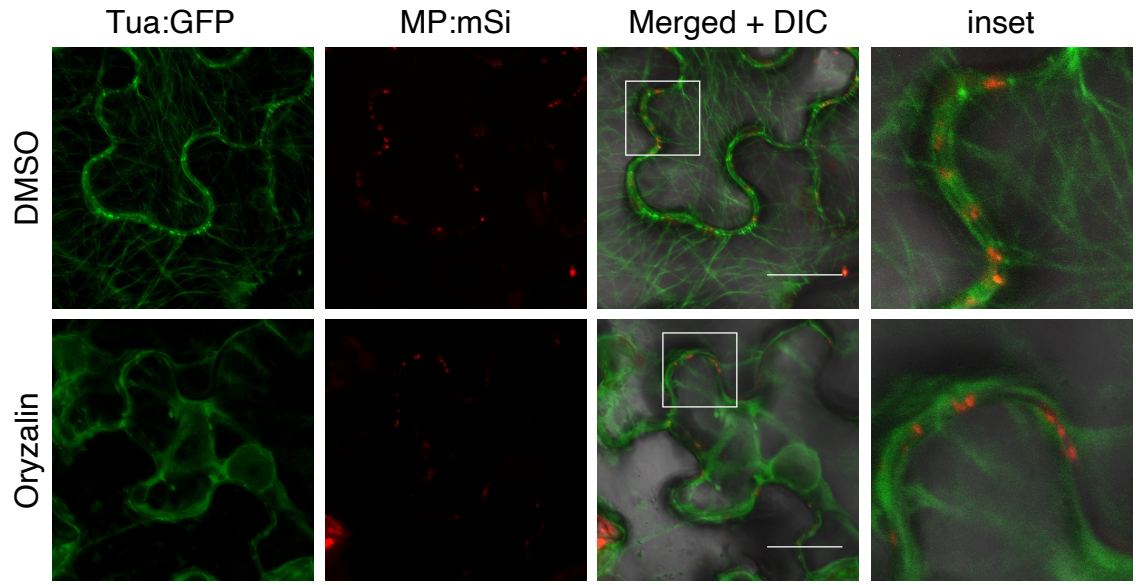

Figure II-5. Oryzalin had no effect on the PD targeting of RCNMV MP. *Agrobacterium* harboring a construct encoding RCNMV MP:mSi was infiltrated into transgenic *N. benthamiana* expressing fusion protein of tubulinα and GFP (Tua:GFP). OD_{600} was adjust to 0.4 for MP:mSi. 100 μM Oryzalin or DMSO solution was infiltrated 20 hours post-infiltration of *Agrobacterium*. Representative confocal microscopy images of RCNMV MP:mSi and Tua:GFP localization in *N. benthamiana* epidermal cells at 36 hours post-infiltration. The inset shows an enlarged image of the area surrounded by a white frame in each merged image. All images are confocal projections composed of several sections taken at 2 μm intervals, which range from the surface to the middle of epidermal cells. Scale bars = 20 μm. DIC, differential interference contrast.

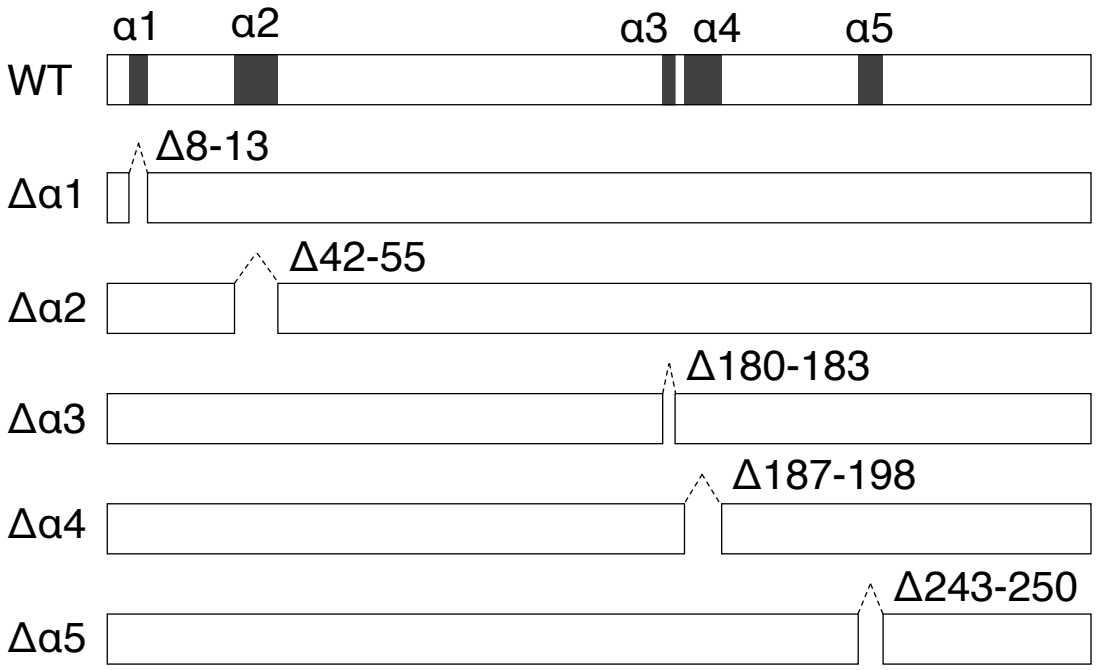

Figure II-6. Maps of MP:sGFP and its derivatives. Five α-helix are predicted in the RCNMV MP using PsiPred, a secondary structure prediction tool. Derivatives of MP:sGFP in which each of five α-helix domains are deleted.

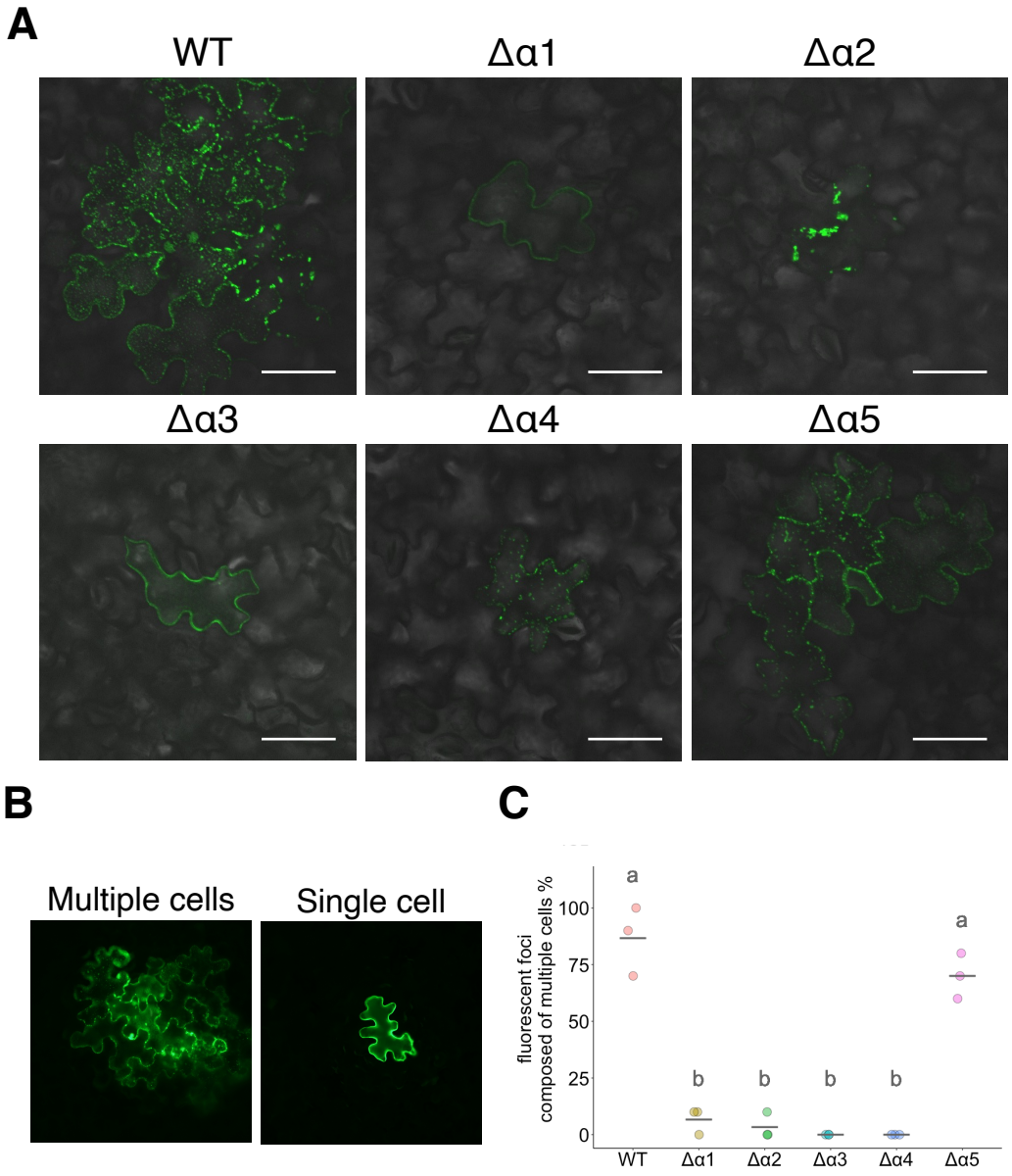

Figure II-7. Deletion of predicted α-helix inhibited viral cell-to-cell movement and appropriate viral subcellular localization. (A) Representative confocal microscopy images of recombinant viruses encoding wt MP or mutants with α-helix deletion (Δα1 to Δα5) at 24 hpi. The images are superimposed images taken with GFP channel and differential interference contrast. Scale bars = 50 μm. (B) Representative epifluorescence microscopy images of infected sites containing multiple fluorescent cells or single cell. (C) Percentage of fluorescent foci composed of multiple cells detected by epifluorescence microscopy at 24 hpi. Dots, the percentage gained from ten images. Bars, the average gained from three independent experiments. Statistical significance is indicated by different letters ($P < 0.05$, one-way ANOVA followed by Tukey's post hoc test).

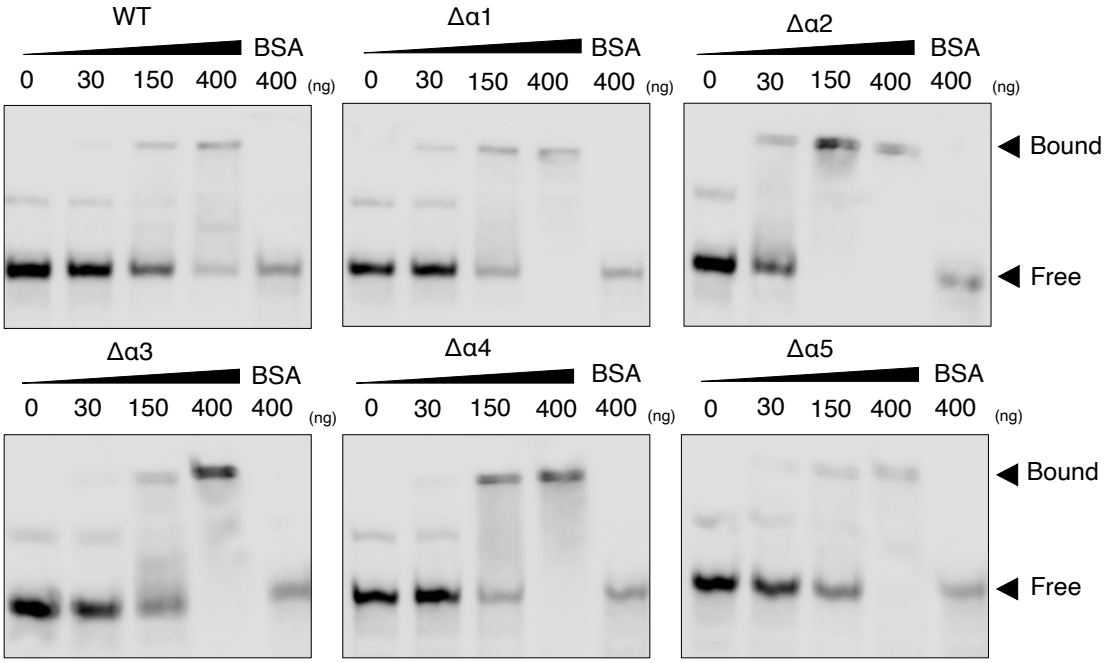

Figure II-8. Deletion mutants retained its RNA binding ability. Specific amount of (His)6-tagged recombinant MP and a-helix mutant, purified from *E. coli* via Ni-NTA column, were incubated with biotin-labeled *in vitro* transcripts derived from a 200-nucleotide fragment of RCNMV RNA2. The resulting RNA–protein complexes were subjected to electrophoresis on a 0.75% agarose gel. Following transfer to a membrane, the labeled RNA was detected using HRP-conjugated streptavidin. BSA, bovine serum albumin used as negative control.

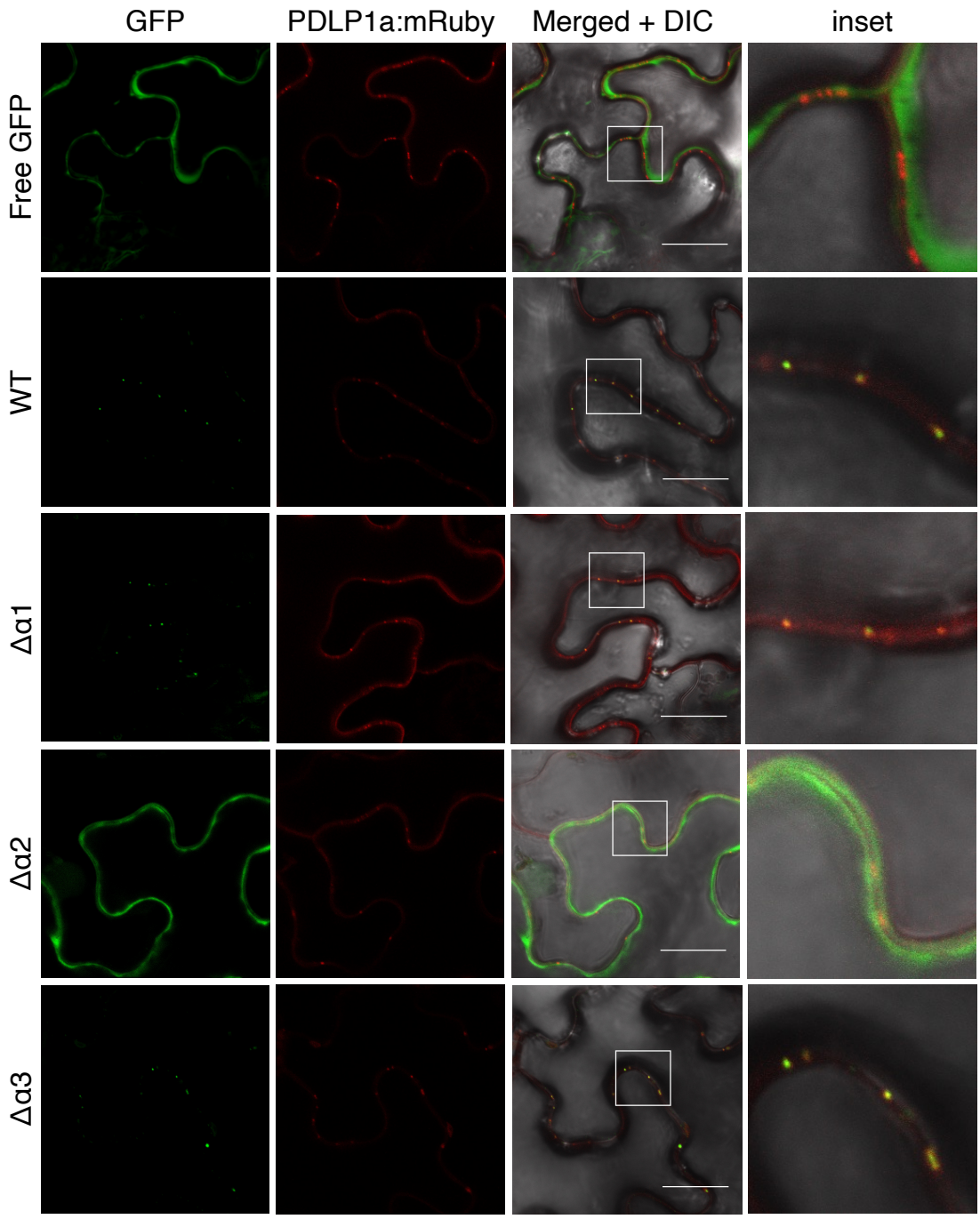

Figure II-9. Deletion of the second α-helix compromised PD localization of MP. *Agrobacterium* containing a construct encoding wt MP:sGFP or its derivatives was infiltrated into *N. benthamiana* together with another containing a construct encoding PDLP1a:mRuby. OD_{600} of each culture was adjust to 0.4. Representative confocal microscopy images in *N. benthamiana* epidermal cells at 48 hours post-infiltration. The inset provides a magnified view of the region delineated by a white frame in each merged image. Scale bars = 20 μm. DIC, differential interference contrast.

A

	42													55 aa
WT	A	S	M	M	S	K	I	T	D	Y	A	K	T	T
α2L	·	A	A	A	A	·	·	·	·	·	·	·	·	·
α2M	·	·	·	·	·	A	A	A	A	A	·	·	·	·
α2R	·	·	·	·	·	·	·	·	·	·	·	A	A	A

B

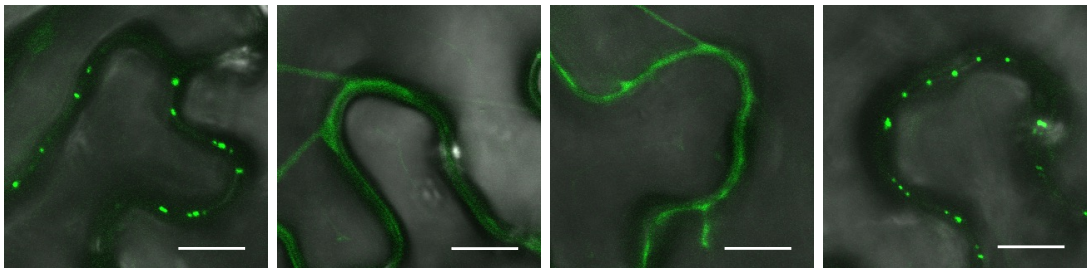

Figure II-10. Alanine substitution of amino acids within the second α-helix interfered with PD localization of MP. *Agrobacterium* harboring a construct encoding wt MP:sGFP or its derivatives was infiltrated into *N. benthamiana.* OD_{600} of each culture was adjust to 0.4. (A) Amino acid sequence of putative second α-helix in wt MP and mutants with alanine substitution. (B) Representative confocal microscopy images in *N. benthamiana* epidermal cells at 48 hours post-infiltration. Scale bars = 10 μm.

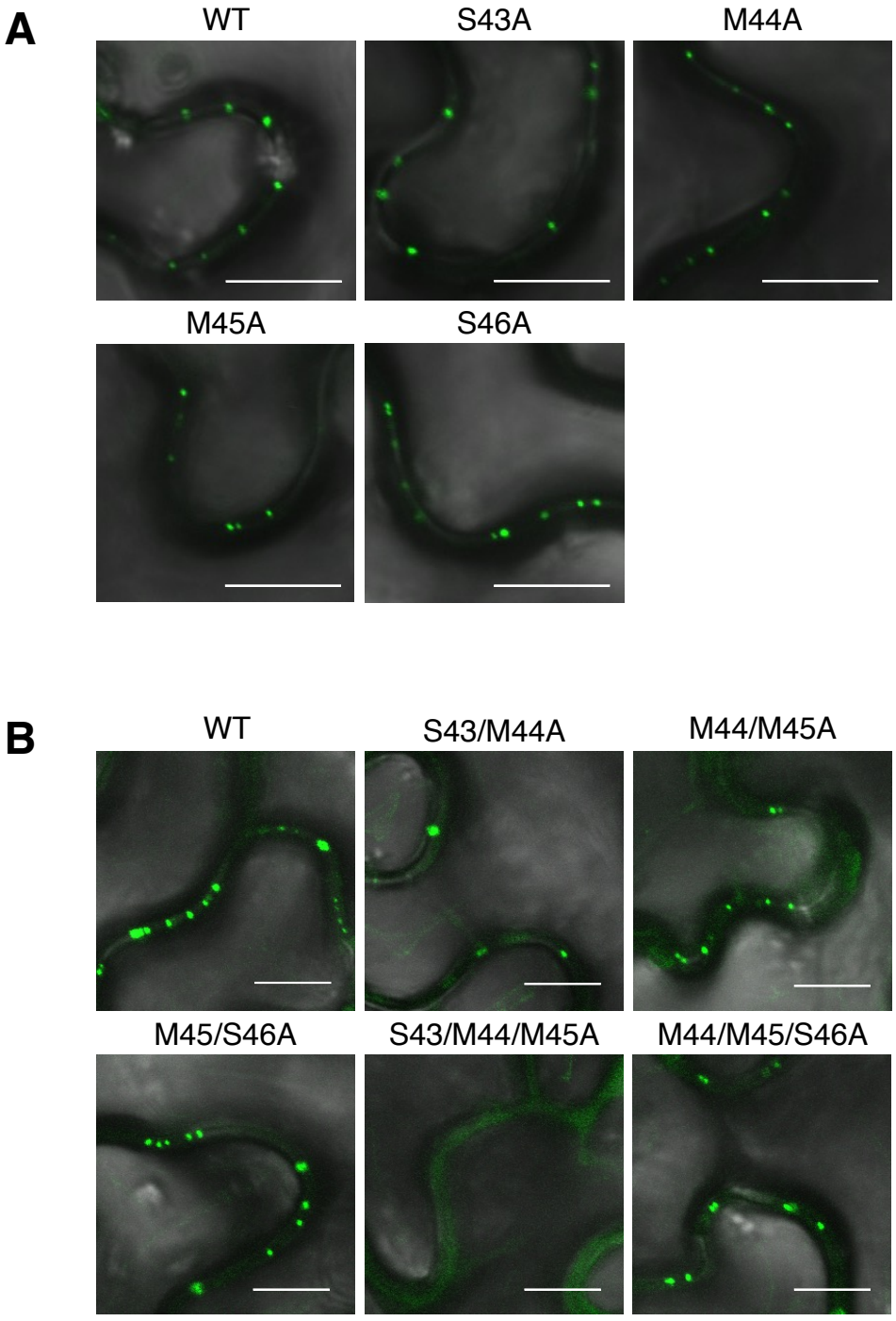

Figure II-11. Alanine substitution of S43/M44/M45 within α2L interfered with PD localization of MP. *Agrobacterium* harboring a construct encoding wt MP:sGFP or its derivatives was infiltrated into *N. benthamiana.* OD_{600} of each culture was adjust to 0.4. Representative confocal microscopy images in *N. benthamiana* epidermal cells at 48 hours post-infiltration. The results of single mutation (A) and multipule mutations (B). Scale bars = 10 μm.

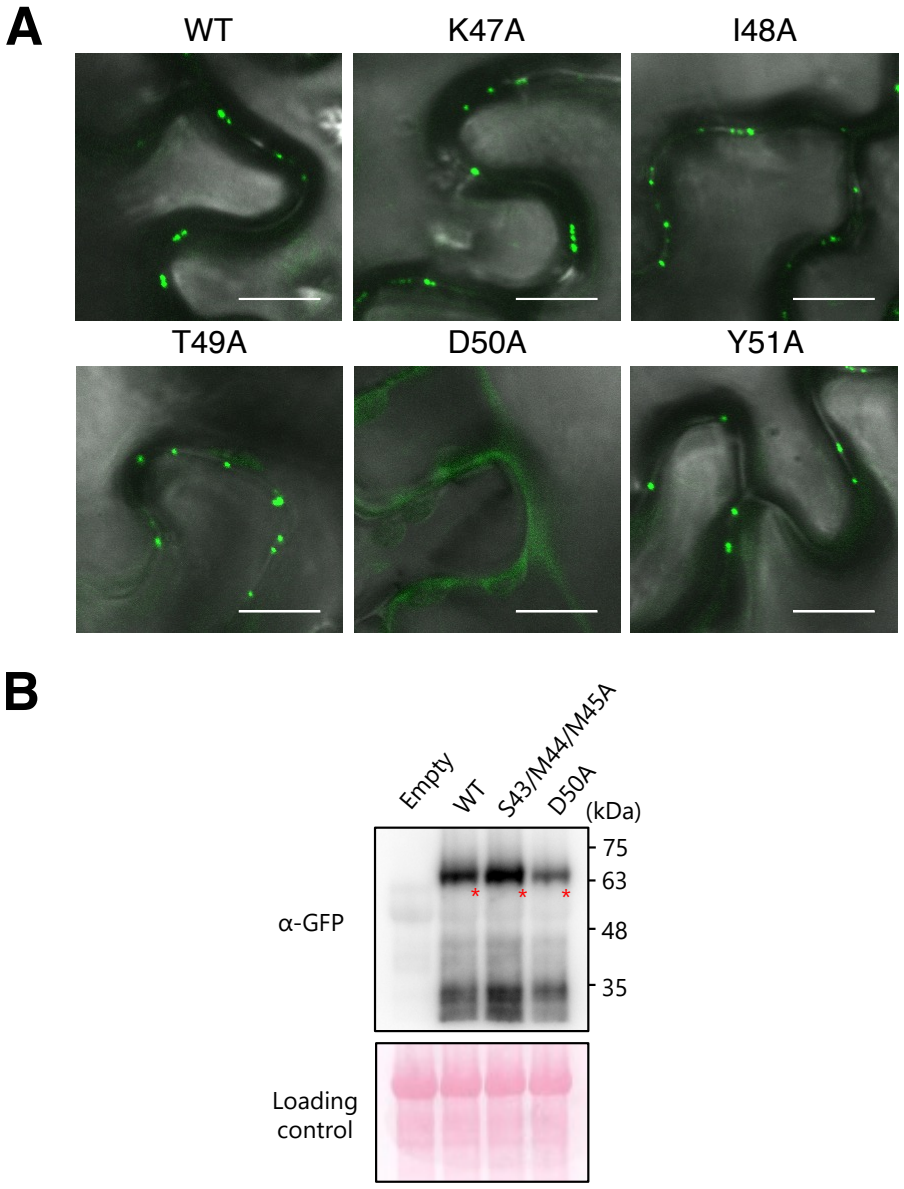

Figure II-12. Alanine substitution of 50th aspartate within α2M interfered with PD localization of MP. Agrobacterium harboring a construct encoding wt MP:sGFP or its derivatives was infiltrated into *N. benthamiana*. OD_{600} of each culture was adjust to 0.4. (A) Representative confocal microscopy images in *N. benthamiana* epidermal cells at 48 hours post-infiltration. Scale bars = 10 μm. (B) Accumulation of MP in the infiltrated leaves at 48 hours post infiltration. Western blot analysis using GFP-specific antibodies confirmed the expression of GFP-tagged wt or mutant MP. Ponceau S staining of membrane served as a loading control.

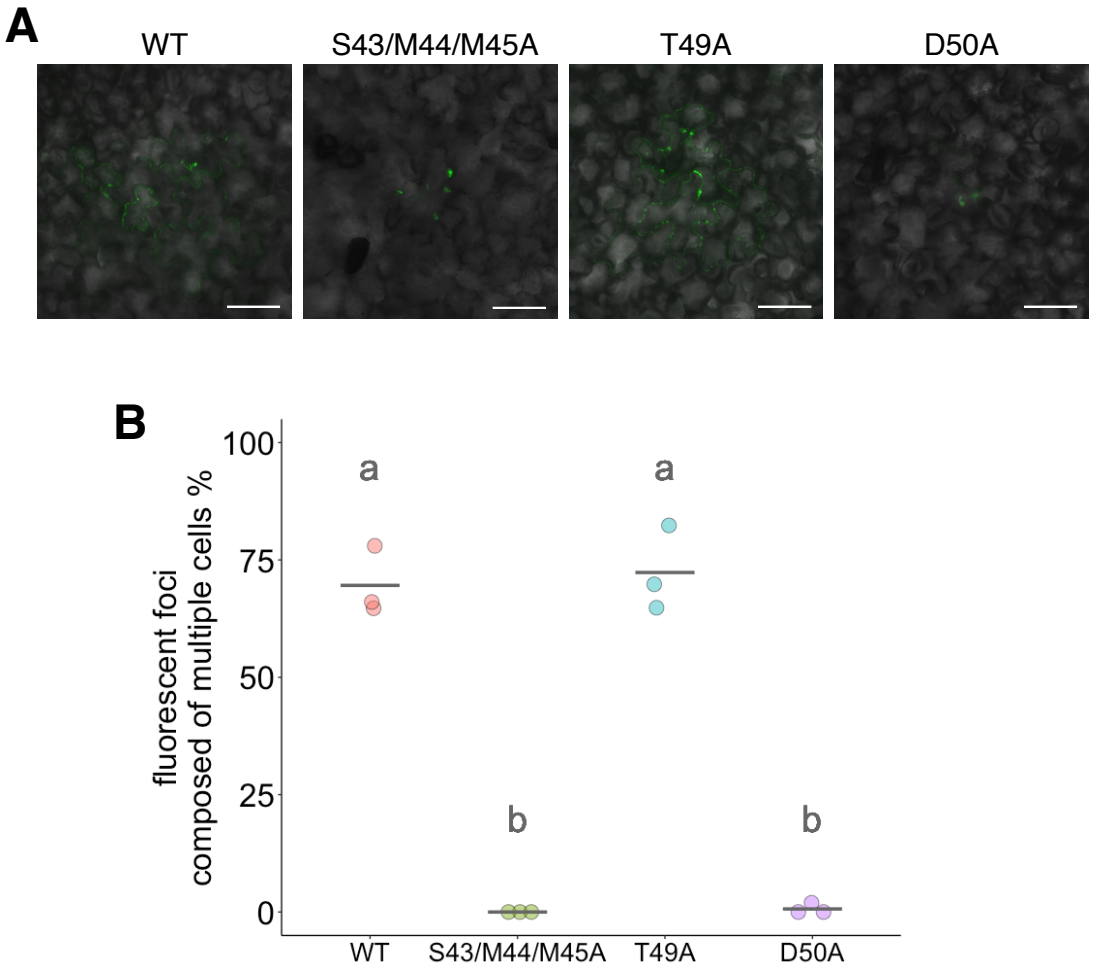

Figure II-13. Alanine substitution at position S43/M44/M45 and D50 completely inhibited viral cell-to-cell movement. (A) Representative confocal microscopy images of recombinant viruses encoding wt MP or mutants with alanine substitution at 24 hpi. The images are superimposed images taken with GFP channel and differential interference contrast. Scale bars = 50 μm. (B) Percentage of fluorescent foci composed of multiple cells detected by epifluorescence microscopy at 24 hpi. Dots, the percentage gained from about 50 images. Bars, the average gained from three independent experiments. Statistical significance is indicated by different letters ($P < 0.05$, one-way ANOVA followed by Tukey's post hoc test).

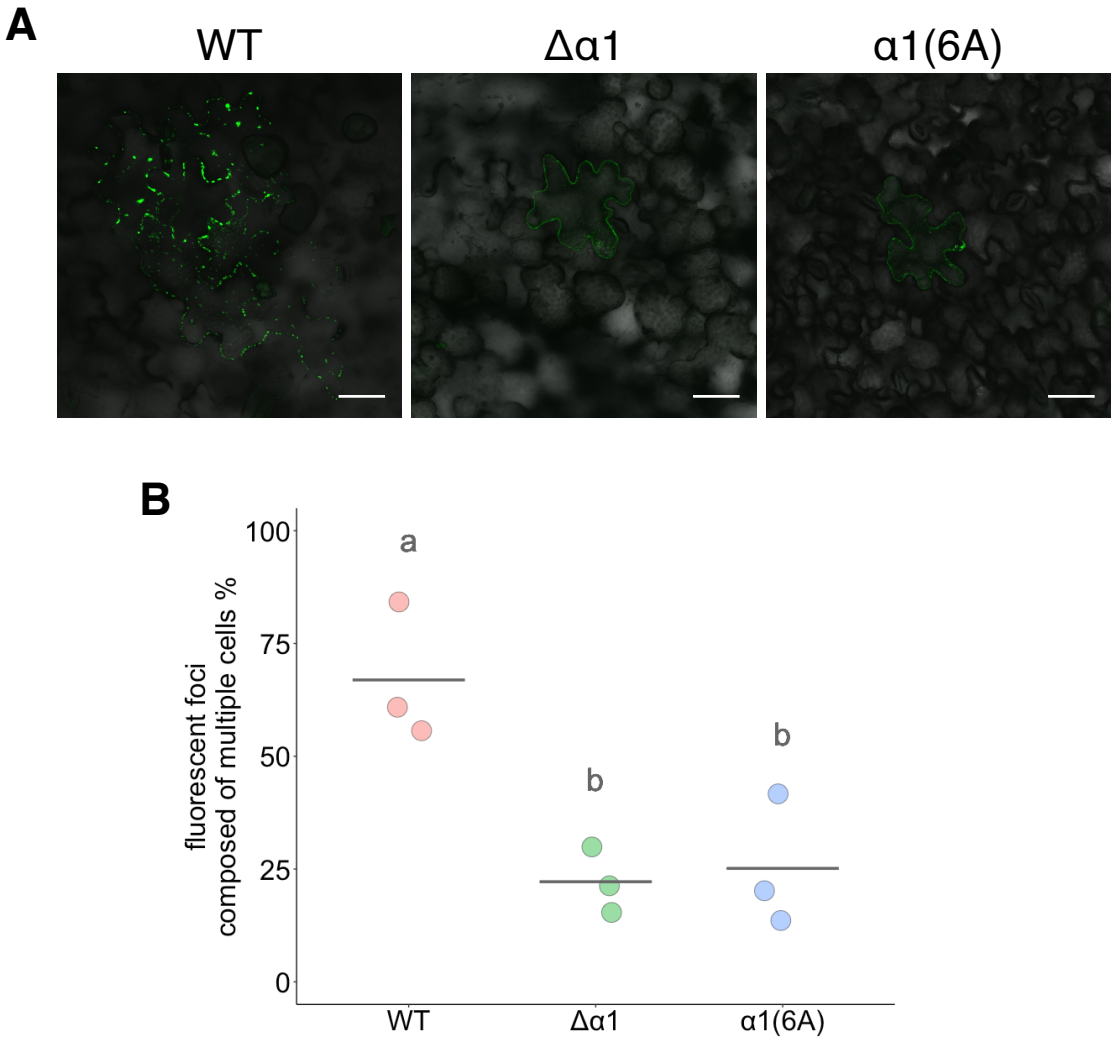

Figure II-14. Deletion of the first α-helix and alanine substitution of all amino acids within the first α-helix inhibits viral cell-to-cell movement. (A) Representative confocal microscopy images of recombinant viruses encoding wt MP or mutants with alanine substitution at 24 hpi. The images are superimposed images taken with GFP channel and differential interference contrast. Scale bars = 50 μm. (B) Percentage of fluorescent foci composed of multiple cells detected by epifluorescence microscopy at 24 hpi. Dots, the percentage gained from about 100 images. Bars, the average gained from three independent experiments. Statistical significance is indicated by different letters ($P < 0.05$, one-way ANOVA followed by Tukey's post hoc test).

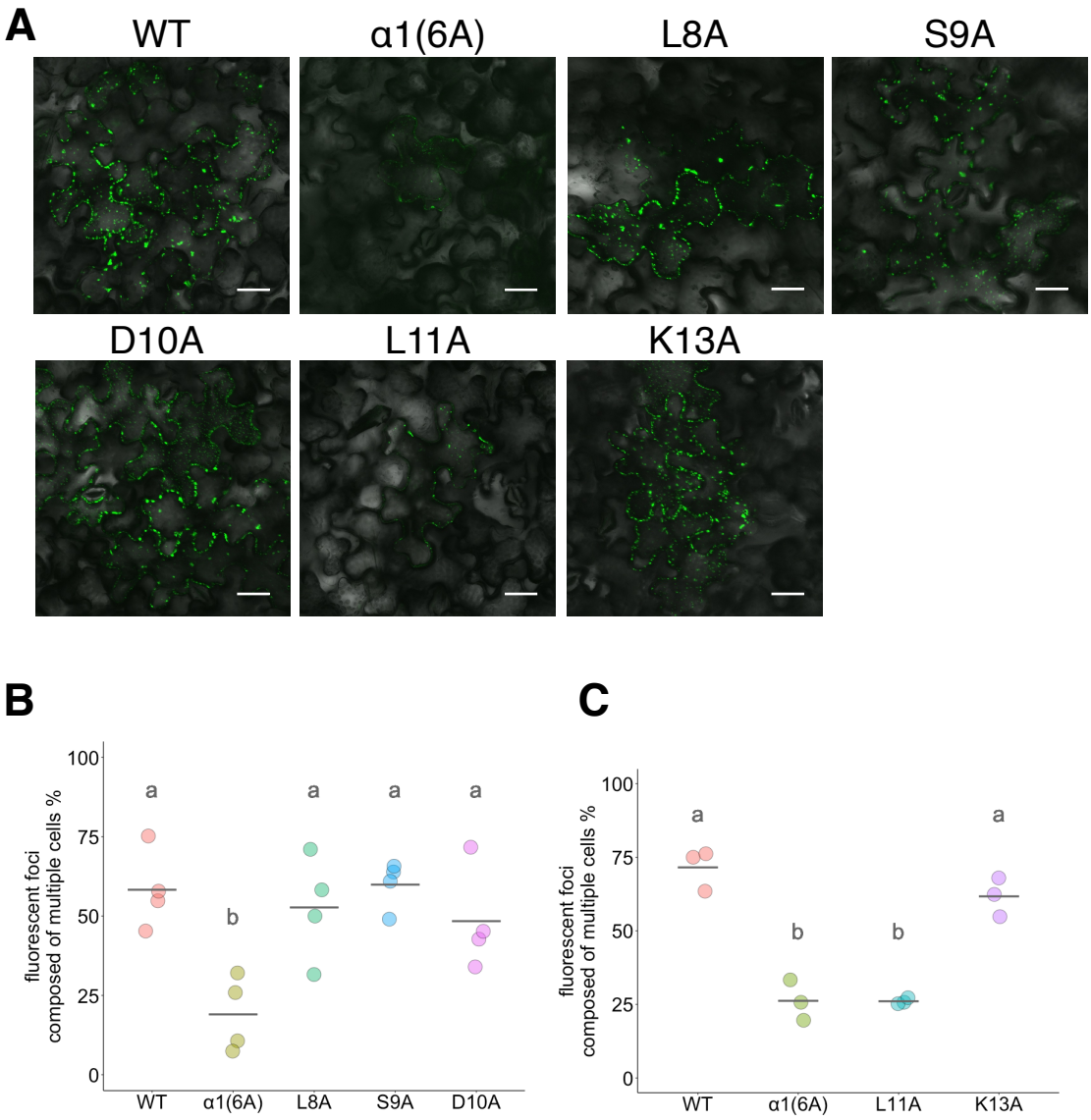

Figure II-15. Alanine substitution of 11th leucine inhibits viral cell-to-cell movement. (A) Representative confocal microscopy images of recombinant viruses encoding wt MP or mutants with alanine substitution at 24 hpi. The images are superimposed images taken with GFP channel and differential interference contrast. Scale bars = 50 μm. (B, C) Percentage of fluorescent foci composed of multiple cells detected by epifluorescence microscopy at 24 hpi. Dots, the percentage gained from about 100 images. Bars, the average gained from three independent experiments. Statistical significance is indicated by different letters ($P < 0.05$, one-way ANOVA followed by Tukey's post hoc test).

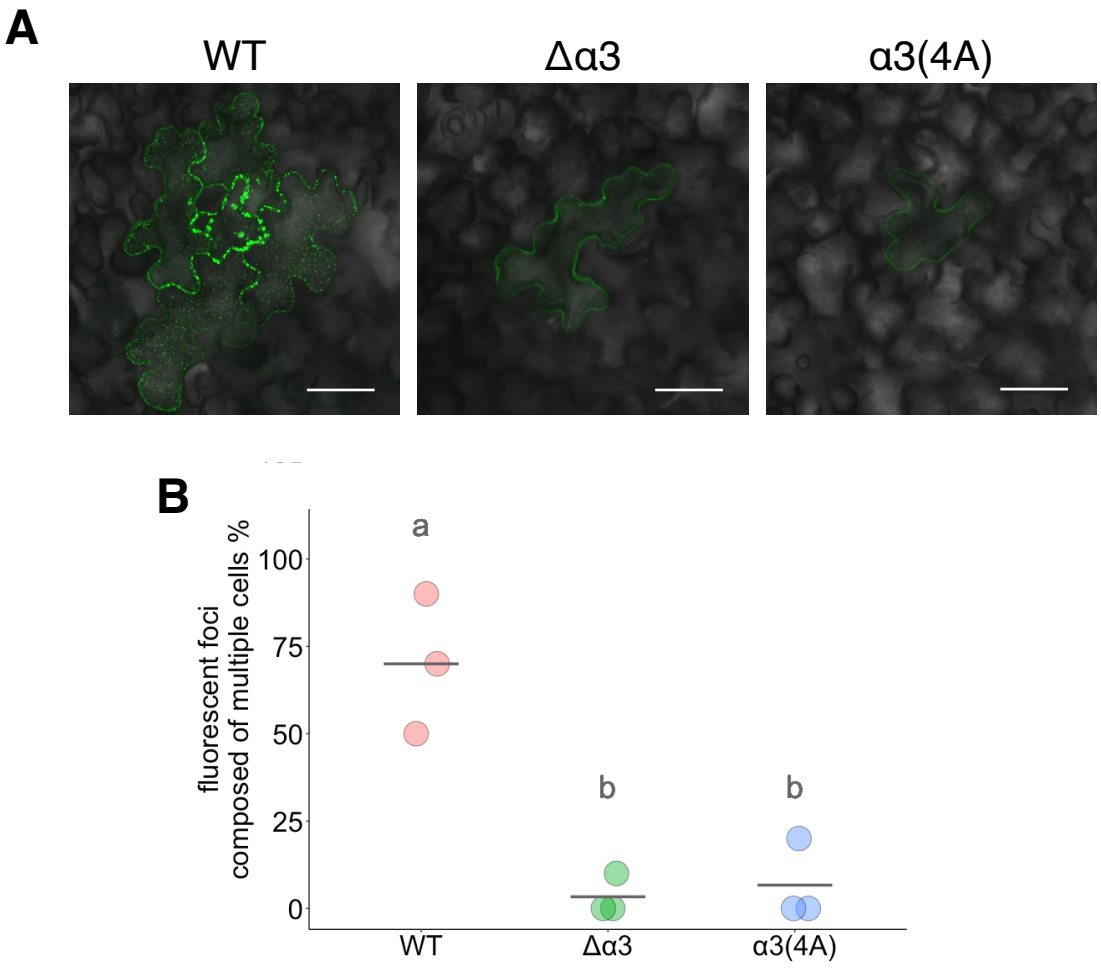

Figure II-16. Deletion of the third α-helix and alanine substitution of all amino acids within the first α-helix inhibits viral cell-to-cell movement. (A) Representative confocal microscopy images of recombinant viruses encoding wt MP or mutants with alanine substitution at 24 hpi. The images are superimposed images taken with GFP channel and differential interference contrast. Scale bars = 50 μm. (B) Percentage of fluorescent foci composed of multiple cells detected by epifluorescence microscopy at 24 hpi. Dots, the percentage gained from about 10 images. Bars, the average gained from three independent experiments. Statistical significance is indicated by different letters ($P < 0.05$, one-way ANOVA followed by Tukey's post hoc test).

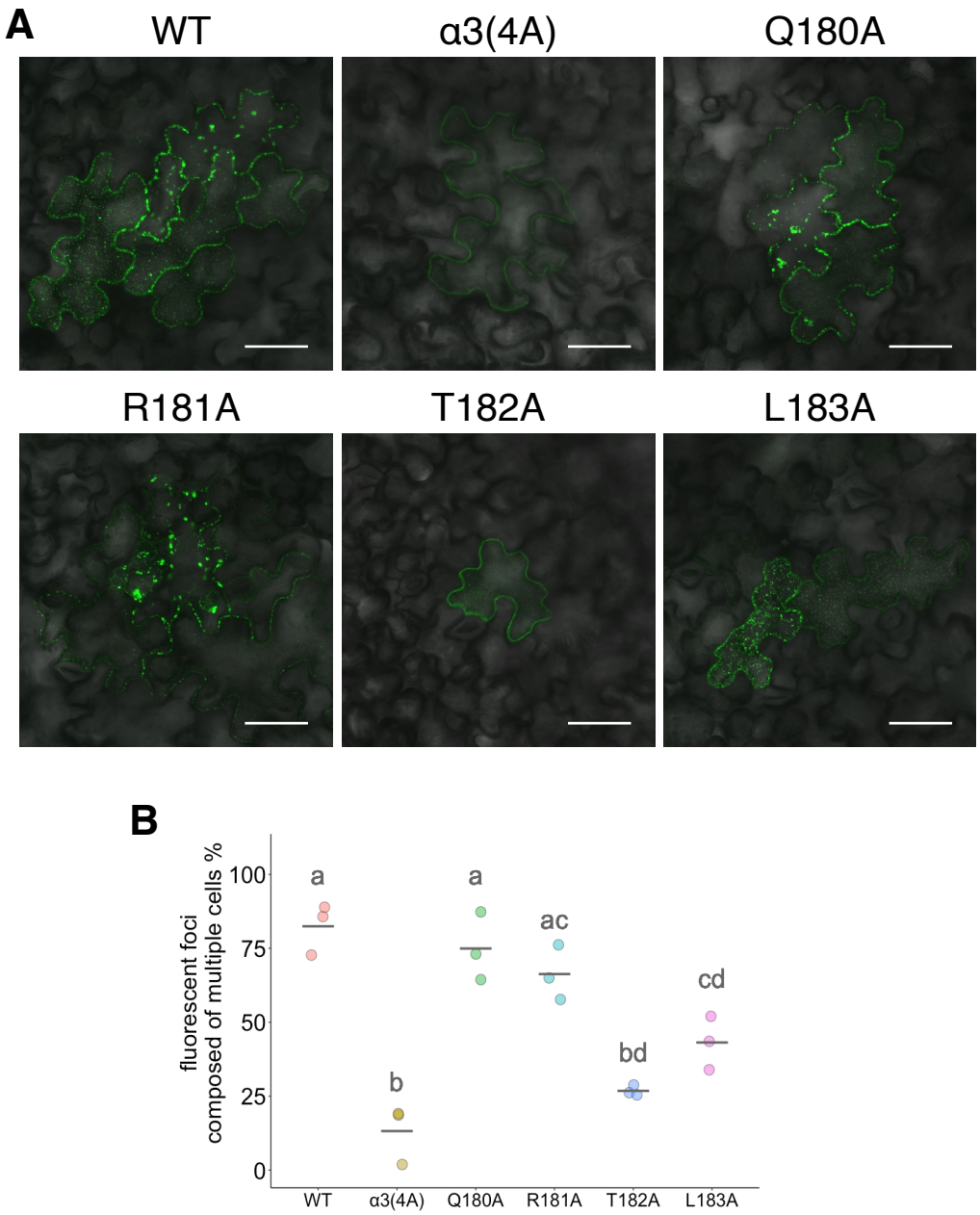

Figure II-17. Alanine substitution of 182nd threonine inhibits viral cell-to-cell movement. (A) Representative confocal microscopy images of recombinant viruses encoding wt MP or mutants with alanine substitution at 24 hpi. The images are superimposed images taken with GFP channel and differential interference contrast. Scale bars = 50 μm. (B) Percentage of fluorescent foci composed of multiple cells detected by epifluorescence microscopy at 24 hpi. Dots, the percentage gained from about 50 images. Bars, the average gained from three independent experiments. Statistical significance is indicated by different letters ($P < 0.05$, one-way ANOVA followed by Tukey's post hoc test)

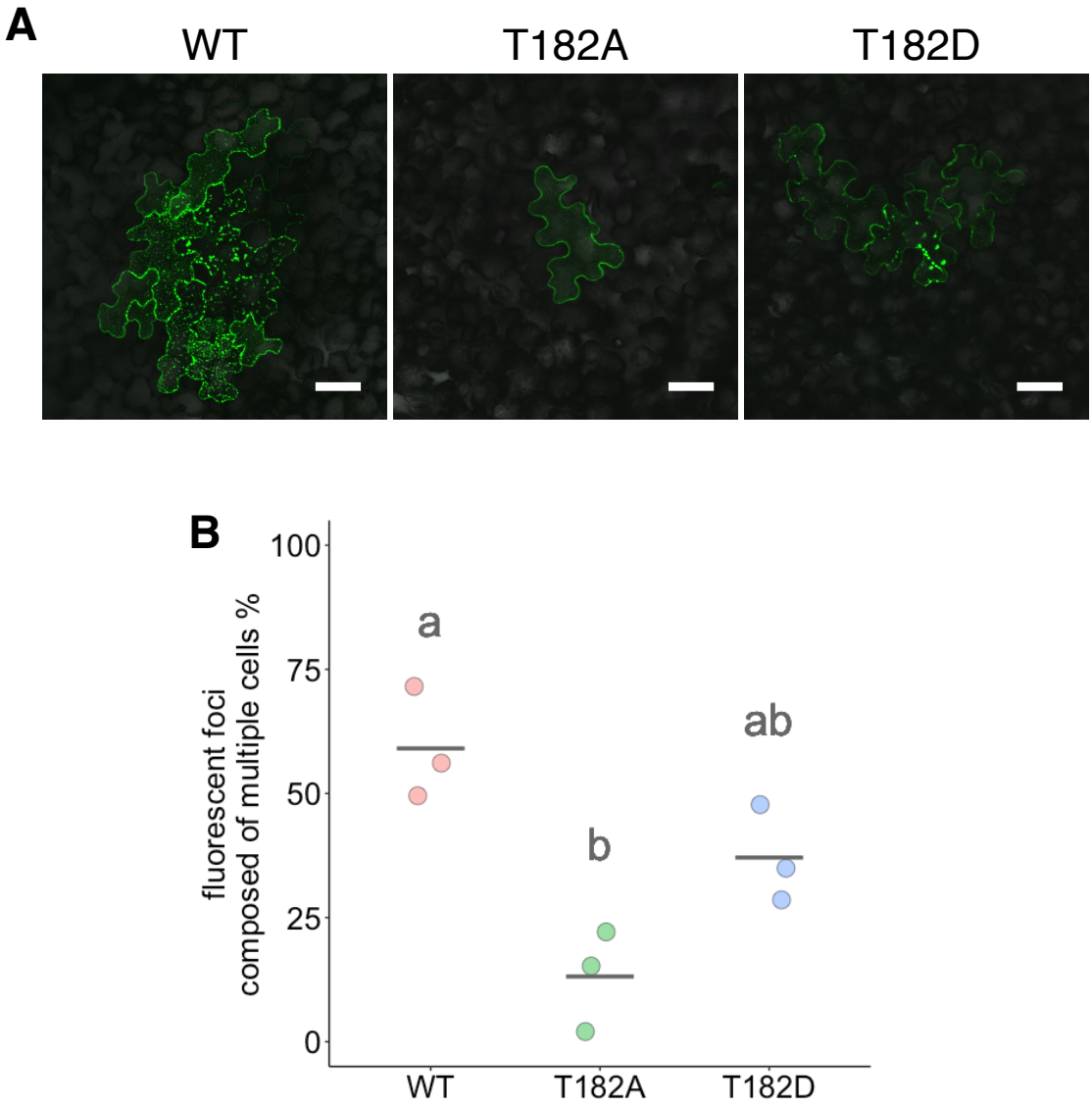

Figure II-18. Phosphorylation mimic mutant retains the ability of localization to aggregated structures and viral cell-to-cell movement. (A) Representative confocal microscopy images of recombinant viruses encoding wt MP or a mutant with aspartic acid at 24 hpi. The images are superimposed images taken with GFP channel and differential interference contrast. Scale bars = 50 μm. (B) Percentage of fluorescent foci composed of multiple cells detected by epifluorescence microscopy at 24 hpi. Dots, the percentage gained from about 100 images. Bars, the average gained from three independent experiments. Statistical significance is indicated by different letters ($P < 0.05$, one-way ANOVA followed by Tukey's post hoc test)

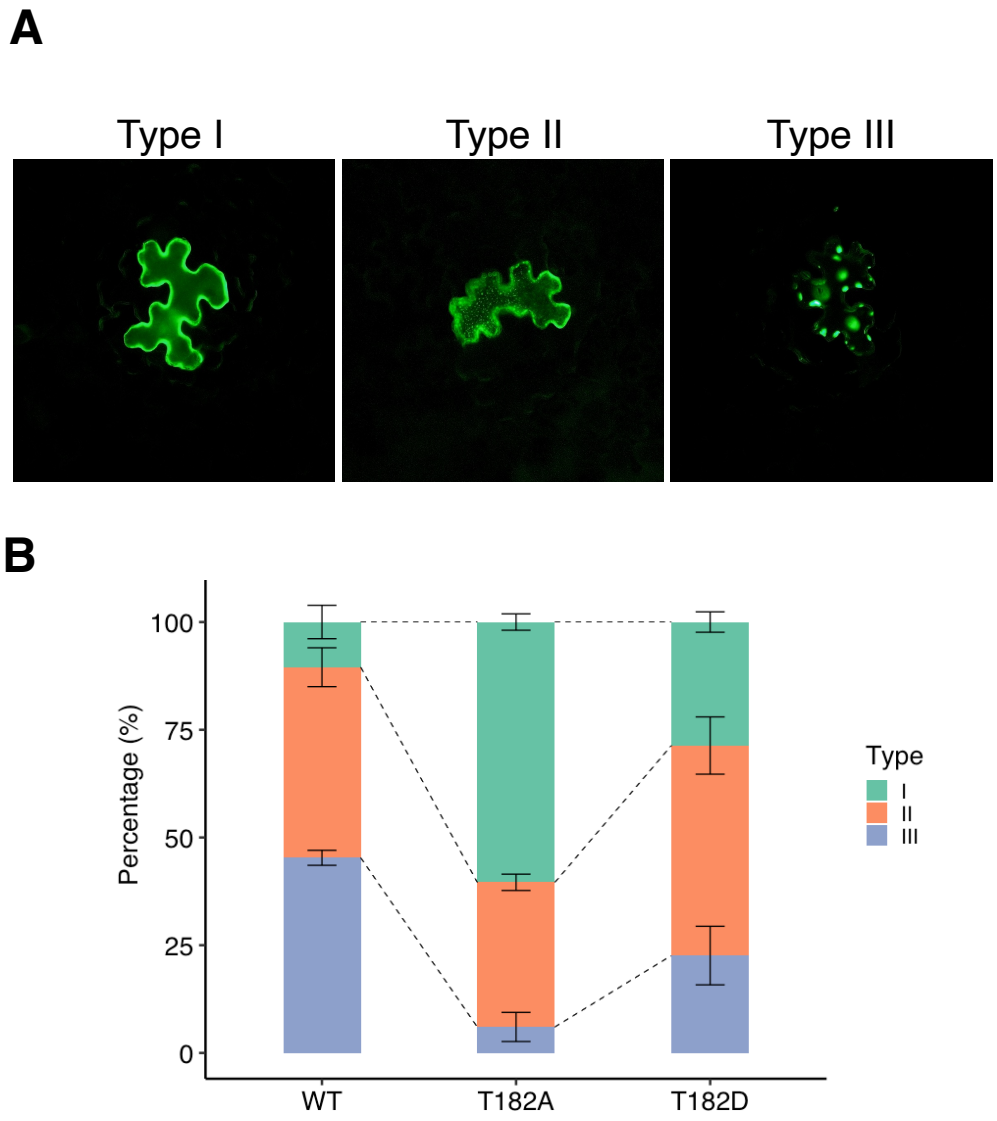

Figure II-19. Quantification of subcellular localization type showed the alanine-substituted mutant was inhibited from forming structures, while the aspartate-substituted mutant had partial aggregation ability. (A) Representative epifluorescence microscopy images of recombinant viruses. Type I, diffusion into cytoplasm. Type II, granular structure. Type III, aggregated structure. (B) Percentage of fluorescent foci showing localization type based on criteria of (A).

SUMMARY

CHAPTER I. Subcellular dynamics of red clover necrotic mosaic virus double-stranded RNAs in infected plant cells

Positive-strand RNA viruses modify cellular organelles to form viral replication complexes (VRCs) for synthesizing viral RNA. VRCs contains dsRNA, which is a viral replication intermediate. Plant viruses transfer between cells using movement proteins (MPs). Their VRCs and MPs often colocalize, likely playing a crucial role in viral movement. Here, to see how VRCs are formed and how MPs colocalize with VRCs, I utilized dsRNA reporter plants (B2-GFP) and investigated the dynamics of viral dsRNA and MP.

In early infection, dsRNA granule structures formed on the cell surface, and MP granule structures formed independently of them. In the late stages of infection, dsRNA and MP granule structures assembled and colocalized with each other. To investigate whether MP is required for dsRNA aggregation, I analyzed the dynamics of mutant viruses that did not express MP. The results showed that aggregation of dsRNA granule structures was observed in the presence or absence of MP, indicating that MP is not required for dsRNA aggregation. When the actin polymerization inhibitor Latrunculin B (Lat B) was used, the aggregation was partially inhibited, suggesting the role of the acto–myosin system in the aggregation of dsRNA structures. Importantly, dsRNA structures were found at sites of viral replication and were associated with the ER membrane. These results suggest that the granule structures of VRCs containing dsRNA and MP are formed independently at different locations, and that dsRNA structures grow larger probably using actin, and MP structures are recruited to the aggregated structures of dsRNA.

CHAPTER II. Unveiling crucial amino acids in red clover necrotic mosaic movement protein for optimal subcellular localization and viral cell-to-cell movement

The previous study employed recombinant RCNMV expressing MP:sGFP from the CP coding region of RNA1, revealing that MP accumulates at PD during early infection and forms aggregation structures at the cell surface over time. Thus, I hypothesized that the localization of MP to PD and VRCs is important for efficient cell-to-cell movement. To explore the mechanisms involved, I initially investigated the impact of inhibiting the ER-actin network, vesicular trafficking, and microtubules, which are known to play roles in MP transport to PD in other viruses. Surprisingly, the inhibition of these pathways did not affect the PD localization of RCNMV MP, suggesting the involvement of an unidentified transport system.

I then searched for functional regions within MP that are important for its subcellular localization and cell-to-cell movement. As no transmembrane domains or signal sequences were predicted for MP localization, I focused on the alpha-helix structure, a fundamental protein structure unit. Mutational analysis of amino acids within the putative alpha-helix region revealed the significance of S43, M44, M45, and D50 in the second alpha-helix for PD localization. L11 in the first alpha-helix and T182 in the third alpha-helix were found to be crucial for the formation of aggregation structures that seem to colocalize with the VRCs. Importantly, mutants in these functional regions demonstrated an inability for cell-to-cell movement, underscoring the importance of PD and VRCs localization for viral intercellular movement.

ACKNOWLEDGEMENTS

I thank Dr. Steven A. Lommel for providing cDNA clones of RCNMV Australian strain. I thank Dr. Christophe Ritzenthaler for providing *N. benthamiana* B2-GFP seeds. I also thank Dr. Mina Ohtsu for providing pPDLP1a:mRuby. This work was supported by JSPS KAKENHI (Grant Number JP21H02199).

I would like to express my sincere gratitude to my advisor, Dr. Masanori Kaido, Laboratory of Plant Environmental Microbiology, Department of Applied Biological Sciences, Setsunan University, for his invaluable guidance, unwavering support, and mentorship throughout the course of this research. I also wish to express my gratitude to Professor Yoshitaka Takano, Laboratory of Plant Pathology, Graduate School of Agriculture, Kyoto University for his continuous support, encouragement, and constructive feedback. His advice always helped me all the time of my study. My sincere thanks also go to Dr. Kazuyuki Mise and Dr. Akira Mine, Laboratory of Plant Pathology, Graduate School of Agriculture, Kyoto University for their exceptional guidance and expertise. I am deeply thankful to Dr. Suthitar Singkaravanit-Ogawa, Dr. Hiroaki Kato, Dr. Rikako Hirata, Dr. Hiroki Matsuo, and Dr. Taiki Ogawa for their continuous encouragement, insightful advice, and kind assistance. I also would like to thank Mrs. Keiko Hashimoto for her continuous support for management of research expenses and administrative procedures during my research work. My heartfelt thanks go to past and present members of Laboratory of Plant Pathology, Graduate School of Agriculture, Kyoto University, for their encouragement and kind friendship. I extend my gratitude to everyone who played a part in this achievement.

Lastly, I would like to express special thanks to my family for their understanding and selfless support, always supporting me.